Title: The Role of Fullerenes in the Environmental Stability of Polymer:Fullerene Solar Cells

Authors:

Harrison K. H. Lee[1], Andrew M. Telford[2], Jason A. Röhr[2], Mark F. Wyatt[3], Beth Rice[2], Jiaying Wu[4], Alexandre de Castro Maciel[2,5], Sachetan M. Tuladhar[2], Emily Speller[1], James McGettrick[1], Sebastian Pont[4], Trystan Watson[1], James R. Durrant[1,4], Wing C. Tsoi[1], Jenny Nelson[1,2]* and Zhe Li[1]*

*Corresponding authors

Contact Information:

[1] Dr. Harrison K. H. Lee, Emily Speller, Dr. James McGettrick, Dr. Trystan Watson, Prof. James R. Durrant, Dr. Wing C. Tsoi, , Prof Jenny Nelson, Dr. Zhe Li

SPECIFIC IKC, College of Engineering, Bay campus, Swansea University, Wales, UK SA1 8EN

[2] Dr. Andrew M. Telford, Jason A. Röhr, Beth Rice, Prof. Alexandre de Castro Maciel, Dr. Sachetan M. Tuladhar, Prof. Jenny Nelson

Department of Physics, Imperial College London, London, UK SW7 2AZ

[3] Dr Mark F. Wyatt

EPSRC UK National Mass Spectrometry Facility (NMSF), Swansea University Medical School, Wales, UK SA2 8PP

[4] Jiaying Wu, Sebastian Pont, Prof. James R. Durrant

Department of Chemistry, Imperial College London, London, UK SW7 2A

[5] Prof. Alexandre de Castro Maciel

Department of Physics, CCN, Federal University of Piauí, Teresina, Brazil, 64049-550

Emails: jenny.nelson@imperial.ac.uk, z.li@swansea.ac.uk

Abstract

Environmental stability is a common challenge for the commercialisation of low cost, encapsulation-free organic opto-electronic devices. Understanding the role of materials degradation is the key to address this challenge, but most such studies have been limited to conjugated polymers. Here we quantitatively study the role of the common fullerene derivative PCBM in limiting the stability of benchmark organic solar cells, showing that a minor fraction (<1%) of photo-oxidised PCBM, induced by short exposure to either solar or ambient laboratory lighting conditions in air, consistent with typical processing and operating conditions, is sufficient to compromise device performance severely. We identify the effects of photo-oxidation of PCBM on its chemical structure, and connect this to specific changes in its electronic structure, which significantly alter the electron transport and recombination kinetics. The effect of photo-oxidation on device current-voltage characteristics, electron mobility and density of states could all be explained with the same model of photoinduced defects as trap states. Our results demonstrate that the photochemical instability of PCBM and chemically similar fullerenes remains a barrier for the commercialisation of organic opto-electronic devices.

Introduction

A common challenge for the commercialisation of organic opto-electronic devices such as solar cells is their typically limited environmental stability. Numerous reports have shown that exposure to air typically results in rapid deterioration of device performance, especially when combined with exposure to light.[1,2] A general strategy to address this challenge is using device encapsulation, thereby creating a physical barrier for the diffusion of molecular oxygen into the device and hindering the reaction route of oxygen induced degradation.[3] However, encapsulation significantly increases the fabrication cost and hence reduces the commercialisation potential of such devices.

Understanding the degradation mechanism and enhancing the intrinsic stability of organic opto-electronic devices is therefore of paramount importance for their commercialisation.

Whilst organic bulk heterojunction solar cells have shown encouraging improvements in performance with efficiencies increasing from 3% to over 13% in the last decade,[4] commercialisation has been limited by their limited operating lifetimes.[3,5,6] Little success has been demonstrated to date in achieving prolonged lifetimes of un-encapsulated devices under exposure to light and oxygen.

The majority of studies of photoactive material stability have addressed the stability of the donor (polymer) component.[3,5,7,8] Despite their common use in solution-processed optoelectronic devices, fullerenes have been known to be sensitive to photo-induced reactions since the early 1990s.[9,10] For example, under UV or visible illumination in inert atmosphere, fullerenes such as phenyl-C61-butyric acid methyl ester (PCBM) can form covalent intermolecular C-C bonds to form dimers or higher oligomers. Such photo-oligomerisation has been correlated with a loss of organic photovoltaic (OPV) device efficiency under irradiation (the "burn-in" effect),[11,12] although modest PCBM photo-oligomerisation can also be beneficial, improving the morphological stability of OPV devices under thermal stress.[13,14] In the presence of oxygen, PCBM and other fullerene derivatives have been shown to undergo photo-oxidation, with two most commonly observed products of photo-oxidation, epoxide and carbonyl, on the fullerene cage.[15] While the photo-oxidation of fullerenes has been investigated in detail by Moons and co-workers,[16,17] little has been reported on its effect on the performance of organic opto-electronic devices, and especially on the exact mechanism of performance loss. A small number of studies have shown that organic solar cells containing deliberately photo-oxidised fullerene derivatives exhibit dramatic losses in their performance,[18,19] but provided no mechanistic explanation, nor proof of relevance to OPV stability. A few groups have suggested the formation of trap states upon fullerene photo-oxidation based on quantum chemical simulations, with limited direct evidence of the relationship of defects to electronic properties.[20,21]

In this paper, we evaluate the impact of PCBM photo-oxidation on the performance and stability of polymer:fullerene bulk heterojunction devices. We found that a minor fraction of photo-oxidised PCBM in blends films with the benchmark polymer Poly[N-9'-heptadecanyl-2,7-carbazole-alt-5,5-(4',7'-di-2-thienyl-2',1',3'-benzothiadiazole)] (PCDTBT), which is the most stable OPV polymer demonstrated so far,[22] induced by exposure to only a few minutes of illumination in air, can result in severe degradation of device performance. We systematically investigated the effect of introducing minor fractions (0.2 to 3.6%) of deliberately photo-oxidised PCBM on the transport and recombination mechanisms in OPV devices, to explain the losses in power conversion efficiency (PCE). We extend our conclusions to OPV devices based on other benchmark polymers, namely P3HT, PTB7, and PTB7-Th. We show that fullerene photo-oxidation can be a primary mechanism dominating the degradation of fullerene-based opto-electronic devices. The highly photoactive nature of fullerenes and strong correlation to device performance suggest that fullerene photo-oxidation must be taken into account in the choice of processing route for fullerene-based electronic devices. The methodology presented here could readily be applied to probe specific degradation pathways in other OPV systems, such as those containing alternative acceptors.

Results

Impact of fullerene photo-oxidation on OPV devices behaviour. We investigated the decrease in performance due to degradation of bulk-heterojunction OPV devices upon exposure to light and oxygen. Previous studies concluded that light and/or oxygen exposure of un-encapsulated devices resulted in rapid device degradation due to diffusion and subsequent reaction of molecular oxygen with the polymer component of the active layer materials.[3] Figure 1(a) shows the evolution of current density-voltage (*J*-*V*) characteristics of typical PCDTBT:PCBM devices having undergone different exposure durations to AM1.5G conditions in air (see also Supplementary Table 1). Exposure prior to electrode deposition allowed the experiments to focus on the underlying kinetics of the PCDTBT:PCBM photo-oxidation independent of lateral oxygen diffusion kinetics; it has previously

been shown that for devices with an oxygen blocking top contact, lateral oxygen diffusion kinetics can extend over days.[23,24] It is striking that only 10 minutes of light exposure result in an overall PCE loss of over 40%, due to simultaneous drops in short-circuit current density (J_{sc}), open-circuit voltage (V_{oc}) and fill factor (FF). After 60 minutes of exposure, a PCE loss of over 70% is seen. Devices exposed to air in the dark show similar performance to the fresh devices (Supplementary Fig. 1 and Table 2), indicating that the degradation process is driven by the combination of light and oxygen. The above experiments were repeated using different interlayers of different polarity (MoO3 and ZnO as well as PEDOT:PSS) underneath the active layer. The results (Supplementary Fig. 2) show similar trend to that in Figure 1(a).

To identify and quantify which photo-oxidised compounds are formed upon degradation, ultraviolet–visible (UV-vis) spectroscopy and matrix-assisted laser desorption/ionization time-of-flight (MALDI-TOF) mass spectrometry were carried out. Degraded blend films were fabricated and exposed in the same way as the films used for the devices in Figure 1(a). No obvious photo-bleaching of the blend films was observed within the timescale studied (Supplementary Fig. 3). The samples for MALDI-TOF measurements were prepared by re-dissolving the blend films after photochemical degradation. By comparing Figure 2(a) with 2(b) it is seen that photo-oxidised PCBM species (with up to 4 oxygen atoms) were formed upon 60 minutes of AM1.5G exposure in air in the blend film with PCDTBT. The degree of oxidation is further increased with exposure duration (up to 7 oxygen atoms after 10 hours) as is seen in figure 2(c). An analysis of the ^{12}C-isotopic peak areas reveals a total of 0.8% oxidised PCBM in the blend film after 1 hour of aging. This is further increased to 4.3% after 10 hours of aging. It thus appears that PCBM can be readily photo-oxidised upon exposure to light and oxygen of unprotected blend films of PCBM with conjugated donor polymers.

Although this study is focussed on the photostability of PCBM in particular, it is relevant to a number of other fullerene materials. As shown in Supplementary Fig. 4, a similar photoxidation process leads to similar or higher concentration of oxidised fullerenes for other derivatives of C_{60} including the bis-adducts of PCBM and the indene derivative fullerene. The sensitivity of C_{60} derivatives to oxidation is

consistent with the finding of Silva et al. that reactivity of fullerenes increases with reducing pyramidalisation angle (i.e. with increasing curvature).[25] In accordance with this we find a lower sensitivity of $PC_{71}BM$ to the same oxidation procedure, indicating that whilst a variety of fullerene derivative are readily oxidised, the chemical structure and shape of the fullerene influence its tendency to oxidise.

To isolate the impact of PCBM photo-oxidation alone (rather than degradation of the polymer) on the performance of OPV devices, we prepared blends of PCDTBT using PCBM that had been separately photo-oxidised in solution. Figure 1(b) shows the current density-voltage characteristics of these devices (see also Supplementary Table 3). The aged PCBM species were also analysed by MALDI-TOF to estimate the fraction of oxidised PCBM as shown in figure 2(d). A PCBM solution exposed to AM1.5G illumination in air for 72 hours contained 3.6% of oxidised PCBM (O-PCBM). Different amounts of degraded PCBM solution were mixed with a fresh PCBM solution to control the fraction of O-PCBM in the fullerene phase of blends with PCDTBT. The total concentration of fullerene (PCBM + O-PCBM) in the blend films was kept constant. Markedly, with only 1% of oxidised PCBM in the fullerene phase a 65% loss in device PCE was observed, which increased to ~ 90% loss with only 3.6% of O-PCBM. From this it is clear that the photo-oxidation of PCBM, even at low levels, has a significant impact on the performance of OPV devices. Figure 1(c) compares the PCE of devices where the PCDTBT:PCBM films had been exposed to AM1.5G illumination in air and PCDTBT:PCBM devices fabricated using different fractions of O-PCBM. Device PCEs are plotted against the fraction of O-PCBM in the active layer, measured by MALDI-TOF by removing and analysing the active layers. The drop in performance of photo-oxidised PCDTBT:PCBM blends quantitatively matches that of the devices made using O-PCBM. To investigate the generality of this effect, we extended our studies to other benchmark OPV systems, namely P3HT:PCBM, PTB7:PCBM, and PTB7-Th:PCBM blends, which exhibited qualitatively similar effects (Supplementary Fig. 5). It is thus apparent that PCBM photo-oxidation has a drastic impact on the performance of these benchmark OPV systems.

To establish the microscopic mechanism of device performance degradation, we explore the nature of the chemical defects formed upon photo-oxidation, and their effect on charge transport and recombination. As we demonstrate in the following, the insight provided by our study allows us to qualitatively reproduce the observed device behaviour under illumination as shown in Figure 1(d), through simulations, by accounting for deteriorated electronic transport upon PCBM degradation.

Possible mechanisms of fullerene photo-oxidation. The effect of photo-oxidation on the highest occupied molecular orbital (HOMO) and lowest unoccupied molecular orbital (LUMO) levels of PCBM was explored using electronic structure calculations of the products of oxidation, namely PCBM bearing epoxide, diol and carbonyl defects, following the oxidation mechanism reported by Xiao *et al.* as shown in Figure 2(e).[15] For each defect type, we identified all isomers with defects across 6-6 carbon bonds (i.e. two 6 membered rings together) and then calculated HOMO and LUMO energies as well as the total energy of the species using the delta self-consistent field (delta-SCF) method (see Methods section and Supplementary Table 4). Several oxidised species with multiple defects (e.g. two epoxides) and complex defect structures (e.g. two different defects) were included in the study for completeness. To check sensitivity of results to calculation method, the HOMO and LUMO levels were also estimated using Kohn-Sham and time-dependent density functional theory (TD-DFT) methods (Supplementary Table 5 and Table 6). For each method, the differences in HOMO and LUMO energies of any specific O-PCBM isomer relative to those of pristine PCBM were similar.

For each defect type, we calculated average HOMO and LUMO energies by including different isomers in proportion to their thermodynamic probability of occurrence, calculated from the total energy for the neutral species in a Boltzmann average (Supplementary Table 7). The oxidised PCBM species with the lowest total energy tend to have defects close to the phenyl butyric acid methyl ester side-chain; examples are shown by the molecular structures in Figure 2(e). The LUMO is depressed for almost all oxidised PCBM species as shown in Figure 2(e) (and Supplementary Table 4-6 for full data set), especially in the case of carbonyl defects. In contrast, the effect on the HOMO is

small in all cases, except for the diol defect. Therefore, we expect the oxidation to affect electronic transport by introducing trap states for electrons, and to have a stronger effect on electron transport than on hole transport in the PCBM phase.

From Figure 2(e) it is evident that, given the electron transport in a blend film takes place in the PCBM phase, the lower LUMO energies of the oxidised molecules will cause electron trapping. The distribution of electron trap states may be expected to extend deep (several tenths of an eV) into the band gap. The shape of the total density of trap states is difficult to predict, since the incidence of different defect types in practice is not known. However, the epoxide and carbonyl species would most likely give rise to both a broadening of the LUMO energies around an energy close to the LUMO of pristine PCBM as well as some deeper electron traps. Additionally, the overall density of defect states will increase with degradation.

Effects of fullerene oxidation on charge transport kinetics in neat PCBM films. To quantify the impact of photodegradation on electron transport we performed space-charge-limited current (SCLC) measurements on electron-only devices with structure (ITO/TiO_2/PCBM:O-PCBM/Ca/Al) made from PCBM solutions with different weight fractions of O-PCBM (0%, 0.2%, 0.9%, 1.8% and 3.6%). Effects of varying device thickness were minimised by comparing devices with approximately the same thickness of 70-80 nm. Representative current density – voltage curves in Supplementary Fig. 7 show that the current density at a given applied voltage drops significantly with increasing fraction of photo-oxidised PCBM in the film. Also shown in Supplementary Fig. 7 are calculated J-V curves obtained by fitting the results of a drift-diffusion model that incorporates charge trapping to the experimental SCLC data.[26] The model of the density of states (DoS) used for these fits consists of a narrow Gaussian distribution of N_t traps states per volume centred around an energy level lying E_t below the conduction band transport level, together with a band electron mobility, μ_0.[27,28] Electrons are trapped and released by the sub-band-gap states according to a multiple-trapping model. Since only a single carrier type is present in SCLC measurements, recombination is negligible in these

simulations. The parameters N_t, E_t, μ_0 and the electron injection barrier are varied to obtain the best fit for each device at each level of degradation. (See Methods for further details). The model of a Gaussian distribution of traps was selected in preference to an exponential tail of states or a more complex DoS with multiple features because it provided the best fit to the data with the fewest fitting parameters. Figure 3(a), (b), and (c) show the obtained values of μ_0, N_t, and E_t, respectively for different fractions of O-PCBM using a large set of nominally identical devices in each case. Note that the range of fitted parameters increases with degradation, due to the microstructural variations inherent in the degradation process.

Figure 3(a) shows that the band mobility obtained by this fitting drops by approximately one order of magnitude when the fraction of O-PCBM is increased from 0% to 3.6% (mobility values are taken as the statistical average of a range of repeated runs of fabrication and measurement for each level of O-PCBM studied). At the same time, the density of traps increases by around an order of magnitude. For less degraded samples the trap level lies around 0.2 eV below the transport level of PCBM, while for higher O-PCBM concentrations the trap level and transport level are seen to approach each other as shown in Figure 3(c), although the sample-to-sample variation in the extracted trap depth becomes large. The barrier for charge injection was found to be insensitive to degradation at around 0.3 eV (Supplementary Fig. 7(f)). The SCLC results are consistent with the formation of both shallow and deep states below the LUMO of the PCBM, as expected from the quantum chemical calculations discussed in the previous section. The shallow states would serve both to push down the effective transport level and to reduce the 'band' mobility. This is illustrated schematically in Figure 3(d).

By accounting for the data calculated in the SCLC analysis, we were able to reproduce the qualitative trend in current-voltage response under solar illumination of devices with increasing fraction of O-PCBM (Figure 1d). We used the parameters obtained from SCLC for the DoS and band electron mobilities of the pristine, 1.8% degraded and 3.6% degraded films to represent the cases of fresh, partly and fully degraded films, respectively, and included band-to-band ($R_{direct} = 2.2 \times 10^{-20}$ m^3s^{-1}) and band-to-trap recombination, governed by the electron and hole densities along the capture and

emission rate coefficients for electrons and holes (which were all set to the same value, $C_0^- = C_+^- = C_0^+ = C_-^+ = 10^{-16}$ m^3s^{-1}), as well as series and shunt resistances (R_S = 4 Ω cm^2 and R_P = 1.9 kΩ cm^2, respectively). Our modelling strategy was to choose the recombination coefficients, parasitic resistances and hole mobility to best fit the J-V curve of the fresh device, and then modify only the parameters relating to electron transport (i.e., the electron band mobility, trap density and position of the electron transport level relative to the trap level) according to the values obtained from the SCLC analysis for different levels of degradation. In this way, we could reproduce the trend in current-voltage sweeps observed in the real devices, specifically, the losses in V_{oc}, J_{sc} and fill factor with increasing O-PCBM content. The effect of degradation modelled this way is less severe than that observed experimentally. This could arise either from the variation in the electronic effect of a given fraction of O-PCBM (evident from the scatter in SCLC device behaviour at high levels of degradation) or from neglect of the impact of O-PCBM on another, secondary quantity, for example on hole mobility. Nevertheless, the qualitative reproduction of the trend in all parameters corroborates the link between traps and device performance.

Effects of fullerene oxidation on blend film recombination and transport kinetics. In order to further understand the effect of fullerene oxidation on device performance, particularly on V_{oc}, charge-carrier densities and lifetimes were measured by transient photocurrent (TPC), transient photovoltage (TPV) and charge extraction (CE) measurements. The measured charge-carrier density at open circuit, as a function of device V_{oc} under increasing illumination intensity, is plotted in Figure 4(a)**.** Figure 4(b) shows the charge carrier lifetimes measured as a function of these charge-carrier densities*,* under the same illumination conditions. As it can be observed in Figure 4(a), in all devices the charge density rises with V_{oc} approximately exponentially, consistent with the presence of a tail of states in the band gap. We also note that these density of states curves are shifted substantially to lower energy with increasing fraction of O-PCBM: for a given charge-carrier density of 4.3 × 10^{16} cm^{-3}, for example, the energetic differences are ≅ 140 mV between the devices with 0% and 0.4% O-PCBM, and ≅ 130 mV between those with 0.4% and 1% O-PCBM. Therefore, in order to achieve the

same electron quasi-Fermi level position and therefore the same V_{oc}, much more charge has to be injected in the devices with O-PCBM, due to the deeper distribution of states within the band gap. Figure 4(d) shows, for comparison, the charge carrier density – V_{oc} behaviour expected for the DoS parameters for differently degraded devices obtained by modelling the devices with the same set of parameters obtained from SCLC analysis and used to model the J-V curves in Fig. 1(d) above. The approximately exponential form of the $n(V_{oc})$ curves and the shift to lower V_{oc} with degradation are reproduced, supporting the idea that the changes in transport and density of states both arise from the introduction of electron trap states.

Figure 4(b) shows that the devices with higher O-PCBM fractions exhibit longer charge lifetimes at fixed charge density. Longer charge-carrier lifetimes are consistent with increased trapping in localized states, which can slow down recombination at a given charge density by reducing the rate at which charge carriers meet. The V_{oc} values calculated from these two opposing effects, i.e. longer lifetimes and higher density of sub-gap states with increasing O-PCBM fraction, match well the measured V_{oc} values at varying illumination intensity as shown in Figure 4(c) (see Supplementary Information for the mathematical background), consistent with this analysis. The introduction of electron trap states results in slower recombination at fixed charge density but that does not benefit V_{oc} because a higher charge density (which leads to faster recombination) is needed to achieve the same quasi-Fermi level separation.

TPV measurement provides information on the total recombination in a device, but cannot discriminate between different mechanisms, such as band-to-band, trap mediated or surface recombination. A first indication of the dominant recombination mechanism comes from the ideality factors measured from the dependence of V_{oc} on light intensity [Figure 4(c)]. The ideality factors are related to the reaction order of recombination such that n_{id} tends to increase from $\cong 1$ to $\cong 2$ either when recombination becomes stronger in the bulk of the active layer compared to its interfaces with the electrodes, or when the recombination involves deeper trap states in the band gap.[29] Here, the

increase in n_{id} with O-PCBM fraction indicates that the recombination mechanism changes with increasing oxidation. Both scenarios (more bulk traps and deeper traps) are consistent with the n_{id} behaviour. The same trends found in devices containing O-PCBM were found in devices prepared from blends degraded as films, as seen in Supplementary Fig. 8, eliminating electrode degradation as the cause of the change in TPV behaviour.

Finally, charge extraction measurements carried out at short circuit (rather than at open circuit as above), allow us to assay the average (combining electron and hole) charge-carrier mobility in the OPV devices. The mobility inferred from these charge extraction data decreased with increasing fraction of O-PCBM (Supplementary Fig. 9), consistent with increased carrier trapping and in qualitative agreement with the SCLC data discussed above. The magnitude of the reduction of mobility upon degradation is lower than obtained by SCLC, however the mobility estimated from charge extraction includes hole mobility, which should be less affected by fullerene oxidation.

Electroluminescence analysis of the effect of fullerene photooxidation on voltage losses. As a complementary probe of the effect of degradation on blend DoS we characterised the series of PCDTBT:(PCBM:O-PCBM) devices using electroluminescence (EL) and sub-band gap external quantum efficiency (EQE) measurements. Shown in Figure 5a are normalised EL spectra for fresh and degraded devices. The peak at ≅ 1.2 eV is assigned to radiative decay of the charge-transfer state at the PCDTBT:PCBM interface, in agreement with previous measurements.[30] Control experiments on pure PCDTBT or PCBM confirmed that the emission did not arise from band-to-band recombination from either species (Supplementary Fig. 10). The emission of the charge-transfer state is shifted to slightly lower energies in samples containing increasing fractions of O-PCBM, and its quantum yield decreases (higher injection current is required to obtain a detectable emission). The lower emission efficiency observed in devices with oxidised PCBM is consistent with both poorer transport and a higher degree of non-radiative recombination compared to radiative recombination.

Also shown in Figure 5(a) are sub-band gap EQE spectra, obtained by combining measured EQE with the measured EL spectra, using a detailed balance approach (for devices containing other fractions of O-PCBM see Supplementary Fig. 11).[31] The presence of an increasing fraction of charge-transfer states with lower energy than in fresh blends is evident from the decreasing slope of the sub-band-gap EQE curves, which indicates that the contribution to EQE of the sub-band-gap density of states becomes more pronounced with increasing O-PCBM fraction.

From the sub-band-gap EQE data we were able to calculate the V_{oc} that could theoretically be obtained if the only loss mechanism was radiative recombination ($V_{oc,rad}$) following a previously reported approach.[31] This value is normally lower than the V_{oc} in the Shockley–Queisser limit for single junction solar cells because of the non-step-like absorption profile of practical devices such as these. The difference between the resulting radiative-limit $V_{oc,rad}$ and the measured V_{oc} can be assigned to non-radiative recombination losses ($\Delta V_{oc,non\text{-}rad}$). Shown in Figure 5(b) are the contributions to V_{oc} losses. The relative size of the $\Delta V_{oc,non\text{-}rad}$ component for different devices in a series should reflect the degree of non-radiative recombination, as described above, for devices with different fractions of O-PCBM. The losses due to non-radiative recombination clearly increase with increasing fraction of O-PCBM, consistent with the formation of sub-band gap trap states that slow down carrier collection and increase the overall likelihood of non-radiative recombination. (See Supplementary Table 8 for all the V_{oc} values.) These results are in good agreement with the clear increase in trap-mediated recombination inferred from the ideality factors (Figure 4(c)).

Discussion

Environmental stability has become a primary concern for the realisation of low-cost manufacture of opto-electronic devices using approaches that typically involve air processing and minimal encapsulation. Despite the significant amount of research effort, the origin of the limited environmental stability of devices such as polymer:fullerene solar cells remains unclear. It is

recognised that different stress factors (oxygen, water, heat) are involved and that different components of the device are vulnerable (semiconductors, interlayers electrodes) but few studies unambiguously relate particular chemical degradation mechanisms to their impact on electrical performance. Whilst substantial research efforts have addressed the photochemical and photophysical stability of conjugated donor polymers ,[1,3,5,32] the environmental stability of fullerenes and their impact on device performance have received relatively little attention.[16-19] A further consideration is that in most studies to date the chemical nature of defects is not identified and so the precise relationship between degradation mechanism and device behaviour cannot be explored. Here, we used a systematic study of the impact of fullerene oxidation on solar cell performance to demonstrate that common products of the photo-oxidation of PCBM, specifically fullerene epoxides and carbonyls, act as electron traps in OPV devices. Whilst prior studies had shown that epoxides[21] and other oxygenic defects[15,25] were expected to form on fullerenes, and that in practice oxygen exposure changes the electronic structure of fullerenes[16] with impact on device performance,[17] the link between chemical nature of such defects and electrical properties of devices had not previously been investigated. Previous approaches to simulate the effect of degradation have typically addressed the effect on photocurrent collection of oxidative p-doping of the active layer,[33,34] or invoked trap states to explain changes in electrical response,[35-37] but without a clear origin for those defects. In this work, we have established a quantitative relationship between the presence of specific oxidative defects which act as electron traps and the resulting change in electronic properties of the OPV devices made from the oxidised fullerene. Specifically, electron mobility, charge lifetime and density of states measurements are all consistent with the presence of a distribution of electron trap states centred around 0.2 eV below the conduction band edge, which increases with fraction of oxidised fullerene. Shallow traps in this energy range have been previously observed in PCBM without any intentional degradation.[38] By using a device model to account for the effect of these trap states on charge carrier densities, electron transport and recombination, we could show how the introduction of oxidised PCBM causes losses in device open-circuit voltage,

short-circuit current and fill factor. More generally, this study demonstrates, at least for similar systems, that when the chemical mechanism of degradation, or the degradation products, are known, we can, in principle, predict the consequences for electronic processes.

Interestingly, we have found that even exposure to low light conditions, typical of laboratory environments, is sufficient to drive the photo-oxidation of fullerenes in polymer:fullerene solar cells, corroborating previous studies on fullerene films (Supplementary Fig. 1).[16] This observation suggests that inadvertent exposure to light and oxygen during sample preparation and characterisation (e.g. optical measurements) is as problematic as illumination of the device under operation. Finally, the results reported herein suggest that PCBM, one of the most commonly used fullerene derivatives in the community to date, may not be an ideal candidate for the commercialisation of stable opto-electronic devices due to their intrinsic instability. Alternative small-molecular acceptor materials, which do not undergo epoxide formation so readily as fullerenes, could be good candidates to extend the lifetime of organic solar cells. Preliminary studies suggest that photodegradation is slower using some non-fullerene acceptors,[39] but more detailed studies are needed. Our findings thus highlight the importance of developing alternative electron accepting/transporting materials with improved photochemical stability. Our findings are also relevant for stability of perovskite devices, where PCBM is commonly used as an electron collecting interlayer.[40]

It should be re-iterated that the degradation of organic solar cells involves multiple concurrent pathways, typically induced by different environmental stress factors. In order to achieve overall environmental stability of organic solar cells, all of these degradation mechanisms need to be identified and addressed. While the work presented here demonstrates the important role of fullerenes in the environmental stability of organic solar cells, the development of environmentally stable donor materials, interlayers and electrodes are of equal importance in addressing the stability challenge of organic electronic devices.

Methods

Materials. PCDTBT was purchased from 1-Materials. All fullerene were purchased from Solenne BV. Chlorobenzene (CB), zinc acetate dihydrate, 2-methoxyethanol, and ethanolamine were purchased from Sigma Aldrich. MoO_3 was purchased from Strem Chemicals. All materials were used as received.

Device fabrication. ITO glass substrates were cleaned sequentially with Hellmanex detergent, deionized water, acetone, and isopropyl alcohol in ultrasonic bath. Poly(3,4-ethylenedioxythiophene)-poly(styrenesulfonate), Heraeus Clevios P VP AI 4083, (PEDOT:PSS) or ZnO precursor solution (109.8 mg of zinc acetate dihydrate dissolved in 1 ml of 2-methoxyethanol and 30.2 µl of ethanolamine) was spin-coated on plasma treated ITO substrates at 4000 rpm for 40 s, followed by thermal annealing at 150 ^{o}C for 10 minutes. For the devices using MoO_3 as the interlayer, 10 nm of MoO_3 was thermally evaporated on the ITO coated glasses under vacuum of 2×10^{-5} mbar. PCDTBT and PCBM (1:2) were co-dissolved in CB at 60 °C and stirred at 1300 rpm with a total concentration of 18 mg/ml for over 12 hours in nitrogen filled glovebox. The blend solution was spin-coated on PEDOT:PSS, MoO_3, or ZnO coated substrates in air, resulting in active layers with a thickness of ~70nm. Finally, 30 nm of calcium and 100 nm of aluminium (or 10 nm of MoO_3 and 100 nm of silver for ZnO device) were thermally evaporated on the blend layer under vacuum of 2×10^{-5} mbar, defining active area of 0.15 cm^2. The devices were encapsulated by glass slides using epoxy in nitrogen filled glovebox prior to measurement. Current density–voltage (*J*–*V*) characterizations were performed by a Keithley 2400 sourcemeter under AM1.5G illumination, Newport 92193A-1000 solar simulator with a light intensity of 90 mW/cm^2.

Degradation. PCDTBT:PCBM films fabricated on PEDOT:PSS coated ITO glass substrates were degraded under AM1.5G illumination in dry air (relative humidity ~30%) for different periods of time mentioned in the main text. PCBM solution for selective degradation study was prepared by dissolving PCBM (24 mg) in CB (1 ml) in a 15 ml vial at 60 °C with stir speed of 1300 rpm in a nitrogen filled glovebox for at least 12 hours. The vial of PCBM solution was then filled with air and degraded under AM1.5G illumination with stir speed of 300 rpm for 72 hours in air.

MALDI-TOF measurements. All samples were dissolved in chlorobenzene at an approximate concentration of 1mg/mL. MALDI matrix trans-2-[3-(4-tert-butylphenyl)-2-methyl-2-propenylidene]malononitrile (DCTB) was purchased from Insight Biotechnology Ltd. (Wembley, U.K.), and dissolved in chlorobenzene at 20mg/mL. Solutions of sample and matrix were mixed together so the matrix is in ~250-1000 fold molar excess, typically 1µL of sample to 49µL of matrix. 0.5 µL of each of these mixture solutions for each sample was spotted onto the MALDI plate and dried in air. MALDI-TOF spectra were acquired in negative-reflectron mode using an ultrafleXtreme mass spectrometer (Bruker Daltonics, Bremen, Germany), which is equipped with a Smartbeam-II Nd:YAG laser (λ = 355 nm). Data was acquired using flexControl software v3.4, while post-acquisition processing of data was performed by flexAnalysis software v3.4. PCBM and oxidised analogues were observed as negative radical ion species ($M^{-\bullet}$). Relative semi-quantitative analyses were done via Microsoft Excel.

DFT calculations. We performed single point energy calculations on optimised structures in Gaussian09 for *N, N+1* and *N-1* electron systems. The HOMO (and LUMO) levels are then found by computing the difference between total energy for the *N* electron system with the *N-1* (*N+1*) system. All calculations were done at the B3LYP level of theory with the 6-31g* basis set.[41]

Electroluminescence. EL was measured using a spectrograph (Andor Shamrock 303) combined with a InGaAs photodiode array (Andor iDUS 491) cooled to -90 °C, calibrated with a Bentham CL2 quartz halogen lamp with known emission spectrum. EL spectra were collected at injection current densities up to 100 mA/cm^2, on at least 4 devices for each fraction of O-PCBM.

External quantum efficiency. EQE was measured using a grating spectrometer (CVI DIGIKROM 240) to create monochromatic light combined with a tungsten halogen light source. The monochromatic light was modulated at 290 Hz with a chopper, and a Stanford Research Systems SR380 lock-in amplifier, with an internal transimpedance amplifier of 106 V/A, was used to detect the photocurrent. Long pass filters at 780 and 850 nm were used to filter out the scattered light from

the monochromator. The spectra were taken from 300 to 1000 nm and calibrated by a silicon photodiode.

Electron only devices. glass substrates containing a predefined layer (≈ 70 nm) of indium doped tin oxide (ITO) were ultrasonicated in an acetone bath, and subsequently in an IPA bath, for 10 minutes, respectively. The substrates were dried using nitrogen. Titanium dioxide (TiO_2) films were deposited onto the ITO by spin coating of a precursor solution containing 70 µL titanium isopropoxide, 55 µL ethanolamine and 1 mL 2-methoxyethanol. The substrates were sintered in an oven for 1 hour at 500 °C. The resulting TiO_2 film is approximately 20 nm think. The pre-degraded PCBM was spun onto the substrates with a target film thickness of around 80 nm. The back contact was applied by thermal annealing under high vacuum ($< 5 \cdot 10^{-6}$ Torr). Calcium (Ca) was evaporated at a rate 1 Å/s with a final thickness of around 30 nm. A thick layer of aluminium was subsequently evaporated at a rate of 20 Å/s with a resulting layer thickness of 150 nm. The resulting electron-only device had the following device architecture: glass/ITO/TiO_2/PCBM/Ca/Al. The devices were stored and measured under inert atmosphere (N_2) and in the dark.

SCLC measurements. The current density-voltage (*J–V*) curves were recorded using a source measurement unit (SMU) using a slow scan rate to ensure that the device was in a steady-state condition. J-V curves were recorded in both forward (0 → 5V) and in reverse (0 → -5 V) bias. Since no difference in the magnitude or the shape of the current was observed irrespective of bias polarity, the presence of built-in voltages across the device can be ruled out. The J-V curves were analysed using a commercially available drift-diffusion solver called Advanced Semiconductor Analysis (ASA). The software uses a multiple trapping-release model which assumes that all charge carriers must be released from charge traps to the transport level in order to contribute to the current. Traps were modelled using a Gaussian distribution of states below the conduction band edge, where we allowed for the Gaussian density and the trap level to vary while the Gaussian standard deviation was set to

0.1 eV. To fit the experimental *J–V* curves with the model we allowed the trap density, trap depth, electron band mobility and barrier for electron injection to vary simultaneously.

References

1 Kawano, K. *et al.* Degradation of organic solar cells due to air exposure. *Sol. Energy Mater. Sol. Cells* **90**, 3520-3530 (2006).

2 Ahmed, R., Simbrunner, C., Schwabegger, G., Baig, M. A. & Sitter, H. Air stability of C60 based n-type OFETs. *Synth. Met.* **188**, 136-139 (2014).

3 Jørgensen, M., Norrman, K. & Krebs, F. C. Stability/degradation of polymer solar cells. *Sol. Energy Mater. Sol. Cells* **92**, 686-714 (2008).

4 Cui, Y. *et al.* Fine-Tuned Photoactive and Interconnection Layers for Achieving over 13% Efficiency in a Fullerene-Free Tandem Organic Solar Cell. *J. Am. Chem. Soc.* **139**, 7302-7309 (2017).

5 Jørgensen, M. *et al.* Stability of Polymer Solar Cells. *Adv. Mater.* **24**, 580-612 (2012).

6 Emmott, C. J. M. *et al.* In-situ, long-term operational stability of organic photovoltaics for off-grid applications in Africa. *Sol. Energy Mater. Sol. Cells* **149**, 284-293 (2016).

7 Soon, Y. W. *et al.* Correlating triplet yield, singlet oxygen generation and photochemical stability in polymer/fullerene blend films. *Chem. Commun. (Cambridge, U. K.)* **49**, 1291-1293 (2013).

8 Distler, A. *et al.* Effect of PCBM on the Photodegradation Kinetics of Polymers for Organic Photovoltaics. *Chem. Mater.* **24**, 4397-4405 (2012).

9 Rao, A. M. *et al.* Photoinduced Polymerization of Solid C_{60} Films. *Science* **259**, 955-957 (1993).

10 Eklund, P. C., Rao, A. M., Zhou, P., Wang, Y. & Holden, J. M. Photochemical transformation of C_{60} and C_{70} films. *Thin Solid Films* **257**, 185-203 (1995).

11 Heumueller, T. *et al.* Morphological and electrical control of fullerene dimerization determines organic photovoltaic stability. *Energy Environ. Sci.* **9**, 247-256 (2016).

12 Distler, A. *et al.* The Effect of PCBM Dimerization on the Performance of Bulk Heterojunction Solar Cells. *Adv. Energy Mater.* **4**, 1300693 (2014).

13 Li, Z. *et al.* Performance enhancement of fullerene-based solar cells by light processing. *Nat. Commun.* **4:2227** (2013).

14 Piersimoni, F. *et al.* Influence of fullerene photodimerization on the PCBM crystallization in polymer: Fullerene bulk heterojunctions under thermal stress. *J. Polym. Sci. Part B: Polym. Phys.* **51**, 1209-1214 (2013).

15 Xiao, Z. *et al.* Synthesis of [59]Fullerenones through Peroxide-Mediated Stepwise Cleavage of Fullerene Skeleton Bonds and X-ray Structures of Their Water-Encapsulated Open-Cage Complexes. *J. Am. Chem. Soc.* **129**, 16149-16162 (2007).

16 Anselmo, A. S., Dzwilewski, A., Svensson, K. & Moons, E. Photodegradation of the electronic structure of PCBM and C60 films in air. *Chem. Phys. Lett.* **652**, 220-224 (2016).

17 Hansson, R. *et al.* Photo-degradation in air of the active layer components in a thiophene-quinoxaline copolymer:fullerene solar cell. *Phys. Chem. Chem. Phys.* **18**, 11132-11138 (2016).

18 Yamane, S. *et al.* Photooxidation studies on indene-C60 adducts. *Sol. Energy Mater. Sol. Cells* **143**, 135-140 (2015).

19 Matsuo, Y. *et al.* Deterioration of bulk heterojunction organic photovoltaic devices by a minute amount of oxidized fullerene. *Chem. Commun. (Cambridge, U. K.)* **48**, 3878-3880 (2012).

20 Volonakis, G., Tsetseris, L. & Logothetidis, S. Impurity-related degradation in a prototype organic photovoltaic material: A first-principles study. *Org. Electron.* **14**, 1242-1248 (2013).

21 Reese, M. O. *et al.* Photoinduced Degradation of Polymer and Polymer–Fullerene Active Layers: Experiment and Theory. *Adv. Funct. Mater.* **20**, 3476-3483 (2010).

22 Peters, C. H. *et al.* High Efficiency Polymer Solar Cells with Long Operating Lifetimes. *Adv. Energy Mater.* **1**, 491-494 (2011).

23 Jeranko, T., Tributsch, H., Sariciftci, N. S. & Hummelen, J. C. Patterns of efficiency and degradation of composite polymer solar cells. *Sol. Energy Mater. Sol. Cells* **83**, 247-262 (2004).

24 Shoaee, S. & Durrant, J. R. Oxygen diffusion dynamics in organic semiconductor films. *J. Mater. Chem. C* **3**, 10079-10084 (2015).

25 Silva, H. S., Cresson, J., Rivaton, A., Bégué, D. & Hiorns, R. C. Correlating geometry of multidimensional carbon allotropes molecules and stability. *Org. Electron.* **26**, 395-399 (2015).

26 Zeman, M. & Krc, J. Optical and electrical modeling of thin-film silicon solar cells. *J. Mater. Res.* **23**, 889-898 (2008).

27 Dacuña, J. & Salleo, A. Modeling space-charge-limited currents in organic semiconductors: Extracting trap density and mobility. *Phys. Rev. B* **84**, 195209 (2011).

28 Nicolai, H. T., Mandoc, M. M. & Blom, P. W. M. Electron traps in semiconducting polymers: Exponential versus Gaussian trap distribution. *Phys. Rev. B* **83**, 195204 (2011).

29 Kirchartz, T., Deledalle, F., Tuladhar, P. S., Durrant, J. R. & Nelson, J. On the Differences between Dark and Light Ideality Factor in Polymer:Fullerene Solar Cells. *J. Phys. Chem. Lett.* **4**, 2371-2376 (2013).

30 Faist, M. A. *et al.* Competition between the Charge Transfer State and the Singlet States of Donor or Acceptor Limiting the Efficiency in Polymer:Fullerene Solar Cells. *J. Am. Chem. Soc.* **134**, 685-692 (2012).

31 Yao, J. *et al.* Quantifying Losses in Open-Circuit Voltage in Solution-Processable Solar Cells. *Phys. Rev. Applied* **4**, 014020 (2015).

32 Nicolai, H. T. *et al.* Unification of trap-limited electron transport in semiconducting polymers. *Nat. Mater.* **11**, 882-887 (2012).

33 Seemann, A. *et al.* Reversible and irreversible degradation of organic solar cell performance by oxygen. *Solar Energy* **85**, 1238-1249 (2011).

34 Schafferhans, J., Baumann, A., Wagenpfahl, A., Deibel, C. & Dyakonov, V. Oxygen doping of P3HT:PCBM blends: Influence on trap states, charge carrier mobility and solar cell performance. *Org. Electron.* **11**, 1693-1700 (2010).

35 Khelifi, S. *et al.* Investigation of defects by admittance spectroscopy measurements in poly (3-hexylthiophene):(6,6)-phenyl C61-butyric acid methyl ester organic solar cells degraded under air exposure. *J. Appl. Phys.* **110**, 094509 (2011).

36 Lenes, M. *et al.* Electron Trapping in Higher Adduct Fullerene-Based Solar Cells. *Adv. Funct. Mater.* **19**, 3002-3007 (2009).

37 Pacios, R. *et al.* Effects of Photo-oxidation on the Performance of Poly[2-methoxy-5-(3′,7′-dimethyloctyloxy)-1,4-phenylene vinylene]:[6,6]-Phenyl C61-Butyric Acid Methyl Ester Solar Cells. *Adv. Funct. Mater.* **16**, 2117-2126 (2006).

38 Schafferhans, J., Deibel, C. & Dyakonov, V. Electronic Trap States in Methanofullerenes. *Adv. Energy Mater.* **1**, 655-660 (2011).

39 Baran, D. *et al.* Reducing the efficiency-stability-cost gap of organic photovoltaics with highly efficient and stable small molecule acceptor ternary solar cells. *Nat. Mater.* **16**, 363-369 (2017).

40 Correa-Baena, J.-P. *et al.* The rapid evolution of highly efficient perovskite solar cells. *Energy Environ. Sci.* **10**, 710-727 (2017).

41 Jones, R. O. & Gunnarsson, O. The density functional formalism, its applications and prospects. *Rev. Mod. Phys.* **61**, 689-746 (1989).

Author Contributions

Device fabrication and stability studies were carried out by H.K.H.L. and Z.L. MALDI-TOF measurements were carried out by M.F.W. DFT calculations were performed by B.R. EL measurements were performed by A.M.T., and sub-band gap EQE measurements were carried out by S.M.T. and A.D.C.M. SCLC measurements and *J–V* simulations were carried out by J.A.R. TPV and CE measurements were carried out by J.W. J.M., T.W., E.S. and S.P. contributed to sample preparation and device fabrication. H.K.H.L., J.R.D., A.M.T. and W.C.T. contributed to project planning and discussions. Z.L. and J.N. had the idea, led the project, and prepared the manuscript. All authors contributed to the manuscript preparation.

Acknowledgements

The authors would like to acknowledge the funding support from the Welsh Assembly Government funded Sêr Cymru Solar Project, and the National Research Network in Advanced Engineering and Materials, the European Commission's CHEETAH Project (FP7-Energy-2013- Grant no. 609788) and EPSRC grants EP/M025020/1 and EP/K030671/1. ZL thanks the Welsh Assembly Government Sêr Cymru II fellowship scheme, AMT thanks the Imperial College Junior Research Fellowship scheme, ADCM thanks CNPq-Brazil PDE fellowship (Grant 207507/2014-7), JAR thanks the EPSRC Doctoral Training Centre in Plastic Electronics (EP/G037515/1) and BR thanks the EPSRC Doctoral Training Centre in Theory and Simulation of Materials (EP/G036888/1) for funding.

Competing Financial Interests Statement

The authors declare no competing financial interests.

Figure legends

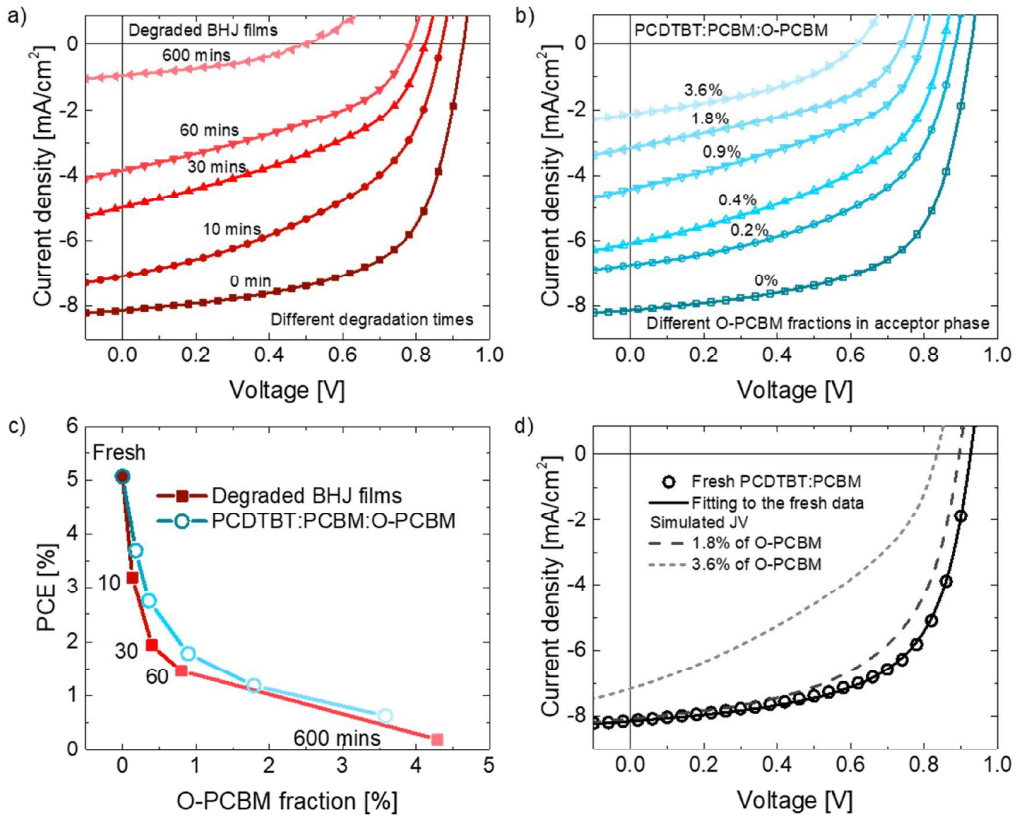

Figure 1 Impact of fullerene photo-oxidation on OPV devices behaviour. (a) Current density-voltage (*J-V*) characteristic of ITO/PEDOT:PSS/PCDTBT:PCBM (1:2)/Ca/Al devices with different degradation times under simulated AM1.5G illumination in air (the films were exposed to solar simulated light prior to back contact deposition); (b) *J-V* characteristic of PCDTBT:PCBM blend devices made with different fractions of degraded PCBM (the PCBM was degraded in solution prior to active layer processing), the percentages indicating the mass fraction of O-PCBM in the fullerene phase. All devices were encapsulated in nitrogen before characterisation. (c) PCE as a function of O-PCBM fraction for degraded PCDTBT:PCBM devices and pre-degraded PCBM devices; and (d) experimental (open circles) and simulated *J-V* characteristics for a device with pristine PCDTBT:PCBM (black); also simulated *J-V* characteristics for devices with increasing fraction of O-PCBM (dark grey dash line: 1.8 % and light grey short dash line: 3.6 %), reconstructed using the mobilities, trap energies and trap

densities obtained from the space-charge-limited current analysis (see Figure 3). Full device parameters are summarised in Supplementary Table 1 and Table 2.

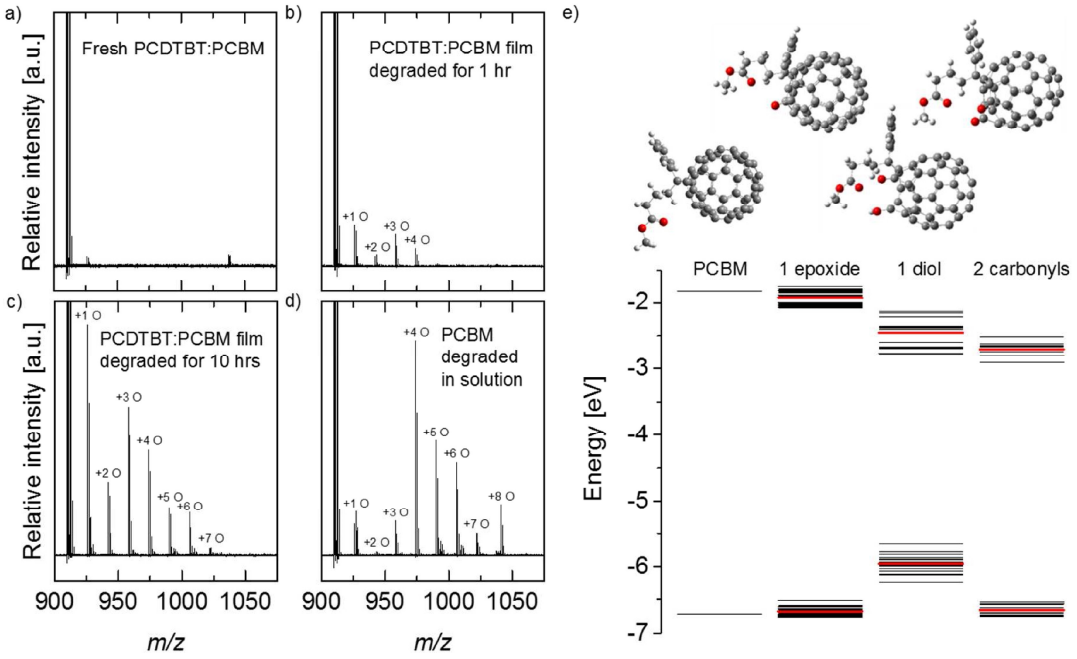

Figure 2 Possible mechanisms of fullerene photo-oxidation. Negative ion mode MALDI-TOF measurement of (a) fresh PCDTBT:PCBM blend films; PCDTBT:PCBM blend films degraded under one sun in dry air for (b) 1 hour and (c) 10 hours; and (d) PCBM degraded in solution under one sun in dry air for 72 hours (see Supplementary Fig. 6 for raw data). (e) From left to right: HOMO and LUMO energies (calculated using a delta-SCF method) for neat PCBM, PCBM with one epoxide, PCBM with one diol and PCBM with two carbonyls defects. The different energies correspond to different possible positions of the defects on the fullerene cage. Boltzmann averages, based on total energy calculations, are given by the red lines. The molecular structures of PCBM, and an example of each defect type, are shown above their corresponding energy level diagram.

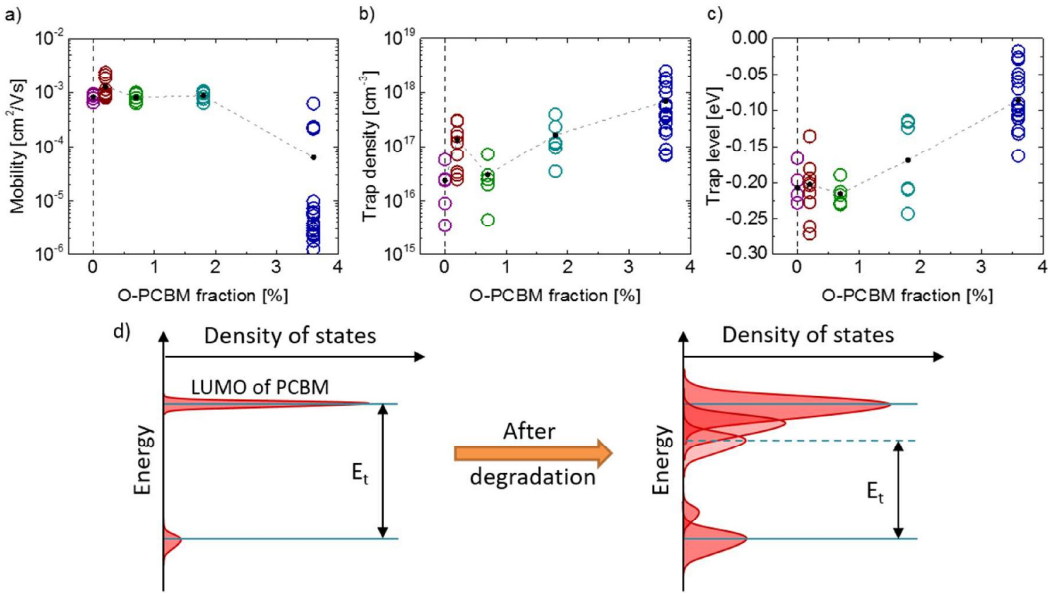

Figure 3 Effects of fullerene oxidation on charge transport kinetics in neat PCBM films. Parameters obtained from analysis of space-charge-limited current measurements for PCBM electron-only devices with increasing fractions of O-PCBM: (a) electron "band" mobilities; (b) density of deep (Gaussian) traps; (c) depth of trap level below the LUMO of the pristine PCBM. (d) Schematic illustrating how the density of electron states may evolve during photo-oxidation. A number of repeated studies of fabrication and measurement were performed due to increasing variations of the band mobility, trap density and trap levels with increasing O-PCBM fraction caused by more severe film irregularity.

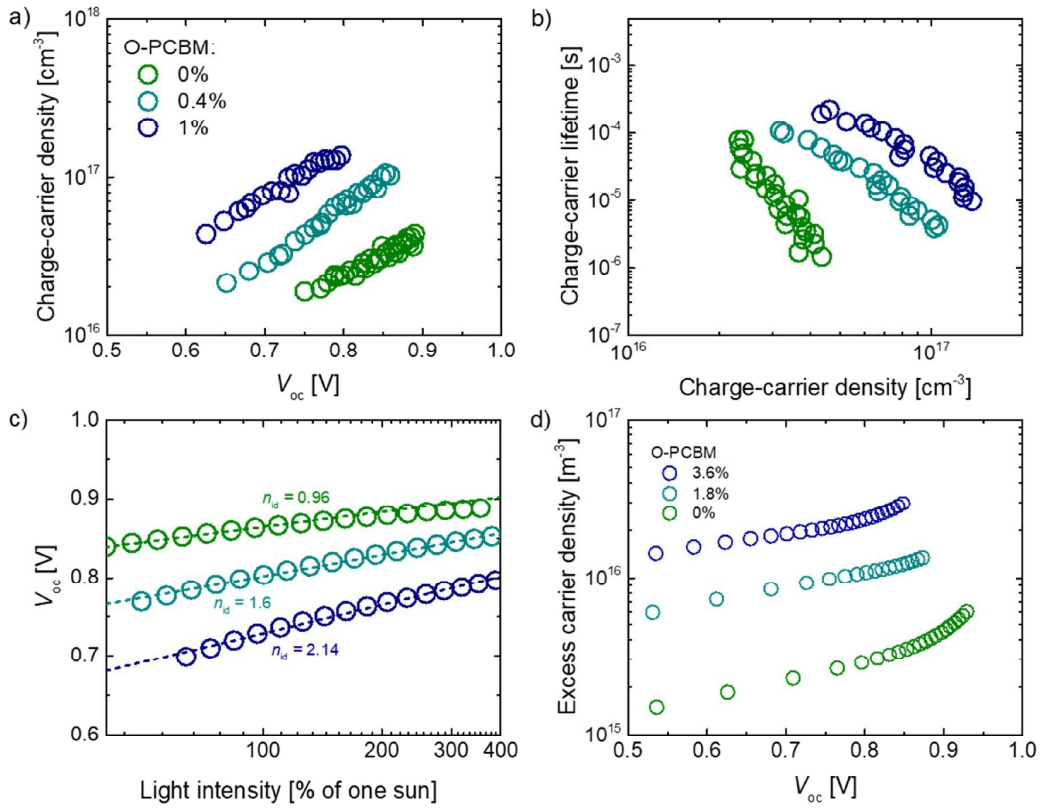

Figure 4 Effects of fullerene oxidation on blend film recombination and transport kinetics. CE,TPV and TPC analysis of PCDTBT:PCBM devices with increasing fraction of O-PCBM: (a) Charge-carrier density at varying V_{oc} (produced by varying the illumination intensity); (b) charge-carrier lifetimes at varying charge-carrier density [calculated from (a)]; (c) measured V_{oc} (open circles) at varying illumination intensities (the dashed lines indicate linear fits to the data); (d) simulated charge carrier density versus V_{oc} for different levels of degradation. Note that the devices under study exhibited high shunt currents under low illumination conditions (below 0.3 suns), and therefore those data were not included in the analysis.

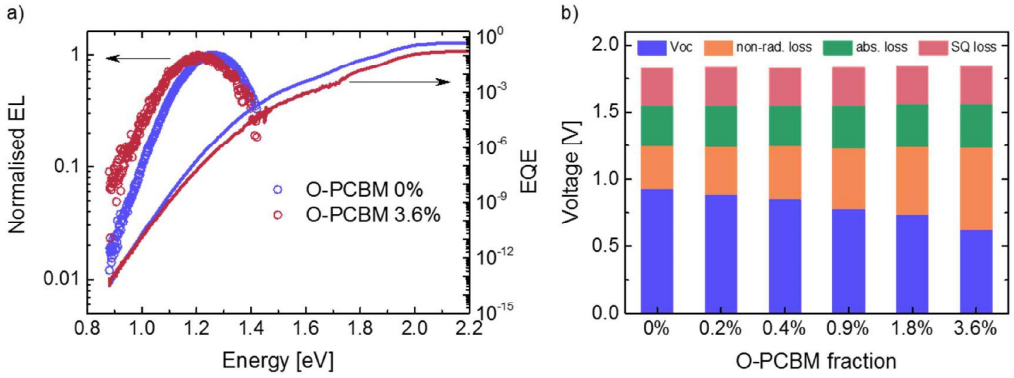

Figure 5 Electroluminescence analysis of the effect of fullerene photooxidation on voltage losses. (a) EL and sub-band gap EQE data for PCDTBT:PCBM with 0% and 3.6% O-PCBM (the data for intermediate concentrations were omitted for clarity; full dataset available in the Supporting Information); the EQE data for energies below ~1.25 eV was calculated from the EL data (b) experimental V_{oc} compared to ideal V_{oc} for devices without non-radiative recombination ($V_{oc,rad}$), and according to the Shockley-Queisser limit ($V_{oc,SQ}$) and the band gap of the polymer (E_g/q).

Supplementary Information of

The Role of Fullerenes in Environmental Stability of Polymer:Fullerene Solar Cells

Harrison K. H. Lee, Andrew M. Telford, Jason A. Röhr, Mark F. Wyatt, Beth Rice, Jiaying Wu, Alexandre de Castro Maciel, Sachetan M. Tuladhar, Emily Speller, James McGettrick, Sebastian Pont, Trystan Watson, James R. Durrant, Wing C. Tsoi, Jenny Nelson* and Zhe Li*

*Corresponding authors

Supplementary Table 1 Summary of device parameters of ITO/PEDOT:PSS/PCDTBT:PCBM(1:2)/Ca/Al devices with different degradation times under simulated AM1.5G illumination in air, before top electrode deposition.

Film degradation time (mins)	J_{SC} (mA/cm^2)	V_{OC} (V)	FF (%)	PCE (%)
0	8.13	0.928	61.5	5.01
10	7.09	0.868	46.5	3.19
30	4.96	0.823	42.4	1.93
60	3.83	0.782	40.5	1.35
600	0.95	0.488	39.5	0.20

Supplementary Table 2 Summary of device parameters of PCDTBT:PCBM devices exposed to air for 60 minutes in the dark and under 1000 lux of compact fluorescent lamp.

Film degradation condition	J_{SC} (mA/cm^2)	V_{OC} (V)	FF (%)	PCE (%)
Fresh	8.13	0.928	61.5	5.01
60 mins under 1000 lux fluorescent lamp in air	7.60	0.903	54.1	4.10
60 mins in dark in air	7.73	0.932	64.5	5.18

Supplementary Table 3 Summary of device parameters of PCDTBT:PCBM blend devices PCDTBT:PCBM blend devices made with different fractions of degraded PCBM, the percentages indicating the relative fraction of O-PCBM in the acceptor phase.

O-PCBM (%)	J_{SC} (mA/cm^2)	V_{OC} (V)	FF (%)	PCE (%)
0	8.13	0.928	61.5	5.01
0.2	6.76	0.885	51.4	3.69
0.4	6.08	0.852	45.7	2.85
0.9	4.42	0.795	42.2	1.78
1.8	3.17	0.740	42.0	1.18
3.6	2.14	0.617	39.8	0.63

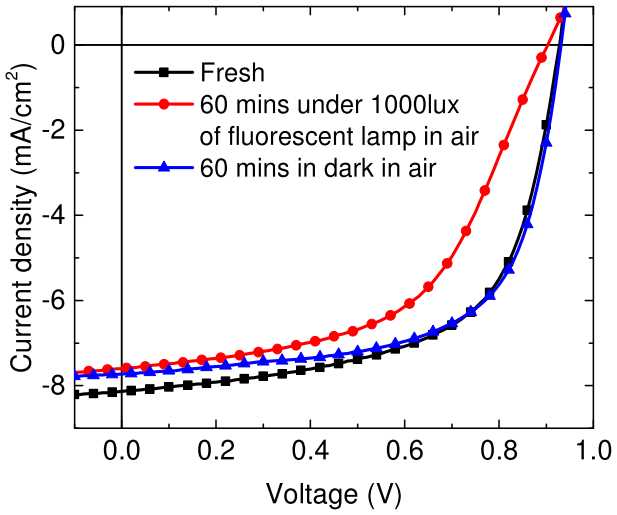

Supplementary Figure 1 *J–V* characteristic of PCDTBT:PCBM devices exposed to air for 60 minutes in the dark and under 1000 lux of compact fluorescent lamp.

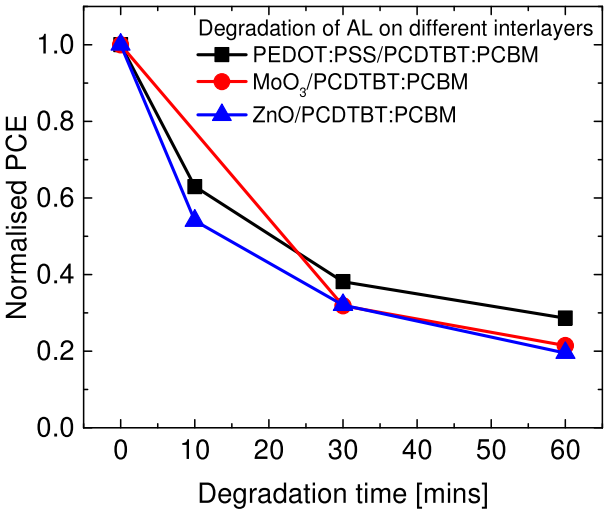

Supplementary Figure 2 Normalised PCE of PCDTBT:PCBM devices with active layers degraded on different interlayers, PEDOT:PSS, MoO_3, and ZnO. The devices using PEDOT:PSS and MoO_3 are finished by Ca/Al as top electrode; the devices using ZnO are finished by MoO_3/Ag as top electrode. The PCEs of the fresh devices using PEDOT:PSS, MoO_3, and ZnO are 5.01%, 4.73%, and 4.43%, respectively.

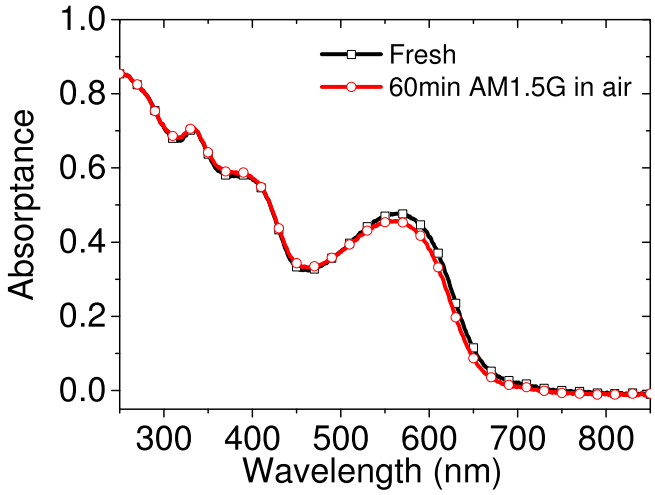

Supplementary Figure 3 Uv-visible spectra of PCDTBT:PCBM blend films without and with 60 minutes of exposure to AM1.5G conditions in dry air.

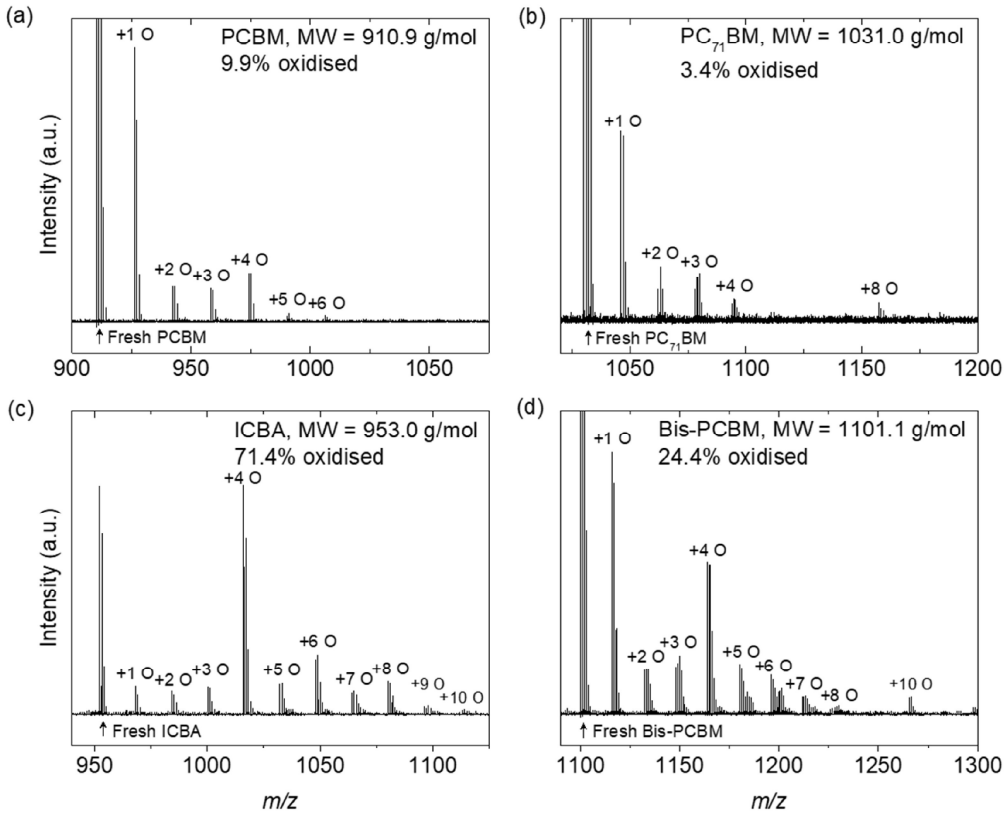

Supplementary Figure 4 MALDI-TOF measurement of (a) PCBM; (b) [6,6]-Phenyl C_{71} butyric acid methyl ester ($PC_{71}BM$); (c) indene-C_{60} bis-adduct (ICBA); and (d) Bis(1-[3-(methoxycarbonyl)propyl]-1-phenyl)-[6,6]C_{62} (Bis-PCBM) degraded in films under one sun in air for 32 hours.

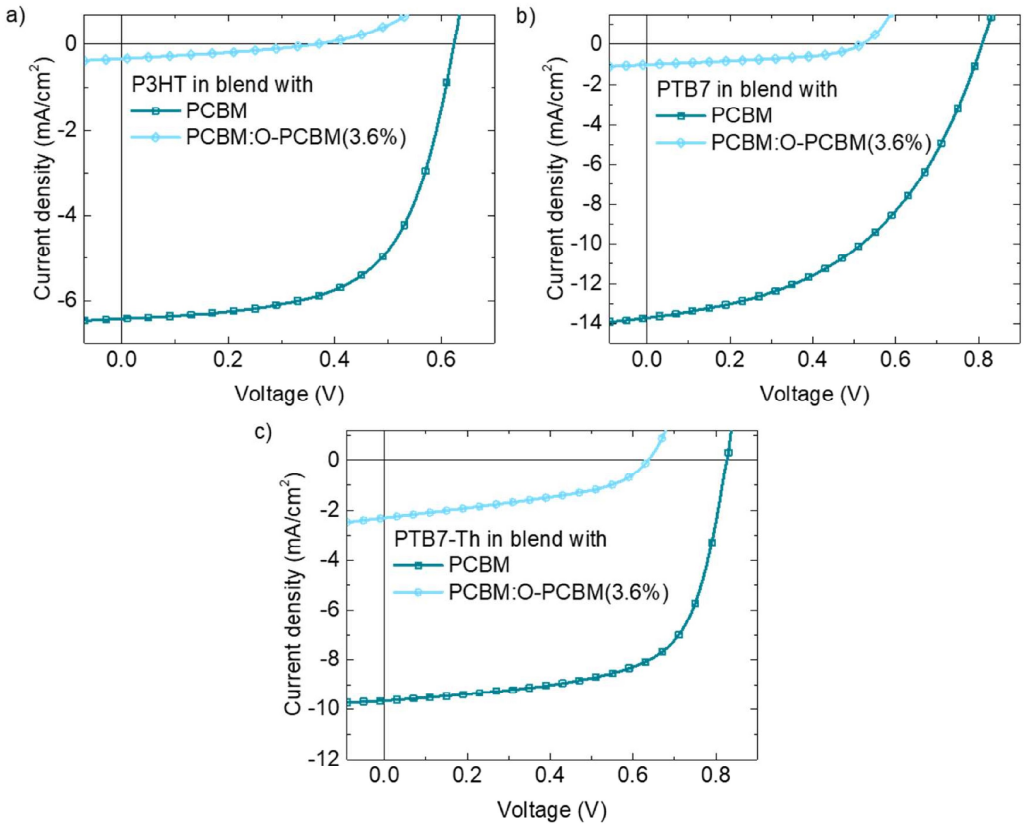

Supplementary Figure 5 *J-V* characteristic of devices using different OPV benchmark polymers (a) P3HT, (b) PTB7, and (c) PTB7-Th (also called PCE10) in blend with fresh PCBM and selectively degraded PCBM containing 3.6% of O-PCBM.

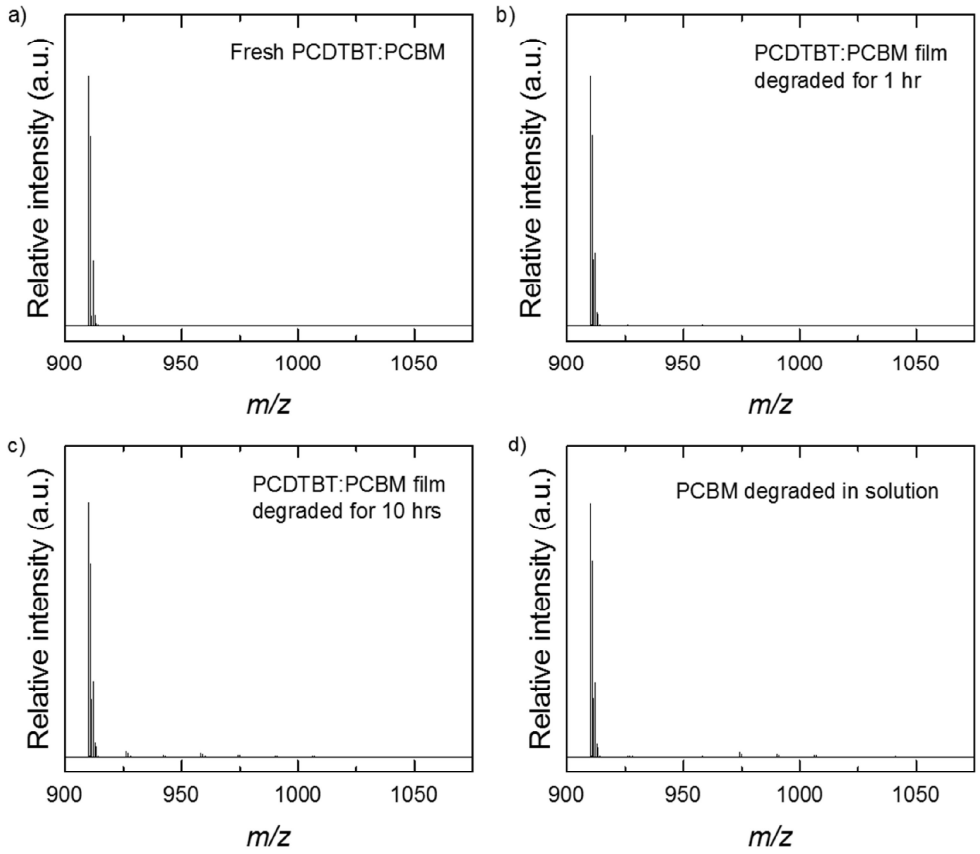

Supplementary Figure 6 Full scale MALDI-TOF measurement of (a) fresh PCDTBT:PCBM blend; (b) PCDTBT:PCBM blend film degraded under one sun in air for 1 hour; (c) PCDTBT:PCBM blend film degraded one sun in air for 10 hour; and (d) PCBM degraded in solution under one sun in air. The main peaks at 910.1 in the plots indicate the PCBM molecules.

HOMO and LUMO simulations on PCBM with multiple defects

Comparison of HOMO-LUMO simulation methods

The HOMO and LUMO levels were calculated with three different methods: (i) delta SCF (see main text); (ii) taking the Kohn-Sham orbitals; (iii) taking the Kohn-Sham orbital for the HOMO and Kohn-Sham HOMO plus the first excitation energy from TD-DFT for the LUMO. All the calculations are done with Gaussian 09, at the B3LYP level of theory with the 6-31g* basis set. The Kohn-Sham orbitals are obtained from a single point energy calculation on the optimised structure. The TD-DFT calculation yields the excitation energies and the first of these is taken to be added to the Kohn-Sham HOMO energy to obtain the LUMO energy.

The levels were also calculated for PCBM with multiple defects: two epoxide defects, one epoxide and one carbonyl defect, and one epoxide and two carbonyl defects. All defects lower the LUMO level and have a small effect on the HOMO level.

The numbering of the position of a PCBM molecule are shown below:

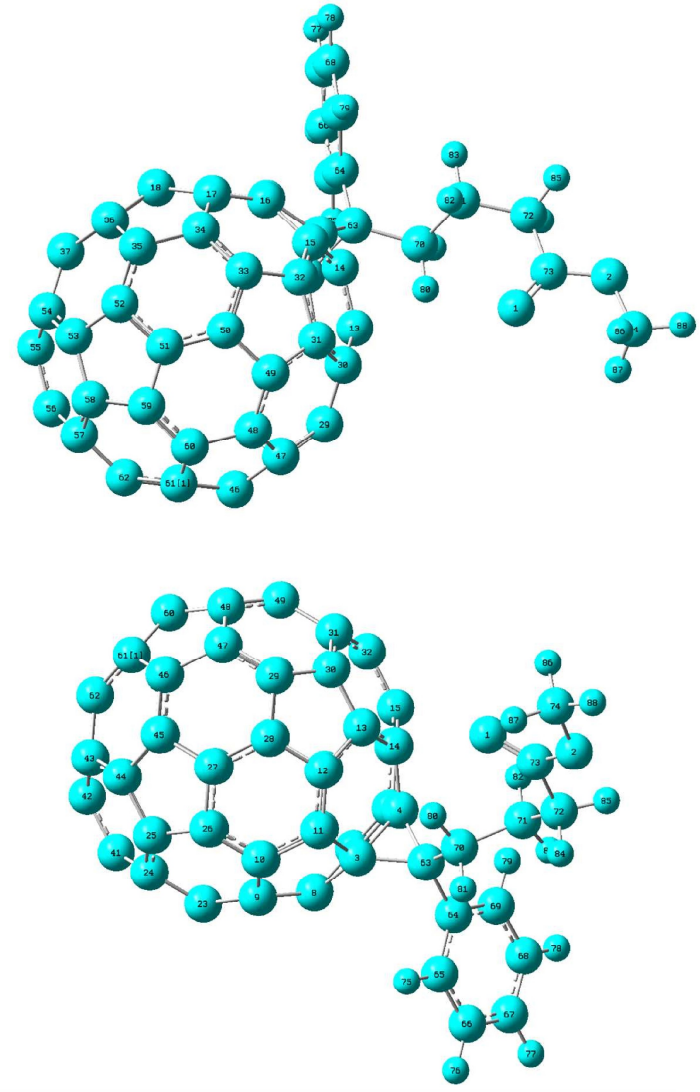

Supplementary Table 4 Delta-SCF HOMO and LUMO simulations of PCBM and PCBM with different oxygen defects. The values marked in red mean the energy levels go down.

Defect type	Defect position on the PCBM	HOMO from delta-SCF (eV)	Change in HOMO (eV)	HOMO from delta-SCF (eV)	Change in LUMO (eV)
No defect	N/A	-6.72	N/A	-1.83	N/A
One epoxide	11,12	-6.77	-0.05	-2.02	-0.19
	7,8	-6.74	-0.02	-2.03	-0.20
	13,14	-6.76	-0.04	-2.02	-0.19
	5,6	-6.77	-0.05	-2.05	-0.22
	24,25	-6.72	-0.01	-1.81	0.02
	33,34	-6.72	0.00	-1.82	0.01
	55,56	-6.72	0.00	-2.05	-0.22
	16,17	-6.73	-0.01	-2.00	-0.17
	20,38	-6.61	0.11	-1.80	0.03
	29,47	-6.59	0.13	-1.80	0.04
	27,28	-6.59	0.12	-1.83	0.00
	48,49	-6.64	0.08	-1.86	-0.03
	15,32	-6.72	0.00	-2.00	-0.17
	21,22	-6.61	0.11	-1.84	-0.01
	30,31	-6.60	0.12	-1.82	0.01
	10,26	-6.71	0.01	-2.00	-0.17
	39,40	-6.65	0.07	-1.85	-0.02
	9,23	-6.72	0.00	-2.00	-0.17
	45,46	-6.64	0.08	-1.86	-0.03
	36,37	-6.66	0.06	-1.85	-0.02
	57,58	-6.74	-0.02	-2.04	-0.21
	61,62	-6.70	0.02	-2.07	-0.24
	59,60	-6.70	0.02	-2.08	-0.25
	53,54	-6.71	0.01	-2.06	-0.23
	41,42	-6.69	0.02	-1.89	-0.06
	43,44	-6.69	0.02	-1.90	-0.06
	50,51	-6.69	0.03	-1.89	-0.06
	35,52	-6.69	0.03	-1.90	-0.07
	18,19	-6.52	0.20	-1.76	0.07
One Carbonyl	13,14	-6.52	0.20	-2.10	-0.27
	11,12	-6.52	0.20	-2.09	-0.26
	7,8	-6.53	0.19	-2.13	-0.30
	16,17	-6.52	0.20	-2.21	-0.38
	10,26	-6.46	0.26	-2.21	-0.38
	20,38	-6.36	0.35	-2.11	-0.28
	29,47	-6.34	0.38	-2.11	-0.28
	9,23	-6.49	0.22	-2.19	-0.36
	15,32	-6.52	0.20	-2.20	-0.37
	21,22	-6.44	0.28	-2.23	-0.39
	33,34	-6.57	0.15	-2.10	-0.27

	24,25	-6.57	0.15	-2.08	-0.25
	27,28	-6.42	0.30	-2.23	-0.40
	18,19	-6.46	0.26	-2.22	-0.39
	30,31	-6.42	0.30	-2.23	-0.40
	39,40	-6.44	0.28	-2.17	-0.34
	45,46	-6.42	0.30	-2.17	-0.34
	48,49	-6.42	0.30	-2.17	-0.34
	36,37	-6.45	0.27	-2.18	-0.35
	41,42	-6.45	0.27	-2.19	-0.36
	43,44	-6.45	0.27	-2.20	-0.37
	50,51	-6.44	0.28	-2.20	-0.37
	59,60	-6.44	0.28	-2.32	-0.49
	55,56	-6.46	0.26	-2.32	-0.49
	53,54	-6.45	0.28	-2.32	-0.49
	61,62	-6.45	0.27	-2.32	-0.49
	5,6	-6.59	0.13	-2.27	-0.43
	35,52	-6.46	0.26	-2.18	-0.35
	57,58	-6.47	0.25	-2.22	-0.39
Two epoxides	11,12/13,14	-6.68	0.04	-2.25	-0.41
	5,6/7,8	-6.69	0.03	-2.27	-0.44
	11,12/10,26	-6.70	0.02	-2.03	-0.20
	11,12/7,8	-6.74	-0.02	-2.14	-0.31
	5,6/13,14	-6.73	-0.01	-2.16	-0.33
	5,6/20,38	-6.73	-0.01	-2.04	-0.21
Two carbonyls	11,12	-6.74	-0.02	-2.52	-0.69
	20,38	-6.56	0.15	-2.62	-0.79
	29,47	-6.54	0.18	-2.62	-0.79
	16,17	-6.73	-0.01	-2.66	-0.83
	10,26	-6.70	0.02	-2.69	-0.86
	24,25	-6.71	0.01	-2.64	-0.81
	45,46	-6.63	0.09	-2.71	-0.88
	36,37	-6.65	0.07	-2.72	-0.88
	43,44	-6.67	0.05	-2.70	-0.87
	59,60	-6.66	0.06	-2.80	-0.97
	35,52	-6.67	0.05	-2.71	-0.88
	18,19	-6.57	0.15	-2.91	-1.08
	53,54	-6.67	0.05	-2.80	-0.96
	27,28	-6.54	0.18	-2.90	-1.07
	5,6	-6.75	-0.03	-2.67	-0.84
	57,58	-6.69	0.03	-2.74	-0.91
One epoxide and one carbonyl	10,26/24,25	-6.61	0.11	-2.08	-0.25
	10,26/7,8	-6.53	0.19	-2.23	-0.40
	10,26/30,31	-6.43	0.29	-2.39	-0.56
	10,26/20,38	-6.41	0.31	-2.28	-0.45
	10,26/31,30	-6.43	0.29	-2.47	-0.64
	10,26/52,35	-6.40	0.32	-2.34	-0.51
One epoxide	11,12/10,26	-6.76	-0.05	-2.48	-0.65

and two carbonyls	11,12/27,28	-6.79	-0.07	-2.56	-0.73
	11,12/29,47	-6.75	-0.03	-2.65	-0.82
	11,12/43,44	-6.60	0.12	-2.81	-0.98
	11,12/59,60	-6.69	0.03	-2.85	-1.01
	11,12/15,32	-6.72	0.00	-2.81	-0.98
One diol	11,12	-5.65	1.07	-2.13	-0.30
	10,26	-5.93	0.79	-2.41	-0.58
	18,19	-5.99	0.73	-2.15	-0.32
	27,28	-5.97	0.75	-2.13	-0.30
	24,25	-5.78	0.94	-2.21	-0.38
	16,17	-5.86	0.86	-2.76	-0.93
	29,47	-6.11	0.61	-2.69	-0.85
	20,38	-6.13	0.59	-2.69	-0.86
	45,46	-5.88	0.84	-2.38	-0.55
	36,37	-5.89	0.82	-2.38	-0.55
	35,52	-5.93	0.79	-2.37	-0.54
	59,60	-6.07	0.65	-2.60	-0.77
	43,44	-5.99	0.73	-2.67	-0.84
	53,54	-6.23	0.48	-2.78	-0.95
	57,58	-6.03	0.69	-2.45	-0.62
	5,6	-5.80	0.91	-2.36	-0.53

Supplementary Table 5 Kohn-Sham HOMO and LUMO simulations of PCBM and PCBM with different oxygen defects. The values marked in red mean the energy levels go down.

Defect type	Defect position on the PCBM	HOMO from Kohn-Sham (eV)	Change in HOMO (eV)	LUMO from Kohn-Sham LUMO (eV)	Change in LUMO (eV)
No defect	N/A	-5.56	N/A	-3.00	N/A
One epoxide	11,12	-5.62	-0.06	-3.16	-0.16
	7,8	-5.61	-0.05	-3.17	-0.17
	13,14	-5.61	-0.05	-3.16	-0.16
	5,6	-5.64	-0.08	-3.19	-0.19
	24,25	-5.58	-0.02	-2.95	0.05
	33,34	-5.57	-0.01	-2.95	0.05
	55,56	-5.58	-0.02	-3.19	-0.19
	16,17	-5.59	-0.03	-3.13	-0.13
	20,38	-5.48	0.08	-2.94	0.06
	29,47	-5.46	0.10	-2.93	0.07
	27,28	-5.47	0.09	-2.97	0.03
	48,49	-5.50	0.06	-3.00	0.00
	15,32	-5.58	-0.02	-3.13	-0.13
	21,22	-5.48	0.08	-2.98	0.02
	30,31	-5.47	0.09	-2.96	0.04
	10,26	-5.58	-0.02	-3.13	-0.13
	39,40	-5.52	0.04	-2.99	0.01
	9,23	-5.58	-0.02	-3.14	-0.14
	45,46	-5.51	0.05	-3.00	0.00
	36,37	-5.52	0.04	-2.99	0.01
	57,58	-5.57	-0.01	-3.18	-0.18
	61,62	-5.56	0.00	-3.21	-0.21
	59,60	-5.56	0.00	-3.22	-0.22
	53,54	-5.56	0.00	-3.20	-0.20
	41,42	-5.55	0.01	-3.03	-0.03
	43,44	-5.55	0.01	-3.04	-0.04
	50,51	-5.54	0.02	-3.04	-0.04
	35,52	-5.54	0.02	-3.04	-0.04
	18,19	-5.39	0.17	-2.90	0.10
One carbonyl	13,14	-5.39	0.17	-3.21	-0.21
	11,12	-5.39	0.17	-3.21	-0.21
	7,8	-5.39	0.17	-3.25	-0.25
	16,17	-5.38	0.18	-3.33	-0.33
	10,26	-5.33	0.23	-3.34	-0.34
	20,38	-5.24	0.32	-3.27	-0.27
	29,47	-5.22	0.34	-3.26	-0.26
	9,23	-5.38	0.18	-3.33	-0.33
	15,32	-5.41	0.15	-3.34	-0.34
	21,22	-5.33	0.23	-3.34	-0.34
	33,34	-5.44	0.12	-3.24	-0.24

	24,25	-5.44	0.12	-3.22	-0.22
	27,28	-5.31	0.25	-3.34	-0.34
	18,19	-5.34	0.22	-3.34	-0.34
	30,31	-5.31	0.25	-3.34	-0.34
	39,40	-5.32	0.24	-3.32	-0.32
	45,46	-5.30	0.26	-3.32	-0.32
	48,49	-5.30	0.26	-3.32	-0.32
	36,37	-5.32	0.24	-3.33	-0.33
	41,42	-5.31	0.25	-3.35	-0.35
	43,44	-5.31	0.25	-3.35	-0.35
	50,51	-5.31	0.25	-3.35	-0.35
	59,60	-5.30	0.26	-3.46	-0.46
	55,56	-5.32	0.24	-3.46	-0.46
	53,54	-5.31	0.25	-3.46	-0.46
	61,62	-5.31	0.25	-3.47	-0.47
	5,6	-5.46	0.10	-3.37	-0.37
	35,52	-5.32	0.24	-3.33	-0.33
	57,58	-5.33	0.23	-3.37	-0.37
Two epoxides	11,12/13,14	-5.54	0.02	-3.38	-0.38
	5,6/7,8	-5.56	0.00	-3.40	-0.40
	11,12/10,26	-5.56	0.00	-3.17	-0.17
	11,12/7,8	-5.60	-0.04	-3.28	-0.28
	5,6/13,14	-5.60	-0.04	-3.29	-0.29
	5,6/20,38	-5.60	-0.04	-3.16	-0.16
One epoxide, one carbonyl	10,26/24,25	-5.48	0.08	-3.23	-0.23
	10,26/7,8	-5.40	0.16	-3.35	-0.35
	10,26/30,31	-5.33	0.23	-3.50	-0.50
	10,26/20,38	-5.29	0.27	-3.43	-0.43
	10,26/31,30	-5.33	0.23	-3.59	-0.59
	10,26/52,35	-5.27	0.29	-3.50	-0.50
One epoxide, two carbonyls	11,12/10,26	-5.63	-0.07	-3.61	-0.61
	11,12/27,28	-5.67	-0.11	-3.71	-0.71
	11,12/29,47	-5.62	-0.06	-3.80	-0.80
	11,12/43,44	-5.48	0.08	-3.96	-0.96
	11,12/59,60	-5.56	0.00	-4.00	-1.00
	11,12/15,32	-5.59	-0.03	-3.94	-0.94
Two Carbonyls	11,12	-5.61	-0.05	-3.64	-0.64
	20,38	-5.45	0.11	-3.78	-0.78
	29,47	-5.42	0.14	-3.77	-0.77
	16,17	-5.60	-0.04	-3.80	-0.80
	10,26	-5.58	-0.02	-3.83	-0.83
	24,25	-5.58	-0.02	-3.79	-0.79
	45,46	-5.51	0.05	-3.86	-0.86
	36,37	-5.53	0.03	-3.87	-0.87
	43,44	-5.54	0.02	-3.87	-0.87
	59,60	-5.53	0.03	-3.96	-0.96
	35,52	-5.54	0.02	-3.87	-0.87

	18,19	-5.47	0.09	-4.06	-1.06
	53,54	-5.53	0.03	-3.95	-0.95
	27,28	-5.43	0.13	-4.05	-1.05
	5,6	-5.67	-0.11	-3.78	-0.78
	57,58	-5.55	0.01	-3.91	-0.91
Diol	11,12	-4.67	0.89	-3.00	0.00
	10,26	-4.90	0.66	-3.33	-0.33
	18,19	-5.00	0.56	-3.06	-0.06
	27,28	-4.98	0.58	-3.04	-0.04
	24,25	-4.80	0.76	-3.10	-0.10
	16,17	-5.07	0.49	-3.61	-0.61
	29,47	-4.99	0.57	-3.61	-0.61
	20,38	-5.02	0.54	-3.63	-0.63
	45,46	-4.89	0.67	-3.27	-0.27
	36,37	-4.90	0.66	-3.27	-0.27
	35,52	-4.91	0.65	-3.31	-0.31
	59,60	-5.09	0.47	-3.47	-0.47
	43,44	-5.11	0.45	-3.58	-0.58
	53,54	-5.16	0.40	-3.68	-0.68
	57,58	-5.05	0.51	-3.35	-0.35
	5,6	-4.85	0.71	-3.23	-0.23

Supplementary Table 6 Kohn-Sham HOMO and TD-DFT LUMO simulations of PCBM and PCBM with different oxygen defects. The values marked in red mean the energy levels go down.

Defect type	Defect position on the PCBM	Kohn-Sham HOMO (eV)	Change in HOMO (eV)	1st excited state energy (eV)	TD-DFT LUMO (eV)	Change in LUMO (eV)
No defect	N/A	-5.56	N/A	1.93	-3.63	N/A
One epoxide	11,12	-5.62	-0.06	1.85	-3.77	-0.14
	7,8	-5.61	-0.05	1.84	-3.77	-0.14
	13,14	-5.61	-0.05	1.84	-3.77	-0.14
	5,6	-5.64	-0.07	1.85	-3.79	-0.15
	24,25	-5.58	-0.02	2.03	-3.55	0.08
	33,34	-5.57	-0.01	2.02	-3.55	0.08
	55,56	-5.58	-0.02	1.78	-3.80	-0.17
	16,17	-5.59	-0.03	1.84	-3.75	-0.12
	20,38	-5.48	0.08	1.93	-3.55	0.08
	29,47	-5.46	0.10	1.92	-3.53	0.10
	27,28	-5.47	0.10	1.89	-3.58	0.05
	48,49	-5.50	0.06	1.90	-3.61	0.03
	15,32	-5.58	-0.02	1.83	-3.75	-0.12
	21,22	-5.48	0.08	1.89	-3.59	0.04
	30,31	-5.47	0.09	1.90	-3.57	0.06
	10,26	-5.58	-0.01	1.82	-3.75	-0.12
	39,40	-5.52	0.05	1.93	-3.59	0.04
	9,23	-5.58	-0.02	1.83	-3.75	-0.12
	45,46	-5.51	0.05	1.90	-3.60	0.03
	36,37	-5.52	0.04	1.93	-3.59	0.04
	57,58	-5.57	-0.01	1.77	-3.80	-0.17
	61,62	-5.56	0.00	1.74	-3.82	-0.19
	59,60	-5.56	0.01	1.73	-3.82	-0.19
	53,54	-5.56	0.00	1.75	-3.81	-0.18
	41,42	-5.55	0.02	1.90	-3.65	-0.02
	43,44	-5.55	0.01	1.89	-3.65	-0.02
	50,51	-5.54	0.02	1.89	-3.65	-0.02
	35,52	-5.54	0.02	1.89	-3.65	-0.02
	18,19	-5.39	0.17	1.87	-3.51	0.12
Two Carbonyls	11,12	-5.61	-0.05	1.39	-4.22	-0.59
	20,38	-5.45	0.12	1.03	-4.42	-0.79
	29,47	-5.42	0.14	1.01	-4.41	-0.78
	16,17	-5.60	-0.04	0.97	-4.63	-1.00
	10,26	-5.58	-0.02	0.99	-4.59	-0.96
	24,25	-5.58	-0.02	1.11	-4.48	-0.85
	45,46	-5.51	0.05	1.05	-4.46	-0.82
	36,37	-5.53	0.03	1.04	-4.49	-0.86
	43,44	-5.54	0.02	1.05	-4.49	-0.86
	59,60	-5.53	0.03	1.12	-4.41	-0.78
	35,52	-5.54	0.03	1.04	-4.49	-0.86

	18,19	-5.47	0.10	0.73	-4.74	-1.11
	53,54	-5.53	0.03	1.01	-4.53	-0.89
	27,28	-5.43	0.13	0.70	-4.74	-1.10
	5,6	-5.67	-0.11	1.07	-4.60	-0.97
	57,58	-5.55	0.01	1.28	-4.27	-0.64
Diol	11,12	-4.67	0.90	1.36	-3.31	0.32
	10,26	-4.90	0.66	1.11	-3.79	-0.16
	18,19	-5.00	0.56	1.47	-3.52	0.11
	27,28	-4.98	0.58	1.46	-3.52	0.11
	24,25	-4.80	0.77	1.47	-3.33	0.30
	16,17	-5.07	0.49	0.84	-4.23	-0.60
	29,47	-4.99	0.57	1.46	-3.53	0.10
	20,38	-5.02	0.54	0.73	-4.29	-0.66
	45,46	-4.89	0.67	1.21	-3.68	-0.05
	36,37	-4.90	0.66	1.20	-3.70	-0.07
	35,52	-4.91	0.65	0.71	-4.21	-0.58
	59,60	-5.09	0.48	1.06	-4.02	-0.39
	43,44	-5.11	0.45	0.88	-4.24	-0.60
	53,54	-5.16	0.40	0.92	-4.24	-0.61
	57,58	-5.05	0.51	1.16	-3.89	-0.26
	5,6	-4.85	0.72	1.37	-3.47	0.16

Supplementary Table 7 Change in HOMO and LUMO levels base on the Boltzmann average. The values marked in red mean the energy levels go down.

Defect type	Change in HOMO (delta-SCF)	Change in LUMO (delta-SCF)	Change in HOMO (Kohn-Sham)	Change in LUMO (Kohn-Sham)	Change in LUMO (TD-DFT)
One epoxide	0.04	-0.10	0.02	-0.07	-0.05
One carbonyl	0.25	-0.36	0.22	-0.33	-0.31
Two epoxides	0.01	-0.32	-0.01	-0.29	-0.29
One epoxide, one carbonyl	0.25	-0.47	0.21	-0.43	-0.43
One epoxide, two carbonyls	0.00	-0.86	-0.03	-0.84	-0.81
Two carbonyls	0.06	-0.88	0.03	-0.87	-0.87
Diol	0.77	-0.62	0.60	-0.60	-0.58

Space charge limited current analysis

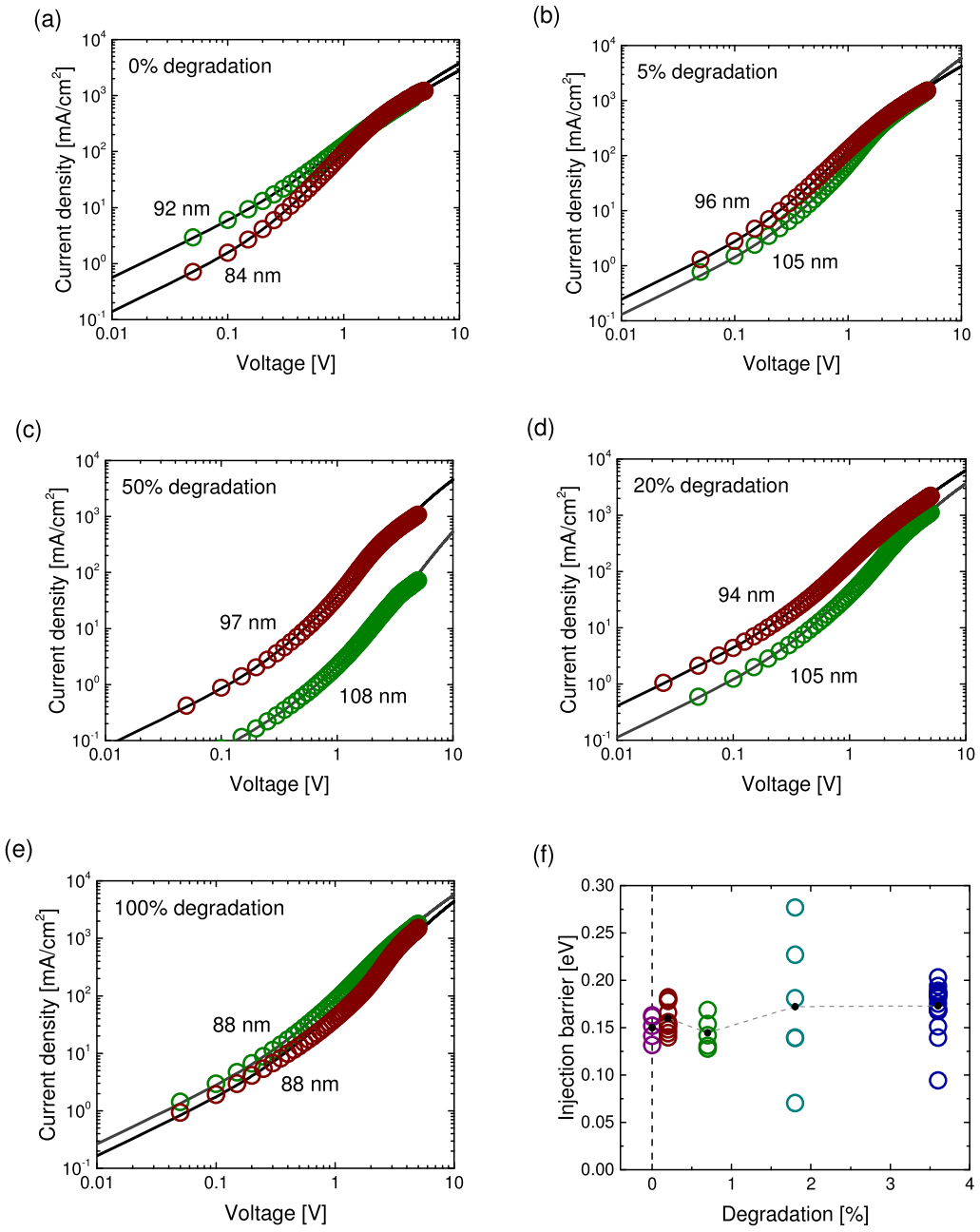

Supplementary Figure 7 (a-e) SCLC current density-voltage data for PCBM electron-only devices with increasing concentrations of O-PCBM. Experimental curves are presented with open circles and the drift-diffusion fits with solid lines. **(f)** Values of the barrier for electron injection into electron only devices containing different fractions of O-PCBM, obtained from the fitting procedure described in the text.

Solar cell *J–V* curve simulations

Both the dark and illuminated solar cell *J-V* curves were simulated using a commercially available drift-diffusion solver called *Advanced Semiconductor Analysis* (ASA) [https://www.cambridge.org/core/journals/journal-of-materials-research/article/optical-and-electrical-modeling-of-thinfilm-silicon-solar-cells/BF97415DB87ACB26ACD99B9FBB32C7B6]. For the illuminated devices, a constant generation rate was chosen to match the current density of the experimental curves when a band gap of 1.4 eV was used. With the presence of a deep Gaussian electron trap level, recombination of trapped electrons and free holes was used along with direct band-to-band recombination. The choice of electron band mobility, Gaussian trap level and Gaussian density was chosen based on the mean values of the SCLC fitting results. All fixed values and varied values are shown in the table below.

Quantity	Value	Units
Fixed values		
Band gap	variable	eV
Effective electron density	10^{19}	cm^{-3}
Effective hole density	10^{19}	cm^{-3}
Dielectric constant	3	-
Active layer thickness	70	nm
Electron band mobility	variable	cm^2/Vs
Hole band mobility	$3 \cdot 10^{-3}$	cm^2/Vs
Injection barrier (electrons)	variable	eV
Injection barrier (holes)	0.2	eV
Gaussian density	variable	cm^{-3}
Gaussian level	variable	eV
Gaussian standard deviation	0.1	eV
Surface recomb. velocity	10^5	m/s
Electron capture rate (neut.)	10^{-10}	$cm^{-3}\,s^{-1}$
Electron capture rate (pos.)	10^{-10}	$cm^{-3}\,s^{-1}$
Hole capture rate (neut.)	10^{-10}	$cm^{-3}\,s^{-1}$
Hole capture rate (neg.)	10^{-10}	$cm^{-3}\,s^{-1}$
Generation rate	$7.7 \cdot 10^{21}$	$cm^{-3}\,s^{-1}$
Direct recombination rate	$7.7 \cdot 10^{-19}$	$cm^{-3}\,s^{-1}$
Series resistance	$3.07 \cdot 10^{-4}$	Ωm^2
Shunt resistance	0.29	Ωm^2
0% O-PCBM device		
Band gap	1.398	eV
Injection barrier	0.2	eV
Electron band mobility	$8.2 \cdot 10^{-4}$	cm^2/Vs
Gaussian density	$2.4 \cdot 10^{16}$	cm^{-3}
Gaussian level	-0.2073	eV
1.8% O-PCBM device		
Band gap	1.363	eV
Injection barrier	0.165	eV
Electron band mobility	$8.8 \cdot 10^{-4}$	cm^2/Vs
Gaussian density	$1.6 \cdot 10^{17}$	cm^{-3}
Gaussian level	-0.1723	eV
3.6% O-PCBM device		
Band gap	1.277	eV
Injection barrier	0.0785	eV
Electron band mobility	$6.3 \cdot 10^{-5}$	cm^2/Vs
Gaussian density	$6.8 \cdot 10^{17}$	cm^{-3}
Gaussian level	-0.086	eV

Charge extraction simulations

The excess charge-carrier density obtained from charge extraction (CE) measurements were simulated by subtracting the total charge-carrier density at V_{oc} under varying illumination by the total charge-carrier density at V = 0 V in the dark. The total charge-carrier density is here the sum of the average values of the electrons densities, hole densities, trap densities and surface charge densities (assuming that enough time has passed that all trapped charge carriers have thermally escaped and are extracted at the contacts).

V_{OC} reconstruction from charge extraction (CE) and transient photovoltage (TPV) measurements

The charge density VS V_{OC} data from CE was fitted with the exponential function:

$$n = n_0 exp\left(\frac{qV_{OC}}{mkT}\right)$$

The lifetime VS V_{OC} data from TPV was fitted with the exponential function:

$$\tau_{\Delta n} = \tau_{\Delta n0} exp\left(-\frac{qV_{OC}}{\vartheta kT}\right)$$

The lifetime of the charge generated by the TPV pulse, $\tau_{\Delta n}$, can be related to the lifetime of the total charge n by the relationship:

$$\tau_n = \delta\tau_{\Delta n}$$

Where:

$$\delta = \frac{m}{\vartheta} + 1$$

Therefore:

$$\tau_n = \delta\tau_{\Delta n0} exp\left(-\frac{qV_{OC}}{\vartheta kT}\right)$$

At open circuit, the generation and recombination currents are equal:

$$J_{gen} \approx J_{SC} = J_{loss} = qd\frac{n}{\tau_n} = qd\frac{n_0 exp\left(\frac{qV_{OC}}{mkT}\right)}{\delta\tau_{\Delta n0} exp\left(-\frac{qV_{OC}}{\vartheta kT}\right)}$$

$$\frac{\delta J_{SC}\tau_{\Delta n0}}{qdn_0} = \frac{exp\left(\frac{qV_{OC}}{mkT}\right)}{exp\left(-\frac{qV_{OC}}{\vartheta kT}\right)}$$

$$\ln\left(\frac{\delta J_{SC}\tau_{\Delta n0}}{qdn_0}\right) = \frac{qV_{OC}}{kT}\left(\frac{1}{m} + \frac{1}{\vartheta}\right)$$

$$V_{OC}\left(\frac{1}{m} + \frac{1}{\vartheta}\right) = \frac{kT}{q} ln\left(\frac{\delta J_{SC}\tau_{\Delta n0}}{qdn_0}\right)$$

$$V_{OC} = \frac{mkT}{q\delta} ln\left(\frac{\delta J_{SC}\tau_{\Delta n0}}{qdn_0}\right)$$

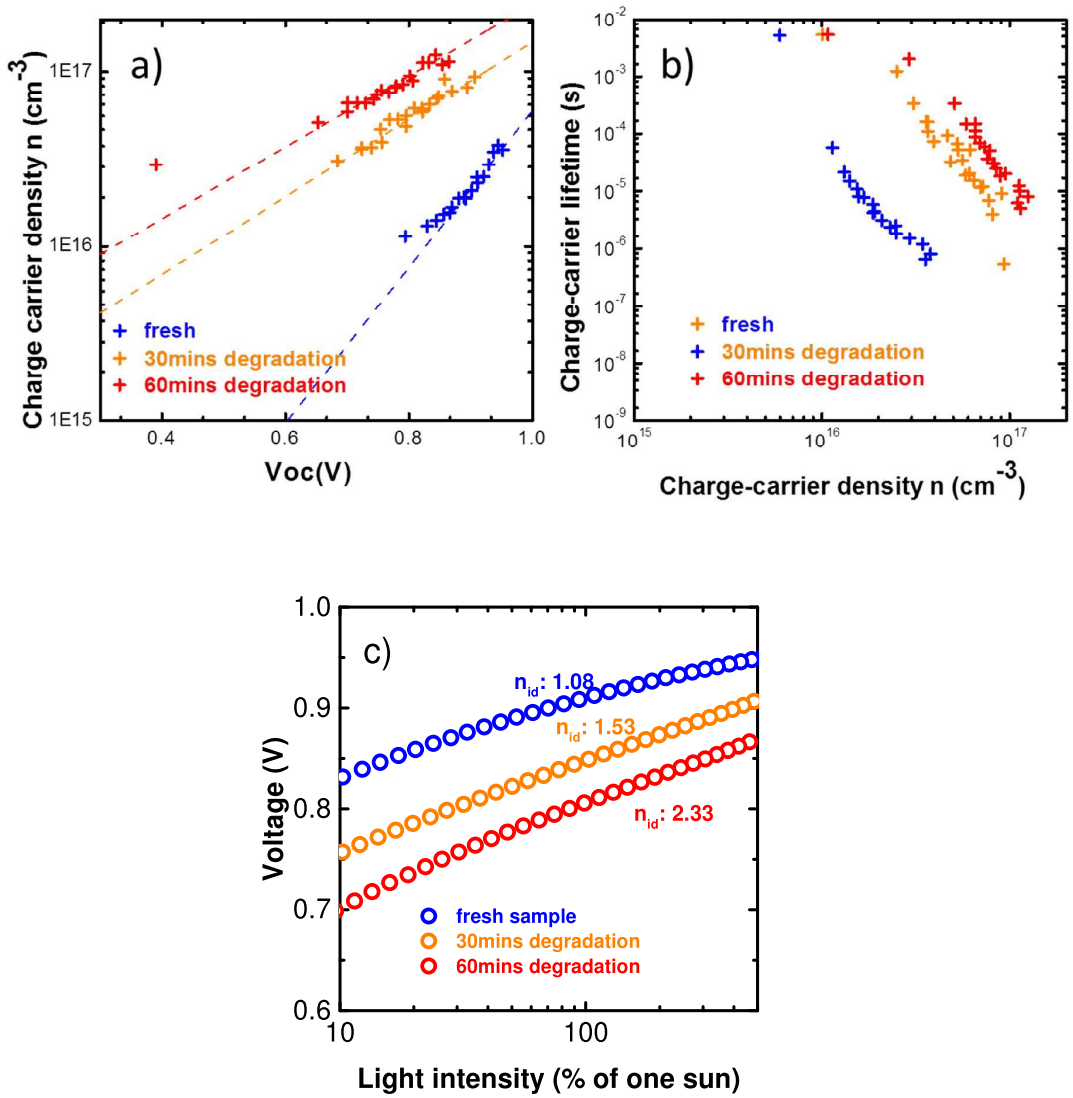

Supplementary Figure 8 CE, TPV, and diode ideality analysis of PCDTBT:PCBM blend devices prepared from blends degraded as films under AM1.5G illumination in dry air for 30 minutes and 60 minutes prior to electrode deposition. (a) Charge-carrier density *n* as a function of V_{oc} as measured from CE (produced by varying the illumination intensity), the dashed line corresponds to mono-exponential fit; (b) charge-carrier lifetimes at varying charge-carrier density as measured from TPV; (c) Measured V_{OC} (open circles) at varying illumination intensities.

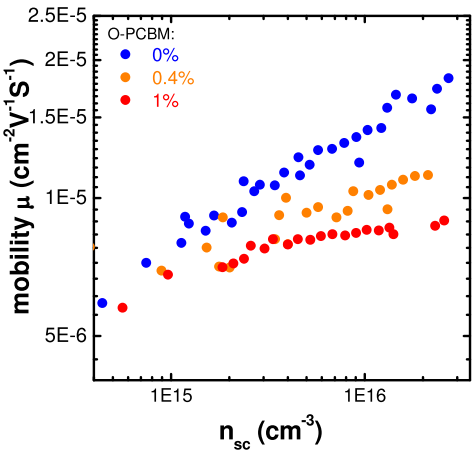

Supplementary Figure 9 Effective mobility measured by charge extraction at short circuit as a function of carrier density for PCDTBT:PCBM blend devices with increasing fraction of O-PCBM.

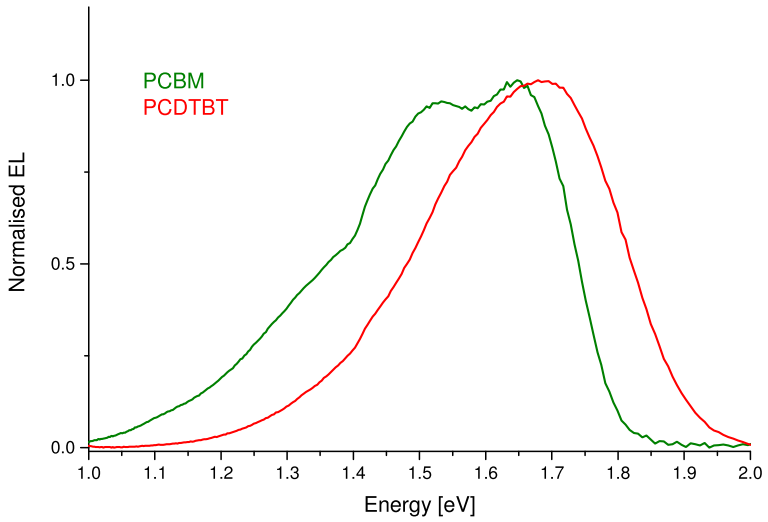

Supplementary Figure 10 Normalised electroluminescence spectra of devices containing only pure PCBM or only pure PCDTBT. Both emissions occur at higher energies than the charge transfer emission recorded in devices containing PCDTBT:PCBM blends.

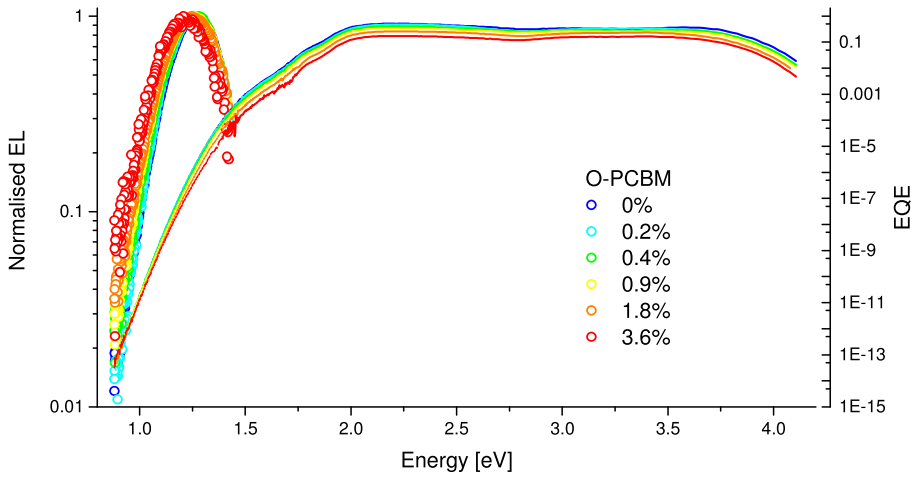

Supplementary Figure 11 Normalised electroluminescence (EL) and absolute external quantum efficiency (EQE) spectra of PCDTBT:PCBM devices containing increasing amounts of photo-oxidised PCBM (O-PCBM). The quantum efficiency data that could be directly collected on our EQE instrument is represented by solid lines (down to about 1.5 eV), while the EQE data below 1.5 eV was obtained from the EL data, after dividing by the black body photon flux and multiplying by a pre-factor to match with the absolute EQE data.

Detailed balance method to calculate voltage losses

The maximum voltage achievable in a solar cell is limited by unavoidable radiative recombination. In the radiative limit, where absorption and emission quantum efficiencies are equal, the maximum voltage achievable can be related to the electroluminescence quantum efficiency (Q_{LED}).

The Q_{LED} is a function of the electroluminescence photo flux and the injection current density:

From the ideal diode equation, we can deduce the open circuit voltage in the radiative limit at open circuit (ideality factor = 1, only radiative recombination):

$$V_{OC,rad} = \frac{kT}{q} ln\left(\frac{J_{SC}(V_{OC,rad})}{J_{0,rad}} + 1\right)$$

Assuming no losses at short circuit (SC):

$$J_{SC}\left(V_{OC,rad}\right) \approx J_{SC}$$

The saturation current in the radiative limit can be calculated from the electroluminescence quantum efficiency (Q_{EL}).

$$J_{0,rad} = q \int Q_{EL}\,(E)\phi_{BB}(E)dE$$

As our electroluminescence system could not measure an absolute value of electroluminescence photon flux, Q_{EL} was obtained by matching the EL data to the calibrated EQE data, by multiplying them by a pre-factor.

Supplementary Table 8 Voltage values calculated for PCDTBT:PCBM devices with increasing fractions of photo-oxidised PCBM (O-PCBM). $V_{OC,SQ}$: Schokley-Queisser limit to V_{OC}; $V_{OC,rad}$: radiative limit to V_{OC}, measured using EQE-EL; V_{OC}: measured using a solar simulator; $\Delta V_{OC,abs}$: voltage losses due to non-ideal absorption (EQE < 1 above the band gap energy and sloped absorption edge); $\Delta V_{OC,non\text{-}rad}$: voltage losses due to non-radiative recombination only.

O-PCBM [%]	$V_{OC,SQ}$ [V]	$V_{OC,rad}$ [V]	V_{OC} [V]	$\Delta V_{OC,abs}$ [V]	$\Delta V_{OC,non\text{-}rad}$ [V]
0	1.545	1.246	0.923	0.299	0.323
0.2	1.545	1.240	0.882	0.305	0.358
0.4	1.545	1.241	0.846	0.303	0.396
0.9	1.545	1.224	0.775	0.321	0.449
1.8	1.555	1.234	0.731	0.320	0.503
3.6	1.555	1.229	0.614	0.326	0.616

Carri Cotton
Publishing Editor
Energy & Environmental Science
Royal Society of Chemistry

Swansea University
Prifysgol Abertawe

24th December 2017

Re: The Role of Fullerenes in The Environmental Stability of Polymer:Fullerene Solar Cells

Manuscript ID: EE-ART-10-2017-002983

Dear Carri,

Thank you very much for your consideration of our manuscript for publication in Energy and Environmental Science. We are pleased to receive the overall very positive comments from all three reviewers and have made changes to the manuscript as requested which, we believe, have addressed all the reviewers' comments. Please find a detailed point-by-point response to the reviewers' comments below, and an amended version of the manuscript attached. We hope you are now able to accept our manuscript for publication in Energy and Environmental Science.

Best regards,

Dr Zhe Li, Swansea University (z.li@swansea.ac.uk) and

Prof Jenny Nelson, Imperial College London (jenny.nelson@imperial.ac.uk)

Point-to-Point response to Reviewers' Comments

Reviewer 1:

"Nevertheless, the interest of this topic is out of a broad section of EES readership, and for this reason I recommend the rejection of this manuscript in Energy Environmental Science since this manuscript would be more suitable for a more specialized journal."

As pointed out by both Reviewers 2 and 3, organic solar cells are an important class of next generation photovoltaic technology and their environmental stability has been widely recognised as a critical challenge for their commercialisation, thereby representing broad research interests and readership. This is evidenced by a range of high impact publications published in recent years addressing the environmental stability of organic solar cells in Energy and Environmental Science and other research journals.[1-5] The field of organic solar cells is further driven by the recent development of non-fullerene acceptor materials, leading to further breakthroughs both in their performance and stability.[6-9] **We have added new text on Pages 3-4 of the main text to emphasise this point.**

"A problem of this manuscript is the partial lack of novelty. The pattern of oxidized PCBM species obtained by MALDI-TOF is known before[1] (the present manuscript should cite this prior work)."

We thank the Reviewer for pointing out an important reference and we have added it into our manuscript. The key novelty of our paper is the quantitative understanding of the unexpected but important role of fullerenes in determining the environmental stability of organic solar cells, which has not been reported previously. The MALDI-TOF data is not a novelty of the paper and was collected as quantitative evidence of the extent of light and oxygen induced fullerene oxidation, the amount of which is further used for our charge transport and modelling studies. **We have added new text on Page 16 of the main text to emphasise the novelty of the work.**

"Interestingly, Yamane et al. found that the P3HT polymer had beneficial effects suppressing further photooxidation of PCBM. Is the polymer used in this work also a photo-oxidization suppressor agent? We do not know because the experiments in the present manuscript were designed to isolate the negative influence of the polymer deterioration in the efficiency loss of the device. Apparently and according to the results reported, this beneficial role of the polymer as oxygen singlet quencher can be neglected here which is a little contradictory thinking that the polymer used here outperforms P3HT."

We thank the Reviewer for raising an interesting point of the potentially beneficial role of the polymer in preventing the photo-oxidation of PCBM. We have previously reported that amorphous polymers typically have higher oxygen solubility and longer triplet lifetimes than crystalline polymers.[10,11] PCDTBT, despite a higher efficiency, is a more amorphous polymer, which is expected to lead to 1) an increased oxygen concentration and 2) an increased triplet lifetime in the blend film, relative to P3HT. Both factors are expected to increase the likelihood of reactions with oxygen. This agrees with the minimal protection effect from the

polymer observed in the paper. **We have added new text on Page 17 in the main text to emphasise these points.**

Although different polymers might have different effects upon the photo-oxidation of fullerenes, the present work both (1) establishes that fullerene photo-oxidation is severe enough to dominate the degradation of common designs of solar cell prepared in common ambient conditions and (2) is able to isolate the fullerene oxidation from any other possible consequence of oxygen exposure. Neither of these findings had previously been reported and the importance of fullerene oxidation was not widely discussed within the community.

"Also, I have a little concern about how the quantity of O-PCBM is determined. According to the Method section this quantity is obtained by doing "relative semi-quantitative analyses were done via MS Excel" but authors may indicate if they used intensity peak height or peak area."

We used peak area as a measure of the quantity of O-PCBM. **We have addressed this comment on Page 19 of the main text.**

"In fact, I consider that this quantity of O-PCBM is a key insight in this work and it should be further confirmed using another alternative technique as for example in-situ XPS. Probably, PCBM and O-PCBM species have a distinctive signature in the C and O signal in XPS measurements."

We thank the reviewer for suggestions of XPS measurements. We have thus collected additional XPS data on the films aged at different levels. Although the XPS results cannot differentiate the degradation of the polymer and fullerenes, the level of bulk oxygen composition obtained by XPS measurements (~1.5±0.4% for 0 hour, ~4.0±1% for 1 hour and ~5.1±0.8% for 10 hours of degradation) is in good agreement with a steady increase in the concentration of oxidised fullerenes with increasing degradation time with similar amplitudes observed to the MALDI-TOF measurements (~0% for 0 hour, ~0.8% for 1 hour and ~4.3% for 10 hours of degradation). **These results have been added in supplementary information, and briefly discussed on Page 6 of the main text.**

"I consider that another useful information as gradient concentration of O-PCBM species was lost when authors redissolved the blend for MALDI-TOF analysis. Probably, the concentration of O-PCBM species in the outter layers exposed to oxygen and light is higher than inner position in the bulk layer. A XPS analysis eroding the layer could help to obtain this gradient concentration of O-PCBM.XPS data added." "Probably, a trap-model including this non-homogeneous concentration of O-PCBM could match better the experimental results."

The Reviewer raised a good point regarding the depth profile of the O-PCBM species in the film. We have thus performed gas cluster ion source depth profiling XPS measurements to obtain the quantitative compositional data through the bulk of the film. We found that the blend films degraded for 0-10 hours in dry air under light and films containing pre-degraded PCBM both show minimal gradient concentration of O-PCBM species other than a high oxygen composition located at the top surface resulting from unavoidable surface

contamination, hence confirming the relevance of our selective degradation approach to real degradation conditions. The uniform distribution of oxidised defects also justifies the use of a numerical model with a spatially uniform distribution of traps states. We also stress that we applied the numerical model only to experimental data collected on samples made with pre-degraded PCBM, i.e. to cases where the chemical composition of the active layer is the most uniform, and the homogenous trap distribution the most relevant. **The depth profile results have been added to the supplementary information, and briefly discussed on Pages 6-7 of the main text.**

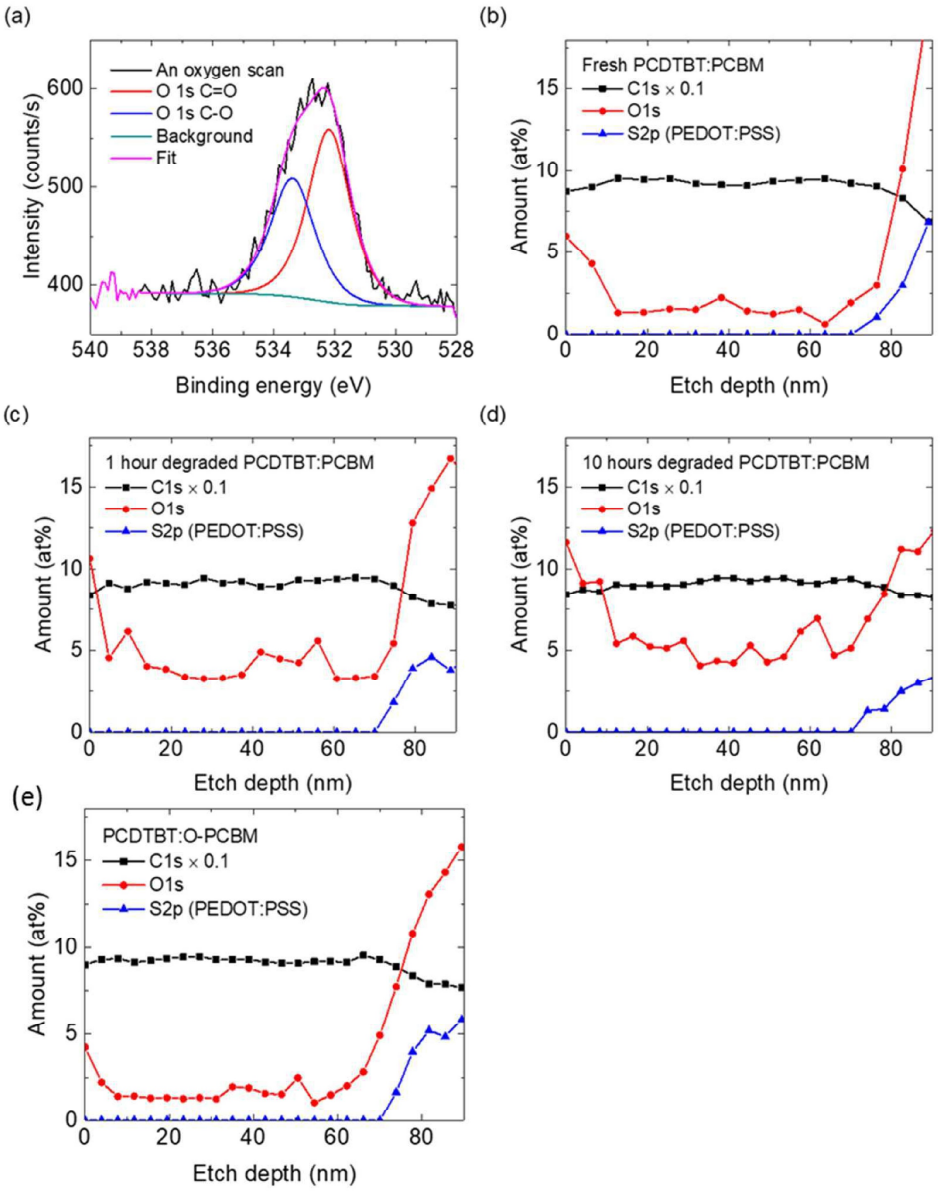

Figure R1 (a) XPS O(1s) spectrum of fresh PCDTBT:PCBM blend films with background and O 1s fitting; XPS C(1s), O(1s) and S(2p) spectrum of (b) fresh PCDTBT:PCBM blend films and PCDTBT:PCBM blend films degraded under one sun in dry air for (c) 1 hour and (d) 10 hours;

(e) XPS C(1s), O(1s) and S(2p) spectrum of PCDTBT:O-PCBM blend films prepared from selectively degraded PCBM.

Reviewer 2:

"This work provides guidance for commercialization of organic solar cells. Therefore, it should be accepted after a revision."

We thank the Reviewer for his or her very positive comments.

"There is no discussion about effects of photo-oxidation PCBM on morphological change. Therefore, we hope that the author could provide the morphology of the blend film with different fractions of photo-oxidation PCBM, like TEM and AFM."

The Reviewer is concerned about the potential morphological changes upon photo-degradation. We have thus performed AFM measurements to investigate the nanoscale morphology of the films. These studies reveal minimal changes in the film morphology upon photo-degradation. **These results have been added to the supplementary information, and are briefly discussed on Page 6 of the main text.**

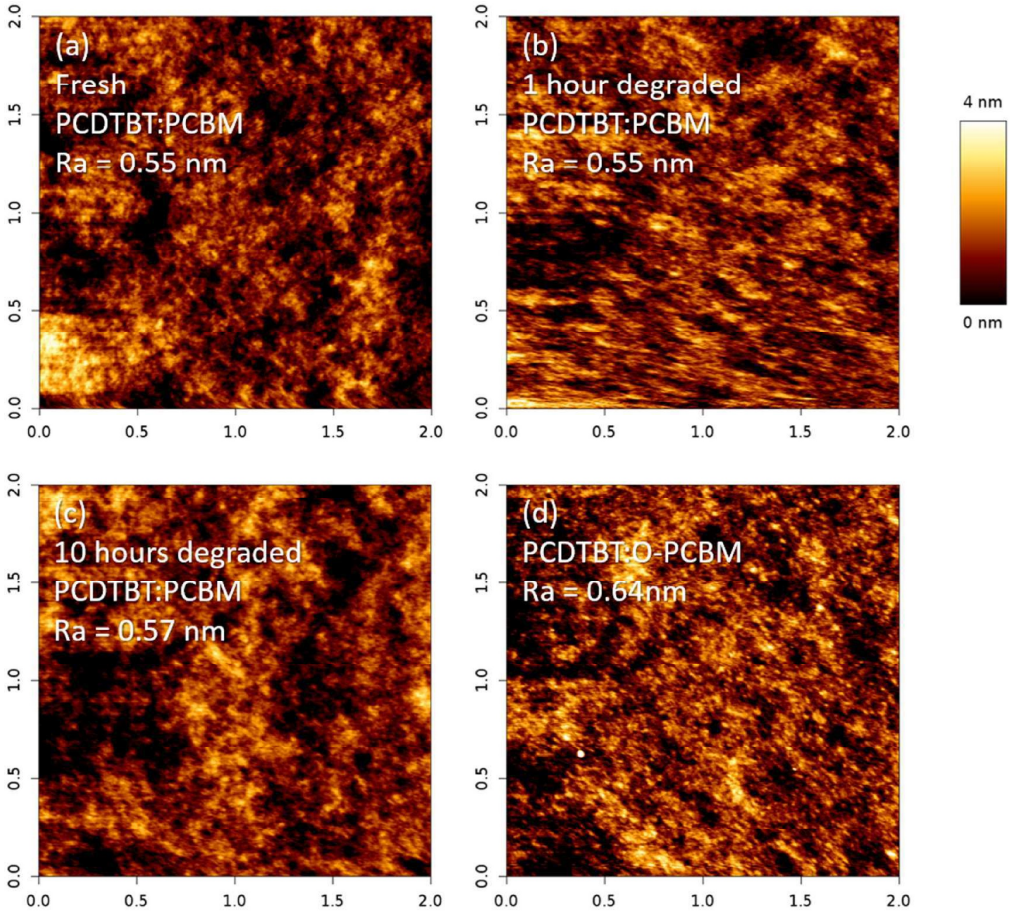

Figure R2 AFM height images and average roughness analysis of (a) fresh PCDTBT:PCBM blend films; PCDTBT:PCBM blend films degraded under one sun in dry air for (b) 1 hour and (c) 10 hours; and (d) PCBM degraded in solution under one sun in dry air for 72 hours.

Reviewer 3:

"This manuscript covers an important topic in OPVs and can reach the bar needed to warrant publication in EES"

We thank the Reviewer for his or her very positive comments.

"Most notably, the depth profile analysis is unclear in the current version. Either a more robust description of the analysis should be provided to give the reader high confidence in the quantitative accuracy, or additional characterization methods should be applied (e.g. XPS)."

We have addressed this comment in our response to Reviewer 1's comments, where we report the depth profile and XPS characterisation of our films.

"The authors are well versed on morphology characterization in such systems. This would indeed also add some value as suggested by one of the reviewers, but this could be considered less important than the earlier comment."

We have addressed this comment in our response to Reviewer 2's comments, where we report on surface morphology characterisation of our samples using AFM.

References

1 Heumueller, T. *et al.* Reducing burn-in voltage loss in polymer solar cells by increasing the polymer crystallinity. *Energy & Environmental Science* **7**, 2974-2980, doi:10.1039/C4EE01842G (2014).

2 Heumueller, T. *et al.* Morphological and electrical control of fullerene dimerization determines organic photovoltaic stability. *Energy & Environmental Science* **9**, 247-256, doi:10.1039/C5EE02912K (2016).

3 Wood, S. *et al.* Natures of optical absorption transitions and excitation energy dependent photostability of diketopyrrolopyrrole (DPP)-based photovoltaic copolymers. *Energy & Environmental Science* **8**, 3222-3232, doi:10.1039/C5EE01974E (2015).

4 Li, Z. *et al.* Performance enhancement of fullerene-based solar cells by light processing. *Nat. Commun.* **4:2227** (2013).

5 Hoke, E. T. *et al.* The Role of Electron Affinity in Determining Whether Fullerenes Catalyze or Inhibit Photooxidation of Polymers for Solar Cells. *Advanced Energy Materials* **2**, 1351-1357, doi:10.1002/aenm.201200169 (2012).

6 Baran, D. *et al.* Reducing the efficiency–stability–cost gap of organic photovoltaics with highly efficient and stable small molecule acceptor ternary solar cells. *Nature Materials* **16**, 363, doi:10.1038/nmat4797 (2016).

7 Holliday, S. *et al.* High-efficiency and air-stable P3HT-based polymer solar cells with a new non-fullerene acceptor. *Nature Communications* **7**, 11585, doi:10.1038/ncomms11585 (2016).

8 Zhao, W. *et al.* Fullerene-Free Polymer Solar Cells with over 11% Efficiency and Excellent Thermal Stability. *Advanced Materials* **28**, 4734-4739, doi:10.1002/adma.201600281 (2016).

9 Cha, H. *et al.* An Efficient, "Burn in" Free Organic Solar Cell Employing a Nonfullerene Electron Acceptor. *Advanced Materials* **29**, 1701156-n/a, doi:10.1002/adma.201701156 (2017).

10 Soon, Y. W. *et al.* Correlating triplet yield, singlet oxygen generation and photochemical stability in polymer/fullerene blend films. *Chemical Communications (Cambridge, United Kingdom)* **49**, 1291-1293, doi:10.1039/c2cc38243a (2013).

11 Soon, Y. W. *et al.* Material Crystallinity as a Determinant of Triplet Dynamics and Oxygen Quenching in Donor Polymers for Organic Photovoltaic Devices. *Advanced Functional Materials*, n/a-n/a, doi:10.1002/adfm.201302612 (2013).

Supplementary Information of

The Role of Fullerenes in Environmental Stability of Polymer:Fullerene Solar Cells

Harrison K. H. Lee, Andrew M. Telford, Jason A. Röhr, Mark F. Wyatt, Beth Rice, Jiaying Wu, Alexandre de Castro Maciel, Sachetan M. Tuladhar, Emily Speller, James McGettrick, Justin R. Searle, Sebastian Pont, Trystan Watson, Thomas Kirchartz, James R. Durrant, Wing C. Tsoi, Jenny Nelson* and Zhe Li*

*Corresponding authors

Supplementary Table 1 Summary of device parameters of ITO/PEDOT:PSS/PCDTBT:PCBM(1:2)/Ca/Al devices with different degradation times under simulated AM1.5G illumination in air, before top electrode deposition.

Film degradation time (mins)	J_{sc} (mA/cm^2)	V_{oc} (V)	FF (%)	PCE (%)
0	8.13	0.928	61.5	5.01
10	7.09	0.868	46.5	3.19
30	4.96	0.823	42.4	1.93
60	3.83	0.782	40.5	1.35
600	0.95	0.488	39.5	0.20

Supplementary Table 2 Summary of device parameters of PCDTBT:PCBM devices exposed to air for 60 minutes in the dark and under 1000 lux of compact fluorescent lamp.

Film degradation condition	J_{sc} (mA/cm^2)	V_{oc} (V)	FF (%)	PCE (%)
Fresh	8.13	0.928	61.5	5.01
60 mins under 1000 lux fluorescent lamp in air	7.60	0.903	54.1	4.10
60 mins in dark in air	7.73	0.932	64.5	5.18

Supplementary Table 3 Summary of device parameters of PCDTBT:PCBM blend devices PCDTBT:PCBM blend devices made with different fractions of degraded PCBM, the percentages indicating the relative fraction of O-PCBM in the acceptor phase.

O-PCBM (%)	J_{sc} (mA/cm^2)	V_{oc} (V)	FF (%)	PCE (%)
0	8.13	0.928	61.5	5.01
0.2	6.76	0.885	51.4	3.69
0.4	6.08	0.852	45.7	2.85
0.9	4.42	0.795	42.2	1.78
1.8	3.17	0.740	42.0	1.18
3.6	2.14	0.617	39.8	0.63

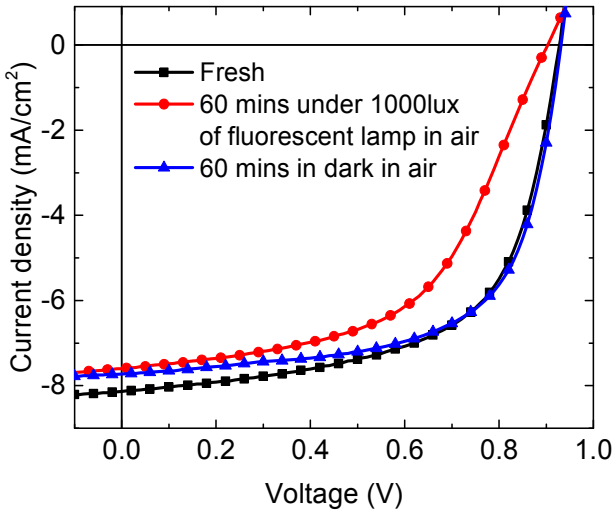

Supplementary Figure 1 *J–V* characteristic of PCDTBT:PCBM devices exposed to air for 60 minutes in the dark and under 1000 lux of compact fluorescent lamp.

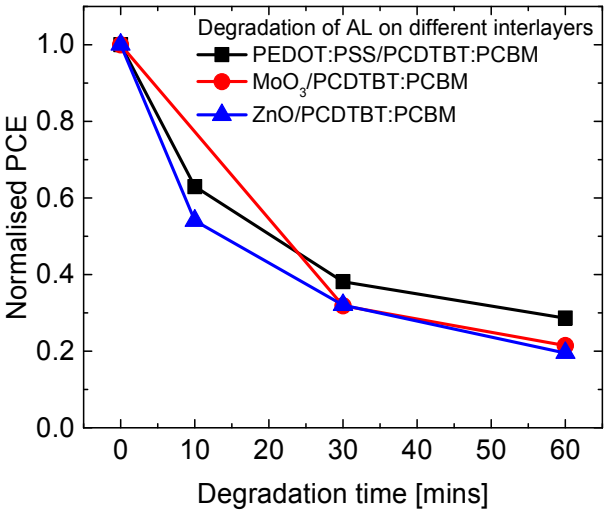

Supplementary Figure 2 Normalised PCE of PCDTBT:PCBM devices with active layers degraded on different interlayers, PEDOT:PSS, MoO_3, and ZnO. The devices using PEDOT:PSS and MoO_3 are finished by Ca/Al as top electrode; the devices using ZnO are finished by MoO_3/Ag as top electrode. The PCEs of the fresh devices using PEDOT:PSS, MoO_3, and ZnO are 5.01%, 4.73%, and 4.43%, respectively.

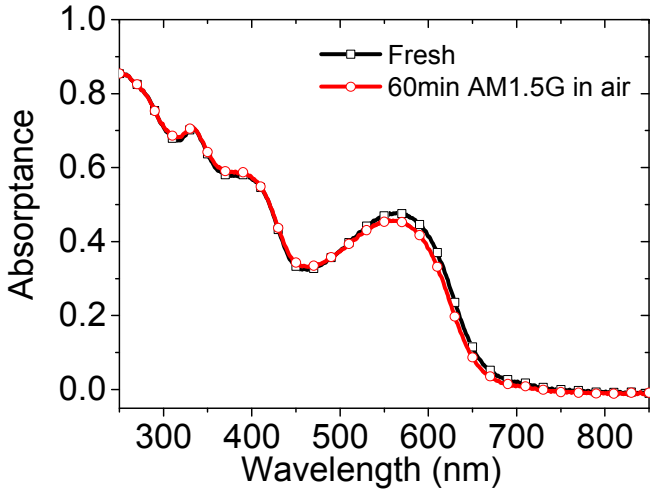

Supplementary Figure 3 UV-visible spectra of PCDTBT:PCBM blend films without and with 60 minutes of exposure to AM1.5G conditions in dry air.

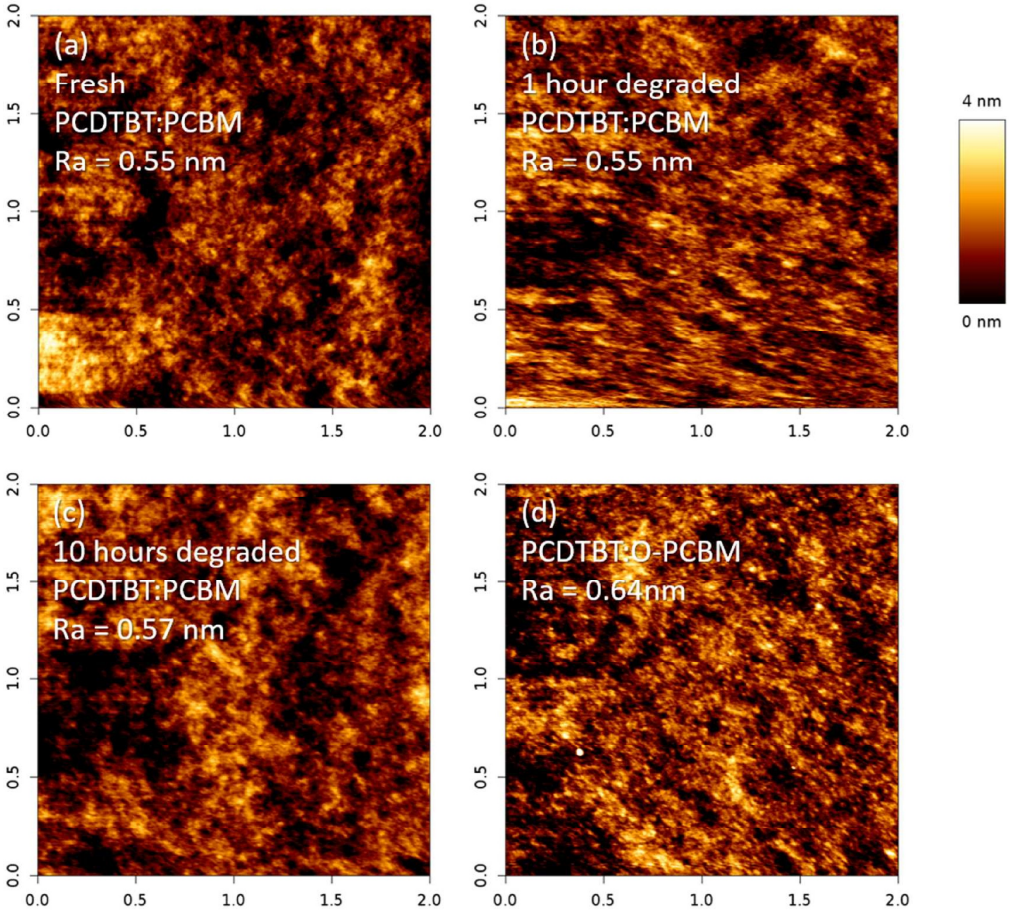

Supplementary Figure 4 AFM height images and average roughness analysis of (a) fresh PCDTBT:PCBM blend films; PCDTBT:PCBM blend films degraded under one sun in dry air for (b) 1 hour and (c) 10 hours; and (d) PCBM degraded in solution under one sun in dry air for 72 hours.

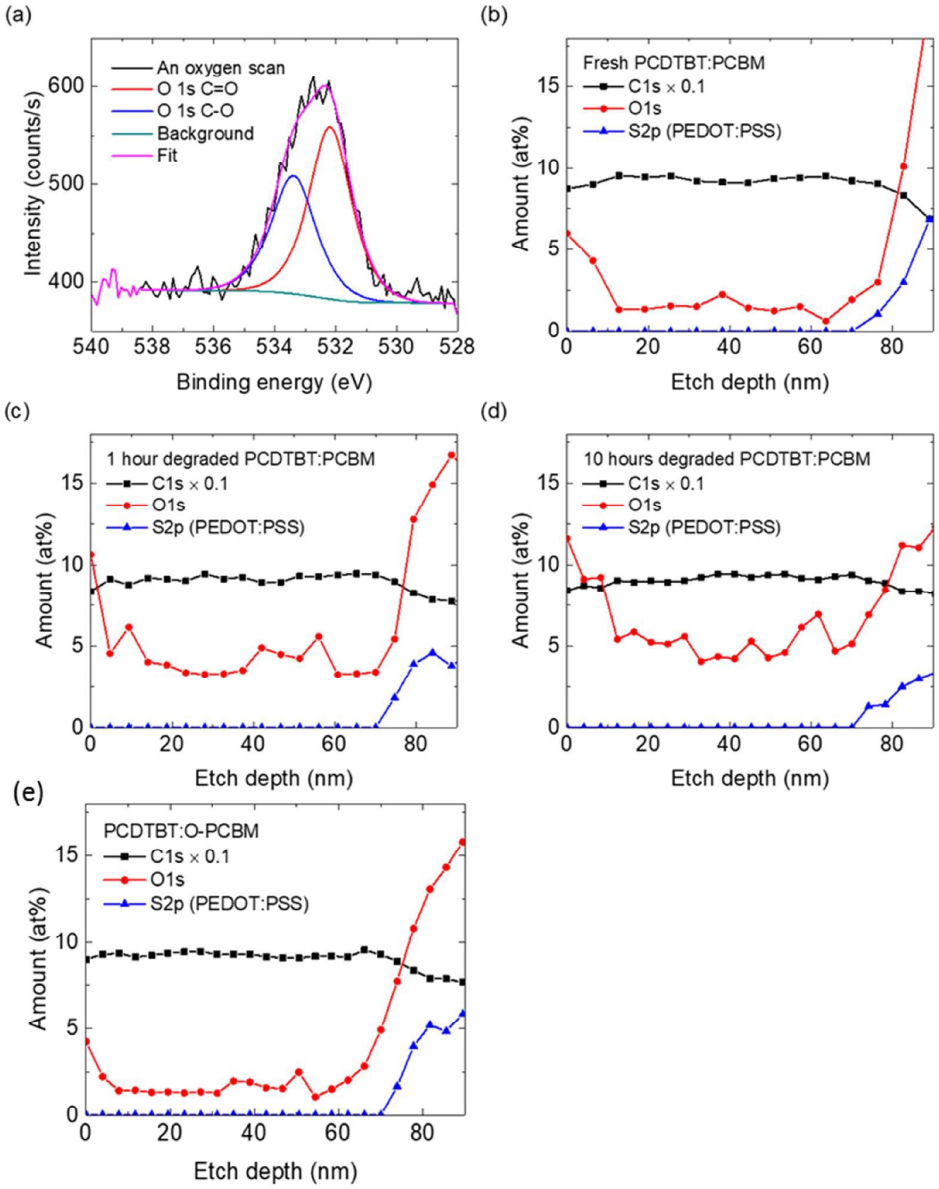

Supplementary Figure 5 (a) XPS O(1s) spectrum of fresh PCDTBT:PCBM blend films with background and O 1s fitting; XPS C(1s), O(1s) and S(2p) spectrum of (b) fresh PCDTBT:PCBM blend films and PCDTBT:PCBM blend films degraded under one sun in dry air for (c) 1 hour and (d) 10 hours; (e) XPS C(1s), O(1s) and S(2p) spectrum of PCDTBT:O-PCBM blend films prepared from selectively degraded PCBM.

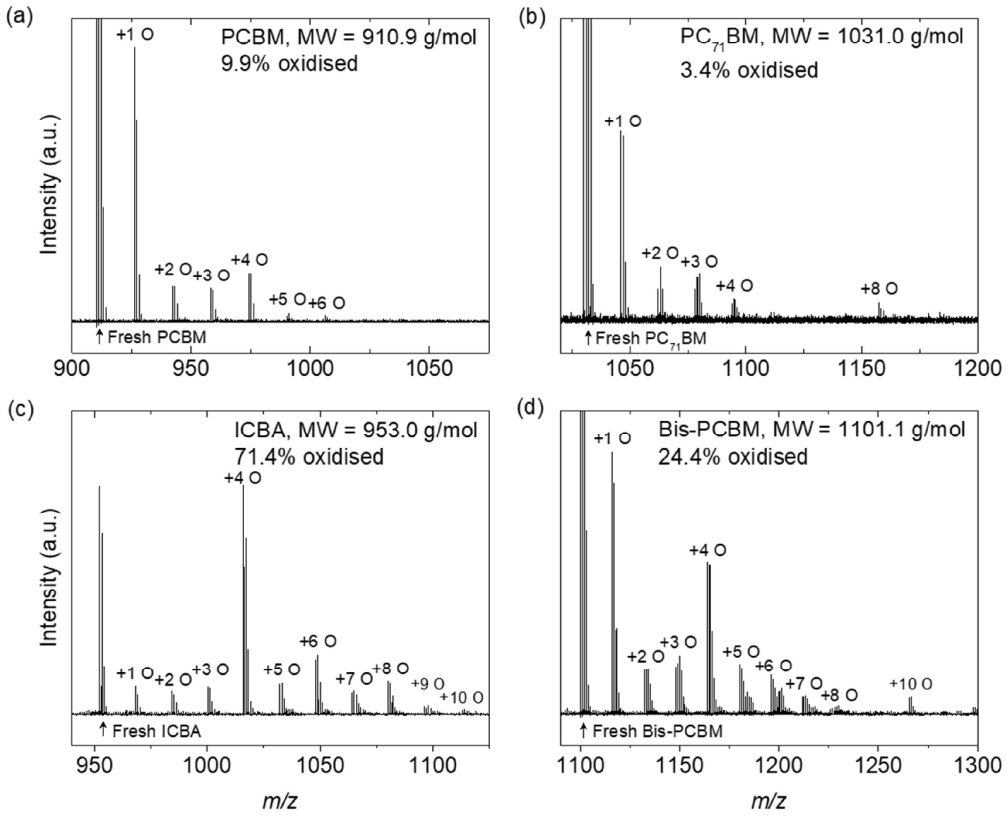

Supplementary Figure 6 MALDI-TOF measurement of (a) PCBM; (b) [6,6]-Phenyl C_{71} butyric acid methyl ester ($PC_{71}BM$); (c) indene-C_{60} bis-adduct (ICBA); and (d) Bis(1-[3-(methoxycarbonyl)propyl]-1-phenyl)-[6,6]C_{62} (Bis-PCBM) degraded in films under one sun in air for 32 hours.

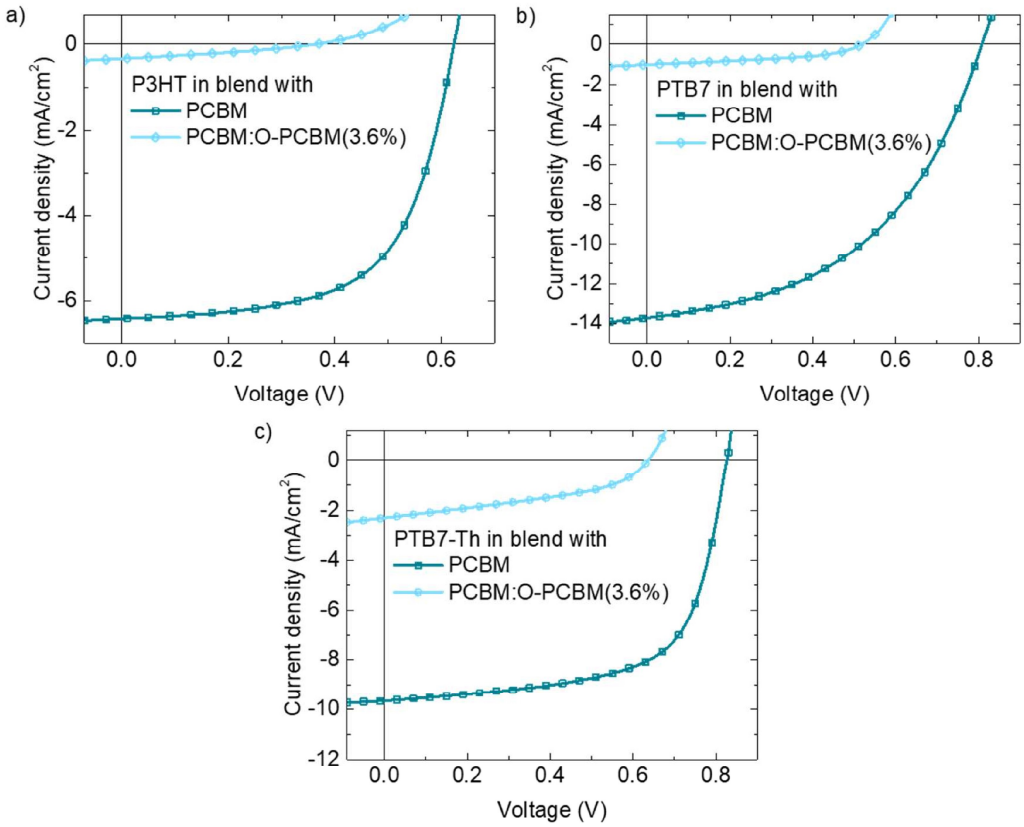

Supplementary Figure 7 *J-V* characteristic of devices using different OPV benchmark polymers (a) P3HT, (b) PTB7, and (c) PTB7-Th (also called PCE10) in blend with fresh PCBM and selectively degraded PCBM containing 3.6% of O-PCBM.

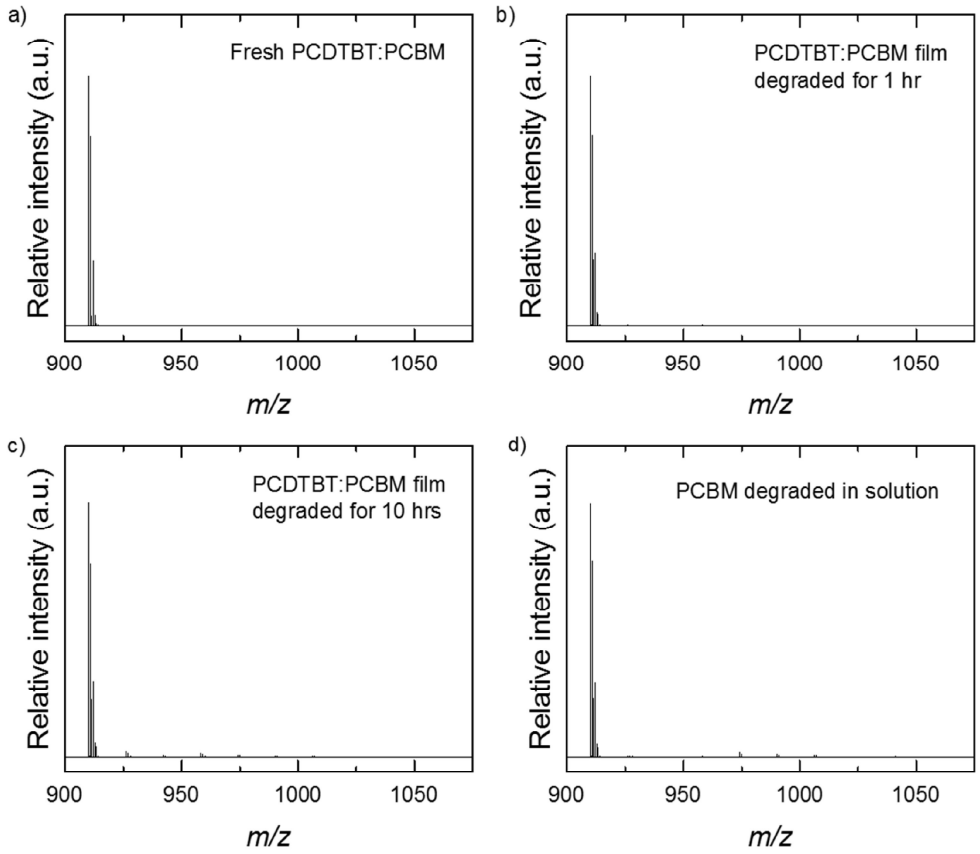

Supplementary Figure 8 Full scale MALDI-TOF measurement of (a) fresh PCDTBT:PCBM blend; (b) PCDTBT:PCBM blend film degraded under one sun in air for 1 hour; (c) PCDTBT:PCBM blend film degraded one sun in air for 10 hour; and (d) PCBM degraded in solution under one sun in air. The main peaks at 910.1 in the plots indicate the PCBM molecules.

HOMO and LUMO simulations on PCBM with multiple defects

Comparison of HOMO-LUMO simulation methods

The HOMO and LUMO levels were calculated with three different methods: (i) delta SCF (see main text); (ii) taking the Kohn-Sham orbitals; (iii) taking the Kohn-Sham orbital for the HOMO and Kohn-Sham HOMO plus the first excitation energy from TD-DFT for the LUMO. All the calculations are done with Gaussian 09, at the B3LYP level of theory with the 6-31g* basis set. The Kohn-Sham orbitals are obtained from a single point energy calculation on the optimised structure. The TD-DFT calculation yields the excitation energies and the first of these is taken to be added to the Kohn-Sham HOMO energy to obtain the LUMO energy.

The levels were also calculated for PCBM with multiple defects: two epoxide defects, one epoxide and one carbonyl defect, and one epoxide and two carbonyl defects. All defects lower the LUMO level and have a small effect on the HOMO level.

The numbering of the position of a PCBM molecule are shown below:

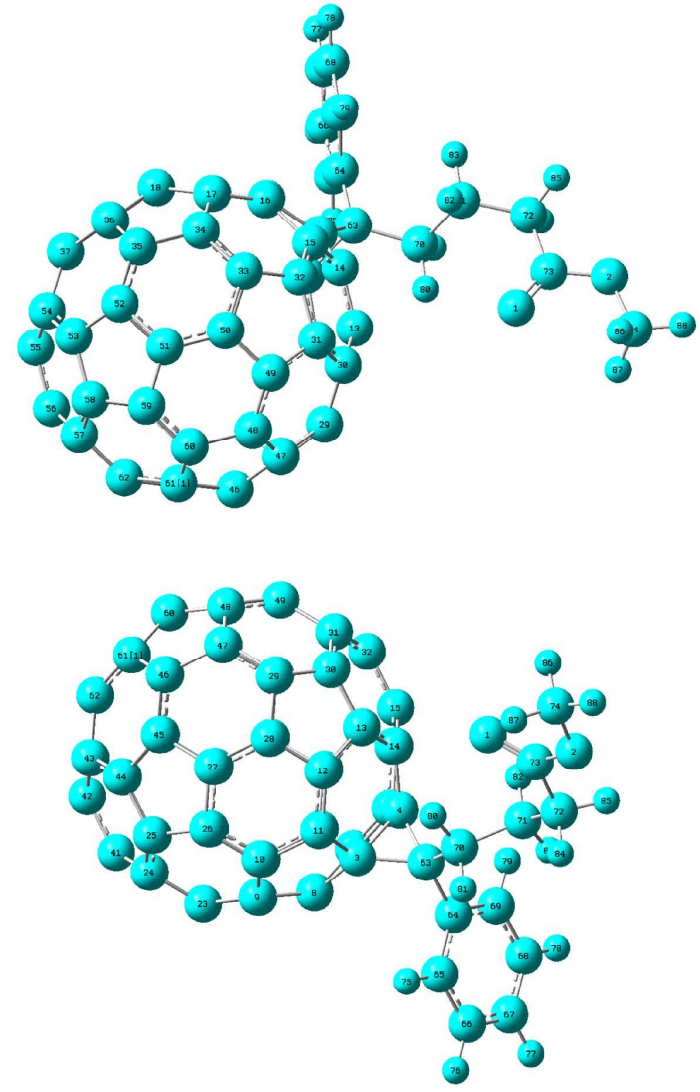

Supplementary Table 4 Delta-SCF HOMO and LUMO simulations of PCBM and PCBM with different oxygen defects. The values marked in red mean the energy levels go down.

Defect type	Defect position on the PCBM	HOMO from delta-SCF (eV)	Change in HOMO (eV)	HOMO from delta-SCF (eV)	Change in LUMO (eV)
No defect	N/A	-6.72	N/A	-1.83	N/A
One epoxide	11,12	-6.77	-0.05	-2.02	-0.19
	7,8	-6.74	-0.02	-2.03	-0.20
	13,14	-6.76	-0.04	-2.02	-0.19
	5,6	-6.77	-0.05	-2.05	-0.22
	24,25	-6.72	-0.01	-1.81	0.02
	33,34	-6.72	0.00	-1.82	0.01
	55,56	-6.72	0.00	-2.05	-0.22
	16,17	-6.73	-0.01	-2.00	-0.17
	20,38	-6.61	0.11	-1.80	0.03
	29,47	-6.59	0.13	-1.80	0.04
	27,28	-6.59	0.12	-1.83	0.00
	48,49	-6.64	0.08	-1.86	-0.03
	15,32	-6.72	0.00	-2.00	-0.17
	21,22	-6.61	0.11	-1.84	-0.01
	30,31	-6.60	0.12	-1.82	0.01
	10,26	-6.71	0.01	-2.00	-0.17
	39,40	-6.65	0.07	-1.85	-0.02
	9,23	-6.72	0.00	-2.00	-0.17
	45,46	-6.64	0.08	-1.86	-0.03
	36,37	-6.66	0.06	-1.85	-0.02
	57,58	-6.74	-0.02	-2.04	-0.21
	61,62	-6.70	0.02	-2.07	-0.24
	59,60	-6.70	0.02	-2.08	-0.25
	53,54	-6.71	0.01	-2.06	-0.23
	41,42	-6.69	0.02	-1.89	-0.06
	43,44	-6.69	0.02	-1.90	-0.06
	50,51	-6.69	0.03	-1.89	-0.06
	35,52	-6.69	0.03	-1.90	-0.07
	18,19	-6.52	0.20	-1.76	0.07
One Carbonyl	13,14	-6.52	0.20	-2.10	-0.27
	11,12	-6.52	0.20	-2.09	-0.26
	7,8	-6.53	0.19	-2.13	-0.30
	16,17	-6.52	0.20	-2.21	-0.38
	10,26	-6.46	0.26	-2.21	-0.38
	20,38	-6.36	0.35	-2.11	-0.28
	29,47	-6.34	0.38	-2.11	-0.28
	9,23	-6.49	0.22	-2.19	-0.36
	15,32	-6.52	0.20	-2.20	-0.37
	21,22	-6.44	0.28	-2.23	-0.39
	33,34	-6.57	0.15	-2.10	-0.27

	24,25	-6.57	0.15	-2.08	-0.25
	27,28	-6.42	0.30	-2.23	-0.40
	18,19	-6.46	0.26	-2.22	-0.39
	30,31	-6.42	0.30	-2.23	-0.40
	39,40	-6.44	0.28	-2.17	-0.34
	45,46	-6.42	0.30	-2.17	-0.34
	48,49	-6.42	0.30	-2.17	-0.34
	36,37	-6.45	0.27	-2.18	-0.35
	41,42	-6.45	0.27	-2.19	-0.36
	43,44	-6.45	0.27	-2.20	-0.37
	50,51	-6.44	0.28	-2.20	-0.37
	59,60	-6.44	0.28	-2.32	-0.49
	55,56	-6.46	0.26	-2.32	-0.49
	53,54	-6.45	0.28	-2.32	-0.49
	61,62	-6.45	0.27	-2.32	-0.49
	5,6	-6.59	0.13	-2.27	-0.43
	35,52	-6.46	0.26	-2.18	-0.35
	57,58	-6.47	0.25	-2.22	-0.39
Two epoxides	11,12/13,14	-6.68	0.04	-2.25	-0.41
	5,6/7,8	-6.69	0.03	-2.27	-0.44
	11,12/10,26	-6.70	0.02	-2.03	-0.20
	11,12/7,8	-6.74	-0.02	-2.14	-0.31
	5,6/13,14	-6.73	-0.01	-2.16	-0.33
	5,6/20,38	-6.73	-0.01	-2.04	-0.21
Two carbonyls	11,12	-6.74	-0.02	-2.52	-0.69
	20,38	-6.56	0.15	-2.62	-0.79
	29,47	-6.54	0.18	-2.62	-0.79
	16,17	-6.73	-0.01	-2.66	-0.83
	10,26	-6.70	0.02	-2.69	-0.86
	24,25	-6.71	0.01	-2.64	-0.81
	45,46	-6.63	0.09	-2.71	-0.88
	36,37	-6.65	0.07	-2.72	-0.88
	43,44	-6.67	0.05	-2.70	-0.87
	59,60	-6.66	0.06	-2.80	-0.97
	35,52	-6.67	0.05	-2.71	-0.88
	18,19	-6.57	0.15	-2.91	-1.08
	53,54	-6.67	0.05	-2.80	-0.96
	27,28	-6.54	0.18	-2.90	-1.07
	5,6	-6.75	-0.03	-2.67	-0.84
	57,58	-6.69	0.03	-2.74	-0.91
One epoxide and one carbonyl	10,26/24,25	-6.61	0.11	-2.08	-0.25
	10,26/7,8	-6.53	0.19	-2.23	-0.40
	10,26/30,31	-6.43	0.29	-2.39	-0.56
	10,26/20,38	-6.41	0.31	-2.28	-0.45
	10,26/31,30	-6.43	0.29	-2.47	-0.64
	10,26/52,35	-6.40	0.32	-2.34	-0.51
One epoxide	11,12/10,26	-6.76	-0.05	-2.48	-0.65

and two carbonyls	11,12/27,28	-6.79	-0.07	-2.56	-0.73
	11,12/29,47	-6.75	-0.03	-2.65	-0.82
	11,12/43,44	-6.60	0.12	-2.81	-0.98
	11,12/59,60	-6.69	0.03	-2.85	-1.01
	11,12/15,32	-6.72	0.00	-2.81	-0.98
One diol	11,12	-5.65	1.07	-2.13	-0.30
	10,26	-5.93	0.79	-2.41	-0.58
	18,19	-5.99	0.73	-2.15	-0.32
	27,28	-5.97	0.75	-2.13	-0.30
	24,25	-5.78	0.94	-2.21	-0.38
	16,17	-5.86	0.86	-2.76	-0.93
	29,47	-6.11	0.61	-2.69	-0.85
	20,38	-6.13	0.59	-2.69	-0.86
	45,46	-5.88	0.84	-2.38	-0.55
	36,37	-5.89	0.82	-2.38	-0.55
	35,52	-5.93	0.79	-2.37	-0.54
	59,60	-6.07	0.65	-2.60	-0.77
	43,44	-5.99	0.73	-2.67	-0.84
	53,54	-6.23	0.48	-2.78	-0.95
	57,58	-6.03	0.69	-2.45	-0.62
	5,6	-5.80	0.91	-2.36	-0.53

Supplementary Table 5 Kohn-Sham HOMO and LUMO simulations of PCBM and PCBM with different oxygen defects. The values marked in red mean the energy levels go down.

Defect type	Defect position on the PCBM	HOMO from Kohn-Sham (eV)	Change in HOMO (eV)	LUMO from Kohn-Sham LUMO (eV)	Change in LUMO (eV)
No defect	N/A	-5.56	N/A	-3.00	N/A
One epoxide	11,12	-5.62	-0.06	-3.16	-0.16
	7,8	-5.61	-0.05	-3.17	-0.17
	13,14	-5.61	-0.05	-3.16	-0.16
	5,6	-5.64	-0.08	-3.19	-0.19
	24,25	-5.58	-0.02	-2.95	0.05
	33,34	-5.57	-0.01	-2.95	0.05
	55,56	-5.58	-0.02	-3.19	-0.19
	16,17	-5.59	-0.03	-3.13	-0.13
	20,38	-5.48	0.08	-2.94	0.06
	29,47	-5.46	0.10	-2.93	0.07
	27,28	-5.47	0.09	-2.97	0.03
	48,49	-5.50	0.06	-3.00	0.00
	15,32	-5.58	-0.02	-3.13	-0.13
	21,22	-5.48	0.08	-2.98	0.02
	30,31	-5.47	0.09	-2.96	0.04
	10,26	-5.58	-0.02	-3.13	-0.13
	39,40	-5.52	0.04	-2.99	0.01
	9,23	-5.58	-0.02	-3.14	-0.14
	45,46	-5.51	0.05	-3.00	0.00
	36,37	-5.52	0.04	-2.99	0.01
	57,58	-5.57	-0.01	-3.18	-0.18
	61,62	-5.56	0.00	-3.21	-0.21
	59,60	-5.56	0.00	-3.22	-0.22
	53,54	-5.56	0.00	-3.20	-0.20
	41,42	-5.55	0.01	-3.03	-0.03
	43,44	-5.55	0.01	-3.04	-0.04
	50,51	-5.54	0.02	-3.04	-0.04
	35,52	-5.54	0.02	-3.04	-0.04
	18,19	-5.39	0.17	-2.90	0.10
One carbonyl	13,14	-5.39	0.17	-3.21	-0.21
	11,12	-5.39	0.17	-3.21	-0.21
	7,8	-5.39	0.17	-3.25	-0.25
	16,17	-5.38	0.18	-3.33	-0.33
	10,26	-5.33	0.23	-3.34	-0.34
	20,38	-5.24	0.32	-3.27	-0.27
	29,47	-5.22	0.34	-3.26	-0.26
	9,23	-5.38	0.18	-3.33	-0.33
	15,32	-5.41	0.15	-3.34	-0.34
	21,22	-5.33	0.23	-3.34	-0.34
	33,34	-5.44	0.12	-3.24	-0.24

	24,25	-5.44	0.12	-3.22	-0.22
	27,28	-5.31	0.25	-3.34	-0.34
	18,19	-5.34	0.22	-3.34	-0.34
	30,31	-5.31	0.25	-3.34	-0.34
	39,40	-5.32	0.24	-3.32	-0.32
	45,46	-5.30	0.26	-3.32	-0.32
	48,49	-5.30	0.26	-3.32	-0.32
	36,37	-5.32	0.24	-3.33	-0.33
	41,42	-5.31	0.25	-3.35	-0.35
	43,44	-5.31	0.25	-3.35	-0.35
	50,51	-5.31	0.25	-3.35	-0.35
	59,60	-5.30	0.26	-3.46	-0.46
	55,56	-5.32	0.24	-3.46	-0.46
	53,54	-5.31	0.25	-3.46	-0.46
	61,62	-5.31	0.25	-3.47	-0.47
	5,6	-5.46	0.10	-3.37	-0.37
	35,52	-5.32	0.24	-3.33	-0.33
	57,58	-5.33	0.23	-3.37	-0.37
Two epoxides	11,12/13,14	-5.54	0.02	-3.38	-0.38
	5,6/7,8	-5.56	0.00	-3.40	-0.40
	11,12/10,26	-5.56	0.00	-3.17	-0.17
	11,12/7,8	-5.60	-0.04	-3.28	-0.28
	5,6/13,14	-5.60	-0.04	-3.29	-0.29
	5,6/20,38	-5.60	-0.04	-3.16	-0.16
One epoxide, one carbonyl	10,26/24,25	-5.48	0.08	-3.23	-0.23
	10,26/7,8	-5.40	0.16	-3.35	-0.35
	10,26/30,31	-5.33	0.23	-3.50	-0.50
	10,26/20,38	-5.29	0.27	-3.43	-0.43
	10,26/31,30	-5.33	0.23	-3.59	-0.59
	10,26/52,35	-5.27	0.29	-3.50	-0.50
One epoxide, two carbonyls	11,12/10,26	-5.63	-0.07	-3.61	-0.61
	11,12/27,28	-5.67	-0.11	-3.71	-0.71
	11,12/29,47	-5.62	-0.06	-3.80	-0.80
	11,12/43,44	-5.48	0.08	-3.96	-0.96
	11,12/59,60	-5.56	0.00	-4.00	-1.00
	11,12/15,32	-5.59	-0.03	-3.94	-0.94
Two Carbonyls	11,12	-5.61	-0.05	-3.64	-0.64
	20,38	-5.45	0.11	-3.78	-0.78
	29,47	-5.42	0.14	-3.77	-0.77
	16,17	-5.60	-0.04	-3.80	-0.80
	10,26	-5.58	-0.02	-3.83	-0.83
	24,25	-5.58	-0.02	-3.79	-0.79
	45,46	-5.51	0.05	-3.86	-0.86
	36,37	-5.53	0.03	-3.87	-0.87
	43,44	-5.54	0.02	-3.87	-0.87
	59,60	-5.53	0.03	-3.96	-0.96
	35,52	-5.54	0.02	-3.87	-0.87

	18,19	-5.47	0.09	-4.06	-1.06
	53,54	-5.53	0.03	-3.95	-0.95
	27,28	-5.43	0.13	-4.05	-1.05
	5,6	-5.67	-0.11	-3.78	-0.78
	57,58	-5.55	0.01	-3.91	-0.91
Diol	11,12	-4.67	0.89	-3.00	0.00
	10,26	-4.90	0.66	-3.33	-0.33
	18,19	-5.00	0.56	-3.06	-0.06
	27,28	-4.98	0.58	-3.04	-0.04
	24,25	-4.80	0.76	-3.10	-0.10
	16,17	-5.07	0.49	-3.61	-0.61
	29,47	-4.99	0.57	-3.61	-0.61
	20,38	-5.02	0.54	-3.63	-0.63
	45,46	-4.89	0.67	-3.27	-0.27
	36,37	-4.90	0.66	-3.27	-0.27
	35,52	-4.91	0.65	-3.31	-0.31
	59,60	-5.09	0.47	-3.47	-0.47
	43,44	-5.11	0.45	-3.58	-0.58
	53,54	-5.16	0.40	-3.68	-0.68
	57,58	-5.05	0.51	-3.35	-0.35
	5,6	-4.85	0.71	-3.23	-0.23

Supplementary Table 6 Kohn-Sham HOMO and TD-DFT LUMO simulations of PCBM and PCBM with different oxygen defects. The values marked in red mean the energy levels go down.

Defect type	Defect position on the PCBM	Kohn-Sham HOMO (eV)	Change in HOMO (eV)	1st excited state energy (eV)	TD-DFT LUMO (eV)	Change in LUMO (eV)
No defect	N/A	-5.56	N/A	1.93	-3.63	N/A
One epoxide	11,12	-5.62	-0.06	1.85	-3.77	-0.14
	7,8	-5.61	-0.05	1.84	-3.77	-0.14
	13,14	-5.61	-0.05	1.84	-3.77	-0.14
	5,6	-5.64	-0.07	1.85	-3.79	-0.15
	24,25	-5.58	-0.02	2.03	-3.55	0.08
	33,34	-5.57	-0.01	2.02	-3.55	0.08
	55,56	-5.58	-0.02	1.78	-3.80	-0.17
	16,17	-5.59	-0.03	1.84	-3.75	-0.12
	20,38	-5.48	0.08	1.93	-3.55	0.08
	29,47	-5.46	0.10	1.92	-3.53	0.10
	27,28	-5.47	0.10	1.89	-3.58	0.05
	48,49	-5.50	0.06	1.90	-3.61	0.03
	15,32	-5.58	-0.02	1.83	-3.75	-0.12
	21,22	-5.48	0.08	1.89	-3.59	0.04
	30,31	-5.47	0.09	1.90	-3.57	0.06
	10,26	-5.58	-0.01	1.82	-3.75	-0.12
	39,40	-5.52	0.05	1.93	-3.59	0.04
	9,23	-5.58	-0.02	1.83	-3.75	-0.12
	45,46	-5.51	0.05	1.90	-3.60	0.03
	36,37	-5.52	0.04	1.93	-3.59	0.04
	57,58	-5.57	-0.01	1.77	-3.80	-0.17
	61,62	-5.56	0.00	1.74	-3.82	-0.19
	59,60	-5.56	0.01	1.73	-3.82	-0.19
	53,54	-5.56	0.00	1.75	-3.81	-0.18
	41,42	-5.55	0.02	1.90	-3.65	-0.02
	43,44	-5.55	0.01	1.89	-3.65	-0.02
	50,51	-5.54	0.02	1.89	-3.65	-0.02
	35,52	-5.54	0.02	1.89	-3.65	-0.02
	18,19	-5.39	0.17	1.87	-3.51	0.12
Two Carbonyls	11,12	-5.61	-0.05	1.39	-4.22	-0.59
	20,38	-5.45	0.12	1.03	-4.42	-0.79
	29,47	-5.42	0.14	1.01	-4.41	-0.78
	16,17	-5.60	-0.04	0.97	-4.63	-1.00
	10,26	-5.58	-0.02	0.99	-4.59	-0.96
	24,25	-5.58	-0.02	1.11	-4.48	-0.85
	45,46	-5.51	0.05	1.05	-4.46	-0.82
	36,37	-5.53	0.03	1.04	-4.49	-0.86
	43,44	-5.54	0.02	1.05	-4.49	-0.86
	59,60	-5.53	0.03	1.12	-4.41	-0.78
	35,52	-5.54	0.03	1.04	-4.49	-0.86

	18,19	-5.47	0.10	0.73	-4.74	-1.11
	53,54	-5.53	0.03	1.01	-4.53	-0.89
	27,28	-5.43	0.13	0.70	-4.74	-1.10
	5,6	-5.67	-0.11	1.07	-4.60	-0.97
	57,58	-5.55	0.01	1.28	-4.27	-0.64
Diol	11,12	-4.67	0.90	1.36	-3.31	0.32
	10,26	-4.90	0.66	1.11	-3.79	-0.16
	18,19	-5.00	0.56	1.47	-3.52	0.11
	27,28	-4.98	0.58	1.46	-3.52	0.11
	24,25	-4.80	0.77	1.47	-3.33	0.30
	16,17	-5.07	0.49	0.84	-4.23	-0.60
	29,47	-4.99	0.57	1.46	-3.53	0.10
	20,38	-5.02	0.54	0.73	-4.29	-0.66
	45,46	-4.89	0.67	1.21	-3.68	-0.05
	36,37	-4.90	0.66	1.20	-3.70	-0.07
	35,52	-4.91	0.65	0.71	-4.21	-0.58
	59,60	-5.09	0.48	1.06	-4.02	-0.39
	43,44	-5.11	0.45	0.88	-4.24	-0.60
	53,54	-5.16	0.40	0.92	-4.24	-0.61
	57,58	-5.05	0.51	1.16	-3.89	-0.26
	5,6	-4.85	0.72	1.37	-3.47	0.16

Supplementary Table 7 Change in HOMO and LUMO levels base on the Boltzmann average. The values marked in red mean the energy levels go down.

Defect type	Change in HOMO (delta-SCF)	Change in LUMO (delta-SCF)	Change in HOMO (Kohn-Sham)	Change in LUMO (Kohn-Sham)	Change in LUMO (TD-DFT)
One epoxide	0.04	-0.10	0.02	-0.07	-0.05
One carbonyl	0.25	-0.36	0.22	-0.33	-0.31
Two epoxides	0.01	-0.32	-0.01	-0.29	-0.29
One epoxide, one carbonyl	0.25	-0.47	0.21	-0.43	-0.43
One epoxide, two carbonyls	0.00	-0.86	-0.03	-0.84	-0.81
Two carbonyls	0.06	-0.88	0.03	-0.87	-0.87
Diol	0.77	-0.62	0.60	-0.60	-0.58

Space charge limited current analysis

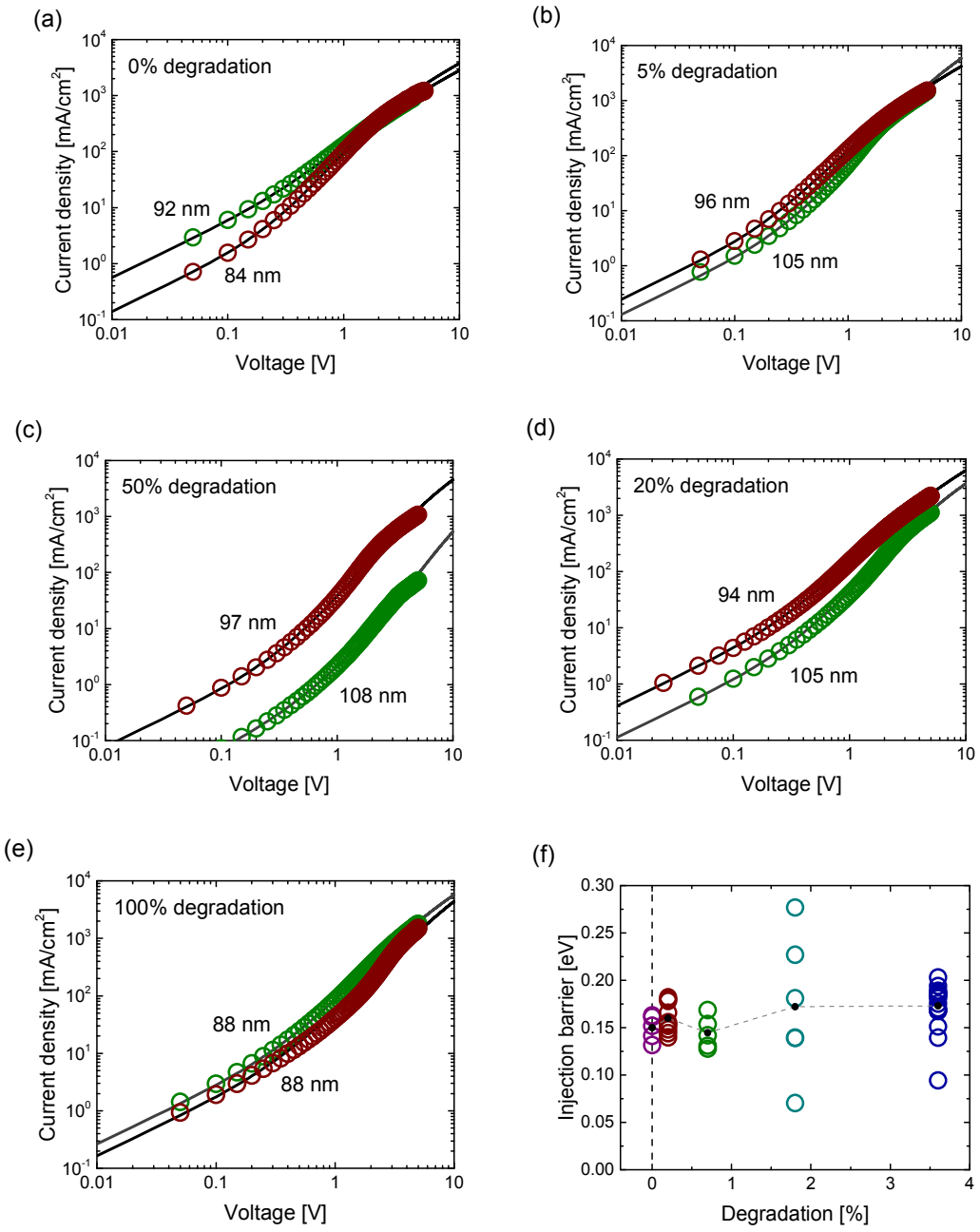

Supplementary Figure 9 (a-e) SCLC current density-voltage data for PCBM electron-only devices with increasing concentrations of O-PCBM. Experimental curves are presented with open circles and the drift-diffusion fits with solid lines. **(f)** Values of the barrier for electron injection into electron only devices containing different fractions of O-PCBM, obtained from the fitting procedure described in the text.

Solar cell *J–V* curve simulations

Both the dark and illuminated solar cell *J-V* curves were simulated using a commercially available drift-diffusion solver called *Advanced Semiconductor Analysis* (ASA) [https://www.cambridge.org/core/journals/journal-of-materials-research/article/optical-and-electrical-modeling-of-thinfilm-silicon-solar-cells/BF97415DB87ACB26ACD99B9FBB32C7B6]. For the illuminated devices, a constant generation rate was chosen to match the current density of the experimental curves when a band gap of 1.4 eV was used. With the presence of a deep Gaussian electron trap level, recombination of trapped electrons and free holes was used along with direct band-to-band recombination. The choice of electron band mobility, Gaussian trap level and Gaussian density was chosen based on the mean values of the SCLC fitting results. All fixed values and varied values are shown in the table below.

Quantity	Value	Units
Fixed values		
Band gap	variable	eV
Effective electron density	10^{19}	cm^{-3}
Effective hole density	10^{19}	cm^{-3}
Dielectric constant	3	-
Active layer thickness	70	nm
Electron band mobility	variable	cm^2/Vs
Hole band mobility	$3 \cdot 10^{-3}$	cm^2/Vs
Injection barrier (electrons)	variable	eV
Injection barrier (holes)	0.2	eV
Gaussian density	variable	cm^{-3}
Gaussian level	variable	eV
Gaussian standard deviation	0.1	eV
Surface recomb. velocity	10^5	m/s
Electron capture rate (neut.)	10^{-10}	$cm^{-3}\,s^{-1}$
Electron capture rate (pos.)	10^{-10}	$cm^{-3}\,s^{-1}$
Hole capture rate (neut.)	10^{-10}	$cm^{-3}\,s^{-1}$
Hole capture rate (neg.)	10^{-10}	$cm^{-3}\,s^{-1}$
Generation rate	$7.7 \cdot 10^{21}$	$cm^{-3}\,s^{-1}$
Direct recombination rate	$7.7 \cdot 10^{-19}$	$cm^{-3}\,s^{-1}$
Series resistance	$3.07 \cdot 10^{-4}$	Ωm^2
Shunt resistance	0.29	Ωm^2
0% O-PCBM device		
Band gap	1.398	eV
Injection barrier	0.2	eV
Electron band mobility	$8.2 \cdot 10^{-4}$	cm^2/Vs
Gaussian density	$2.4 \cdot 10^{16}$	cm^{-3}
Gaussian level	-0.2073	eV
1.8% O-PCBM device		
Band gap	1.363	eV
Injection barrier	0.165	eV
Electron band mobility	$8.8 \cdot 10^{-4}$	cm^2/Vs
Gaussian density	$1.6 \cdot 10^{17}$	cm^{-3}
Gaussian level	-0.1723	eV
3.6% O-PCBM device		
Band gap	1.277	eV
Injection barrier	0.0785	eV
Electron band mobility	$6.3 \cdot 10^{-5}$	cm^2/Vs
Gaussian density	$6.8 \cdot 10^{17}$	cm^{-3}
Gaussian level	-0.086	eV

Charge extraction simulations

The excess charge-carrier density obtained from charge extraction (CE) measurements were simulated by subtracting the total charge-carrier density at V_{oc} under varying illumination by the total charge-carrier density at V = 0 V in the dark. The total charge-carrier density is here the sum of the average values of the electrons densities, hole densities, trap densities and surface charge densities (assuming that enough time has passed that all trapped charge carriers have thermally escaped and are extracted at the contacts).

V_{OC} reconstruction from charge extraction (CE) and transient photovoltage (TPV) measurements

The charge density VS V_{OC} data from CE was fitted with the exponential function:

$$n = n_0 exp\left(\frac{qV_{OC}}{mkT}\right)$$

The lifetime VS V_{OC} data from TPV was fitted with the exponential function:

$$\tau_{\Delta n} = \tau_{\Delta n0} exp\left(-\frac{qV_{OC}}{\vartheta kT}\right)$$

The lifetime of the charge generated by the TPV pulse, $\tau_{\Delta n}$, can be related to the lifetime of the total charge n by the relationship:

$$\tau_n = \delta\tau_{\Delta n}$$

Where:

$$\delta = \frac{m}{\vartheta} + 1$$

Therefore:

$$\tau_n = \delta\tau_{\Delta n0} exp\left(-\frac{qV_{OC}}{\vartheta kT}\right)$$

At open circuit, the generation and recombination currents are equal:

$$J_{gen} \approx J_{SC} = J_{loss} = qd\frac{n}{\tau_n} = qd\frac{n_0 exp\left(\frac{qV_{OC}}{mkT}\right)}{\delta\tau_{\Delta n0} exp\left(-\frac{qV_{OC}}{\vartheta kT}\right)}$$

$$\frac{\delta J_{SC}\tau_{\Delta n0}}{qdn_0} = \frac{exp\left(\frac{qV_{OC}}{mkT}\right)}{exp\left(-\frac{qV_{OC}}{\vartheta kT}\right)}$$

$$\ln\left(\frac{\delta J_{SC}\tau_{\Delta n0}}{qdn_0}\right) = \frac{qV_{OC}}{kT}\left(\frac{1}{m} + \frac{1}{\vartheta}\right)$$

$$V_{OC}\left(\frac{1}{m} + \frac{1}{\vartheta}\right) = \frac{kT}{q} ln\left(\frac{\delta J_{SC}\tau_{\Delta n0}}{qdn_0}\right)$$

$$V_{OC} = \frac{mkT}{q\delta} ln\left(\frac{\delta J_{SC}\tau_{\Delta n0}}{qdn_0}\right)$$

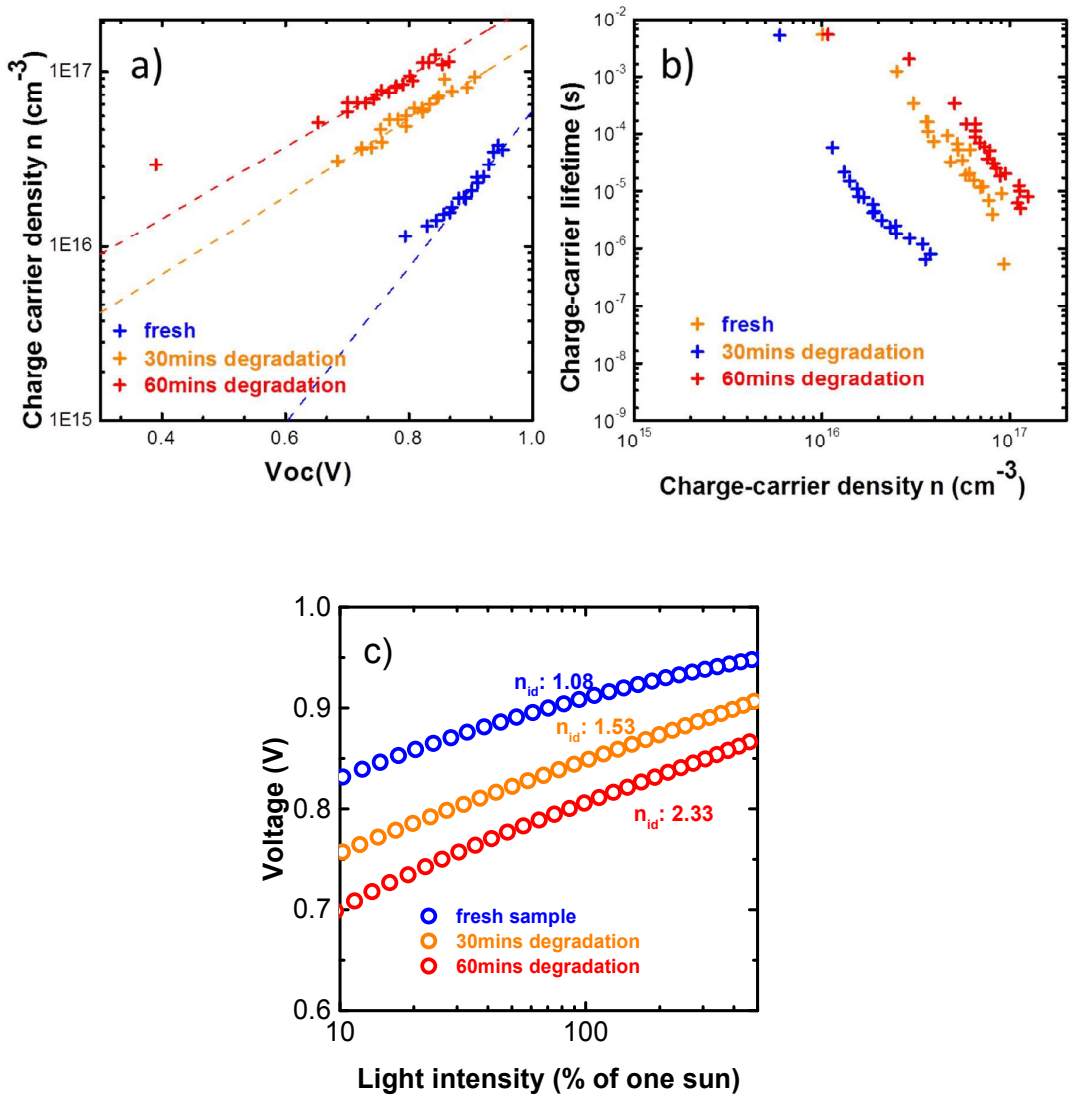

Supplementary Figure 10 CE, TPV, and diode ideality analysis of PCDTBT:PCBM blend devices prepared from blends degraded as films under AM1.5G illumination in dry air for 30 minutes and 60 minutes prior to electrode deposition. (a) Charge-carrier density *n* as a function of V_{oc} as measured from CE (produced by varying the illumination intensity), the dashed line corresponds to mono-exponential fit; (b) charge-carrier lifetimes at varying charge-carrier density as measured from TPV; (c) Measured V_{OC} (open circles) at varying illumination intensities.

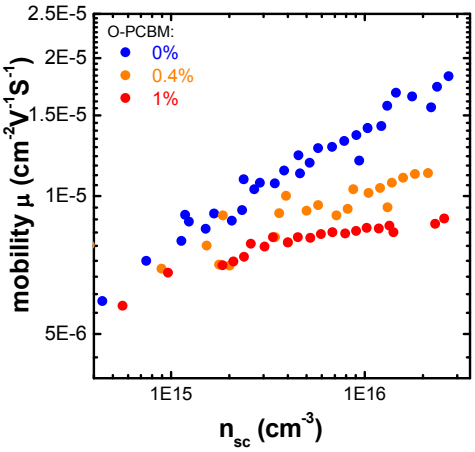

Supplementary Figure 11 Effective mobility measured by charge extraction at short circuit as a function of carrier density for PCDTBT:PCBM blend devices with increasing fraction of O-PCBM.

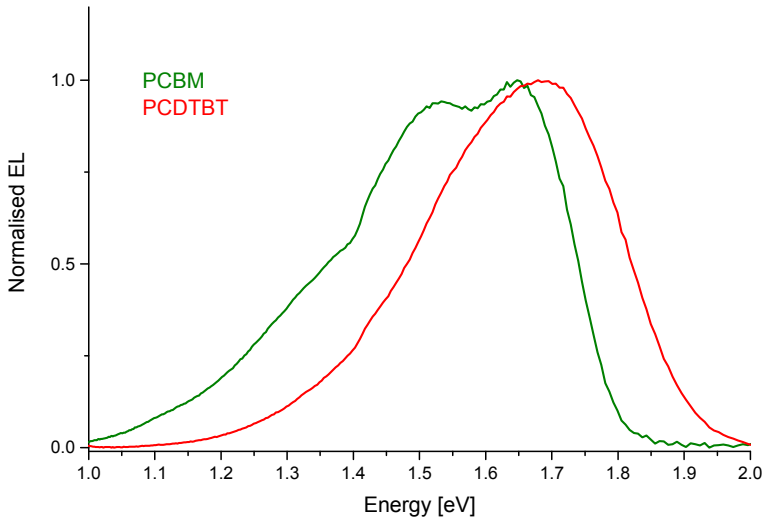

Supplementary Figure 12 Normalised electroluminescence spectra of devices containing only pure PCBM or only pure PCDTBT. Both emissions occur at higher energies than the charge transfer emission recorded in devices containing PCDTBT:PCBM blends.

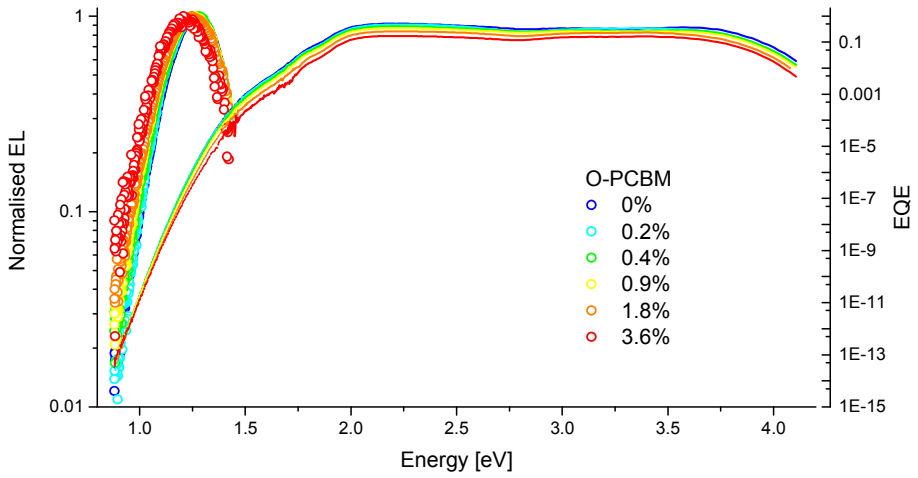

Supplementary Figure 13 Normalised electroluminescence (EL) and absolute external quantum efficiency (EQE) spectra of PCDTBT:PCBM devices containing increasing amounts of photo-oxidised PCBM (O-PCBM). The quantum efficiency data that could be directly collected on our EQE instrument is represented by solid lines (down to about 1.5 eV), while the EQE data below 1.5 eV was obtained from the EL data, after dividing by the black body photon flux and multiplying by a pre-factor to match with the absolute EQE data.

Detailed balance method to calculate voltage losses

The maximum voltage achievable in a solar cell is limited by unavoidable radiative recombination. In the radiative limit, where absorption and emission quantum efficiencies are equal, the maximum voltage achievable can be related to the electroluminescence quantum efficiency (Q_{LED}).

The Q_{LED} is a function of the electroluminescence photo flux and the injection current density:

From the ideal diode equation, we can deduce the open circuit voltage in the radiative limit at open circuit (ideality factor = 1, only radiative recombination):

$$V_{OC,rad} = \frac{kT}{q} ln\left(\frac{J_{SC}(V_{OC,rad})}{J_{0,rad}} + 1\right)$$

Assuming no losses at short circuit (SC):

$$J_{SC}\left(V_{OC,rad}\right) \approx J_{SC}$$

The saturation current in the radiative limit can be calculated from the electroluminescence quantum efficiency (Q_{EL}).

$$J_{0,rad} = q \int Q_{EL}\,(E)\phi_{BB}(E)dE$$

As our electroluminescence system could not measure an absolute value of electroluminescence photon flux, Q_{EL} was obtained by matching the EL data to the calibrated EQE data, by multiplying them by a pre-factor.

Supplementary Table 8 Voltage values calculated for PCDTBT:PCBM devices with increasing fractions of photo-oxidised PCBM (O-PCBM). $V_{OC,SQ}$: Schokley-Queisser limit to V_{OC}; $V_{OC,rad}$: radiative limit to V_{OC}, measured using EQE-EL; V_{OC}: measured using a solar simulator; $\Delta V_{OC,abs}$: voltage losses due to non-ideal absorption (EQE < 1 above the band gap energy and sloped absorption edge); $\Delta V_{OC,non\text{-}rad}$: voltage losses due to non-radiative recombination only.

O-PCBM [%]	$V_{OC,SQ}$ [V]	$V_{OC,rad}$ [V]	V_{OC} [V]	$\Delta V_{OC,abs}$ [V]	$\Delta V_{OC,non\text{-}rad}$ [V]
0	1.545	1.246	0.923	0.299	0.323
0.2	1.545	1.240	0.882	0.305	0.358
0.4	1.545	1.241	0.846	0.303	0.396
0.9	1.545	1.224	0.775	0.321	0.449
1.8	1.555	1.234	0.731	0.320	0.503
3.6	1.555	1.229	0.614	0.326	0.616

Title: The Role of Fullerenes in the Environmental Stability of Polymer:Fullerene Solar Cells

Authors:

Harrison Ka Hin Lee[1], Andrew M. Telford[2], Jason A. Röhr[2], Mark F. Wyatt[3], Beth Rice[2], Jiaying Wu[4], Alexandre de Castro Maciel[2,5], Sachetan M. Tuladhar[2], Emily Speller[1], James McGettrick[1], Justin R. Searle,[1] Sebastian Pont[4], Trystan Watson[1], Thomas Kirchartz,[6] James R. Durrant[1,4], Wing C. Tsoi[1], Jenny Nelson[1,2]* and Zhe Li[1]*

*Corresponding authors

Contact Information:

[1] Dr. Harrison Ka Hin Lee, Emily Speller, Dr. James McGettrick, Dr. Trystan Watson, Prof. James R. Durrant, Dr. Wing C. Tsoi, , Prof Jenny Nelson, Dr. Zhe Li

SPECIFIC IKC, College of Engineering, Bay campus, Swansea University, Wales, UK SA1 8EN

[2] Dr. Andrew M. Telford, Jason A. Röhr, Beth Rice, Prof. Alexandre de Castro Maciel, Dr. Sachetan M. Tuladhar, Prof. Jenny Nelson

Department of Physics, Imperial College London, London, UK SW7 2AZ

[3] Dr Mark F. Wyatt

EPSRC UK National Mass Spectrometry Facility (NMSF), Swansea University Medical School, Wales, UK SA2 8PP

[4] Jiaying Wu, Sebastian Pont, Prof. James R. Durrant

Department of Chemistry, Imperial College London, London, UK SW7 2A

[5] Prof. Alexandre de Castro Maciel

Department of Physics, CCN, Federal University of Piauí, Teresina, Brazil, 64049-550

[6] Prof. Thomas Kirchartz

IEK5-Photovoltaics, Forschungszentrum Jülich, 52425 Jülich, Germany

Faculty of Engineering and CENIDE, University of Duisburg-Essen, Carl-Benz-Str. 199, 47057 Duisburg, Germany

Emails: jenny.nelson@imperial.ac.uk, z.li@swansea.ac.uk

Abstract

Environmental stability is a common challenge for the commercialisation of low cost, encapsulation-free organic opto-electronic devices. Understanding the role of materials degradation is the key to address this challenge, but most such studies have been limited to conjugated polymers. Here we quantitatively study the role of the common fullerene derivative PCBM in limiting the stability of benchmark organic solar cells, showing that a minor fraction (<1%) of photo-oxidised PCBM, induced by short exposure to either solar or ambient laboratory lighting conditions in air, consistent with typical processing and operating conditions, is sufficient to compromise device performance severely. We identify the effects of photo-oxidation of PCBM on its chemical structure, and connect this to specific changes in its electronic structure, which significantly alter the electron transport and recombination kinetics. The effect of photo-oxidation on device current-voltage characteristics, electron mobility and density of states could all be explained with the same model of photoinduced defects acting as trap states. Our results demonstrate that the photochemical instability of PCBM and chemically similar fullerenes remains a barrier for the commercialisation of organic opto-electronic devices.

Broader context

Abundant, low-cost and easily processed materials are urgently needed for applications in energy conversion and storage. In this context, solution processable organic and lead-halide perovskite semiconductors have attracted intense interest for use in solar cells. However, environmental stability of these and other low cost, solution processed electronic devices remains the major

challenge for commercialisation. Solving the device stability issue requires methods to identify the causes of degradation (for example, semiconductor or electrode failure, chemical or electrochemical processes) and to relate changes in electrical performance to specific degradation mechanisms. Here, we identify a degradation pathway that is relevant to many designs of organic and perovskite solar cells, namely, the photochemical oxidation of fullerenes under exposure to ambient light, and show that the effects on charge transport, device photovoltage, and current-voltage characteristic can be related quantitatively to the nature and energy of specific oxidised defects introduced by light. These findings challenge the widely held assumption that the photo-degradation of donor polymers is the primary weakness of organic solar cells and show that exposure to ambient laboratory or factory lighting in air may be sufficient to compromise device performance. The work provides a target and a methodology in the pursuit of superior materials for solar cells, namely, that more robust electron transport materials are needed, and that the viability of candidates can be assessed from knowledge of their oxidation products and the predicted effect on device response. The work thus provides a predictive step in the design of environmentally stable devices.

Introduction

A common challenge for the commercialisation of organic opto-electronic devices such as solar cells is their typically limited environmental stability. Organic solar cells have undergone significant improvements in performance with their efficiencies increasing from 3% to over 13% in the last decade,[1] primarily due to the recent development of a range of high performance donor polymers and non-fullerene acceptors.[2-4] However, their limited environmental stability and short lifetimes have become a major hurdle for commercialisation.[5-7] Numerous reports have shown that exposure to air typically results in rapid deterioration of device performance, especially when combined with exposure to light.[8,9] A general strategy to address this challenge is using device encapsulation, thereby creating a physical barrier for the diffusion of molecular oxygen into the device and hindering the reaction route of oxygen induced degradation.[5] However, encapsulation significantly

increases the fabrication cost, and despite substantial research efforts,[10-13] little success has been demonstrated to date in extending the lifetimes of un-encapsulated devices under exposure to light and oxygen. Understanding the degradation mechanisms and enhancing the intrinsic stability of organic opto-electronic devices is therefore of paramount importance for their commercialisation.

The majority of studies of photoactive material stability have addressed the stability of the donor (polymer) component.[5,6,14,15] Despite their common use in solution-processed optoelectronic devices, fullerenes have been known to be sensitive to photo-induced reactions since the early 1990s.[16,17] For example, under UV or visible illumination in inert atmosphere, fullerenes such as phenyl-C_{61}-butyric acid methyl ester (PCBM) can form covalent intermolecular C-C bonds to form dimers or higher oligomers. Such photo-oligomerisation has been correlated with a loss of organic photovoltaic (OPV) device efficiency under irradiation (the "burn-in" effect),[10,18] although modest PCBM photo-oligomerisation can also be beneficial, improving the morphological stability of OPV devices under thermal stress.[12,19] In the presence of oxygen, PCBM and other fullerene derivatives have been shown to undergo photo-oxidation,[20] with two most commonly observed products of photo-oxidation, epoxide and carbonyl, on the fullerene cage.[21] While the photo-oxidation of fullerenes has been investigated in detail by Moons and co-workers,[22,23] little has been reported on its effect on the performance of organic opto-electronic devices, and especially on the exact mechanism of performance loss. A small number of studies have shown that organic solar cells containing deliberately photo-oxidised fullerene derivatives exhibit dramatic losses in their performance,[24,25] but provided no mechanistic explanation, nor proof of relevance to OPV stability. A few groups have suggested the formation of trap states upon fullerene photo-oxidation based on quantum chemical simulations, with limited direct evidence of the relationship of defects to electronic properties.[26,27]

In this paper, we evaluate the impact of PCBM photo-oxidation on the performance and stability of polymer:fullerene bulk heterojunction devices. We found that a minor fraction of photo-oxidised PCBM in blends films with the benchmark polymer Poly[N-9'-heptadecanyl-2,7-carbazole-alt-5,5-

(4',7'-di-2-thienyl-2',1',3'-benzothiadiazole)] (PCDTBT), which is the most stable OPV polymer demonstrated so far,[28] induced by exposure to only a few minutes of illumination in air, can result in severe degradation of device performance. We systematically investigated the effect of introducing minor fractions (0.2 to 3.6%) of deliberately photo-oxidised PCBM on the transport and recombination mechanisms in OPV devices, to explain the losses in power conversion efficiency (PCE). We extend our conclusions to OPV devices based on other benchmark polymers, namely P3HT, PTB7, and PTB7-Th. We show that fullerene photo-oxidation can be a primary mechanism dominating the degradation of fullerene-based opto-electronic devices. The highly photoactive nature of fullerenes and strong correlation to device performance suggest that fullerene photo-oxidation must be taken into account in the choice of processing route for fullerene-based electronic devices. The methodology presented here could readily be applied to probe specific degradation pathways in other OPV systems, such as those containing alternative acceptors.

Results

Impact of fullerene photo-oxidation on OPV devices behaviour. We investigated the decrease in performance due to degradation of bulk-heterojunction OPV devices upon exposure to light and oxygen. Previous studies concluded that light and/or oxygen exposure of un-encapsulated devices resulted in rapid device degradation due to diffusion and subsequent reaction of molecular oxygen with the polymer component of the active layer materials.[5] Figure 1(a) shows the evolution of current density-voltage (*J*-*V*) characteristics of typical PCDTBT:PCBM devices having undergone different exposure durations to AM1.5G conditions in air (see also Supplementary Table 1). Exposure prior to electrode deposition allowed the experiments to focus on the underlying kinetics of the PCDTBT:PCBM photo-oxidation independent of lateral oxygen diffusion kinetics; it has previously been shown that for devices with an oxygen blocking top contact, lateral oxygen diffusion kinetics can extend over days.[29,30] It is striking that only 10 minutes of light exposure result in an overall PCE loss of over 40%, due to simultaneous drops in short-circuit current density (J_{sc}), open-circuit voltage

(V_{oc}) and fill factor (FF). After 60 minutes of exposure, a PCE loss of over 70% is seen. Devices exposed to air in the dark show similar performance to the fresh devices (Supplementary Fig. 1 and Table 2), indicating that the degradation process is driven by the combination of light and oxygen. The above experiments were repeated using interlayers of different polarity (MoO_3 and ZnO as well as PEDOT:PSS) underneath the active layer. The results (Supplementary Fig. 2) show a similar trend to the one in Figure 1(a).

To identify the origin of device degradation and quantify the degradation products, ultraviolet–visible (UV-vis) spectroscopy, atomic force microscopy (AFM), x-ray photoelectron spectroscopy (XPS) and matrix-assisted laser desorption/ionization time-of-flight (MALDI-TOF) mass spectrometry measurements were carried out. Degraded blend films were fabricated and exposed in the same way as the films used for the devices in Figure 1(a). No obvious photo-bleaching of the blend films was observed within the timescale studied (Supplementary Fig. 3). AFM images reveal minimal changes in surface morphology upon photo-oxidation (Supplementary Fig. 4). XPS measurements reveal a steady increase in bulk oxygen composition with increasing degradation time, and a concentration of oxidised species that is fairly uniform with depth below the surface layers (Supplementary Fig. 5). The samples for MALDI-TOF measurements were prepared by re-dissolving the blend films after photochemical degradation. By comparing Figure 2(a) with 2(b) it is seen that photo-oxidised PCBM species (with up to 4 oxygen atoms) were formed upon 60 minutes of AM1.5G exposure in air in the blend film with PCDTBT. The degree of oxidation is further increased with exposure duration (up to 7 oxygen atoms after 10 hours) as is seen in figure 2(c). An analysis of the ^{12}C-isotopic peak areas reveals a total of 0.8% oxidised PCBM in the blend film after 1 hour of aging. This is further increased to 4.3% after 10 hours of aging. The calculated quantity of photo-oxidised species is in good agreement with the bulk analysis of oxidised species by X-ray photoelectron spectroscopy (XPS) measurement. It thus appears that PCBM can be readily photo-oxidised upon exposure to light and oxygen of unprotected blend films of PCBM with conjugated donor polymers.

Although this study is focussed on the photostability of PCBM in particular, it is relevant to a number of other fullerene materials. As shown in Supplementary Fig. 6, a similar photoxidation process leads to similar or higher concentration of oxidised fullerenes for other derivatives of C_{60} including the bis-adducts of PCBM and the indene derivative fullerene. The sensitivity of C_{60} derivatives to oxidation is consistent with the finding of Silva et al. that reactivity of fullerenes increases with reducing pyramidalisation angle (i.e. with increasing curvature).[31] In accordance with this we find a lower sensitivity of $PC_{71}BM$ to the same oxidation procedure, indicating that whilst a variety of fullerene derivatives are readily oxidised, the chemical structure and shape of the fullerene influence its tendency to oxidise.

To isolate the impact of PCBM photo-oxidation alone (rather than degradation of the polymer) on the performance of OPV devices, we prepared blends of PCDTBT using PCBM that had been separately photo-oxidised in solution. Figure 1(b) shows the current density-voltage characteristics of these devices (see also Supplementary Table 3). The aged PCBM species were also analysed by MALDI-TOF to estimate the fraction of oxidised PCBM as shown in figure 2(d). A PCBM solution exposed to AM1.5G illumination in air for 72 hours contained 3.6% of oxidised PCBM (O-PCBM). Different amounts of degraded PCBM solution were mixed with a fresh PCBM solution to control the fraction of O-PCBM in the fullerene phase of blends with PCDTBT. The total concentration of fullerene (PCBM + O-PCBM) in the blend films was kept constant. XPS measurements of such films show uniform composition with depth, as expected (Supplementary Fig. 5). Markedly, with only 1% of oxidised PCBM in the fullerene phase a 65% loss in device PCE was observed, which increased to ~ 90% loss with only 3.6% of O-PCBM. From this it is clear that the photo-oxidation of PCBM, even at low levels, has a significant impact on the performance of OPV devices. Figure 1(c) compares the PCE of devices where the PCDTBT:PCBM films had been exposed to AM1.5G illumination in air and PCDTBT:PCBM devices fabricated using different fractions of O-PCBM. Device PCEs are plotted against the fraction of O-PCBM in the active layer, measured by MALDI-TOF by removing and analysing the active layers. The drop in performance of photo-oxidised PCDTBT:PCBM blends

quantitatively matches that of the devices made using O-PCBM. To investigate the generality of this effect, we extended our studies to other benchmark OPV systems, namely P3HT:PCBM, PTB7:PCBM, and PTB7-Th:PCBM blends, which exhibited qualitatively similar effects (Supplementary Fig. 7). It is thus apparent that PCBM photo-oxidation has a drastic impact on the performance of these benchmark OPV systems.

To establish the microscopic mechanism of device performance degradation, we explore the nature of the chemical defects formed upon photo-oxidation, and their effect on charge transport and recombination. As we demonstrate in the following, the insight provided by our study allows us to qualitatively reproduce the observed device behaviour under illumination as shown in Figure 1(d), through simulations, by accounting for deteriorated electronic transport and increased recombination upon PCBM degradation.

Possible mechanisms of fullerene photo-oxidation. The effect of photo-oxidation on the highest occupied molecular orbital (HOMO) and lowest unoccupied molecular orbital (LUMO) levels of PCBM was explored using electronic structure calculations of the products of oxidation, namely PCBM bearing epoxide, diol and carbonyl defects, following the oxidation mechanism reported by Xiao *et al.* as shown in Figure 2(e).[21] For each defect type, we identified all isomers with defects across 6-6 carbon bonds (i.e. two 6 membered rings together) and then calculated HOMO and LUMO energies as well as the total energy of the species using the delta self-consistent field (delta-SCF) method (see Methods section and Supplementary Table 4). Several oxidised species with multiple defects (e.g. two epoxides) and complex defect structures (e.g. two different defects) were included in the study for completeness. To check sensitivity of results to the calculation method, the HOMO and LUMO levels were also estimated using Kohn-Sham and time-dependent density functional theory (TD-DFT) methods (Supplementary Table 5 and Table 6). For each method, the differences in HOMO and LUMO energies of any specific O-PCBM isomer relative to those of pristine PCBM were similar.

For each defect type, we calculated average HOMO and LUMO energies by including different isomers in proportion to their thermodynamic probability of occurrence, calculated from the total energy for the neutral species in a Boltzmann average (Supplementary Table 7). The oxidised PCBM species with the lowest total energy tend to have defects close to the phenyl butyric acid methyl ester side-chain; examples are shown by the molecular structures in Figure 2(e). The LUMO is depressed for almost all oxidised PCBM species as shown in Figure 2(e) (and Supplementary Table 4-6 for full data set), especially in the case of carbonyl defects. In contrast, the effect on the HOMO is small in all cases, except for the diol defect. Therefore, we expect the oxidation to affect electronic transport by introducing trap states for electrons, and to have a stronger effect on electron transport than on hole transport in the PCBM phase.

From Figure 2(e) it is evident that, given the electron transport in a blend film takes place in the PCBM phase, the lower LUMO energies of the oxidised molecules will cause electron trapping. The distribution of electron trap states may be expected to extend deep (several tenths of an eV) into the band gap. The shape of the total density of trap states is difficult to predict, since the incidence of different defect types in practice is not known. However, the epoxide and carbonyl species would most likely give rise to both a broadening of the LUMO energies around an energy close to the LUMO of pristine PCBM as well as some deeper electron traps. Additionally, the overall density of defect states will increase with degradation.

Effects of fullerene oxidation on charge transport kinetics in neat PCBM films. To quantify the impact of photodegradation on electron transport we performed space-charge-limited current (SCLC) measurements on electron-only devices with structure (ITO/TiO_2/PCBM:O-PCBM/Ca/Al) made from PCBM solutions with different weight fractions of O-PCBM (0%, 0.2%, 0.9%, 1.8% and 3.6%). Effects of varying device thickness were minimised by comparing devices with approximately the same thickness of 70-80 nm. Representative current density – voltage curves in Supplementary Fig. 9 show that the current density at a given applied voltage drops significantly with increasing fraction of

photo-oxidised PCBM in the film. Also shown in Supplementary Fig. 9 are calculated J-V curves obtained by fitting the results of a drift-diffusion model that incorporates charge trapping to the experimental SCLC data.[32] The model of the density of states (DoS) used for these fits consists of a narrow Gaussian distribution of N_t traps states per volume centred around an energy level lying E_t below the conduction band transport level, together with a band electron mobility, μ_0.[33,34] (Note that the band mobility represents the mobility of charge carriers at the transport level, in the absence of traps, rather than the effective mobility that would be measured.) The trap distribution is assumed constant with depth in accordance with the XPS measurements. Electrons are trapped and released by the sub-band-gap states according to a multiple-trapping model. Since only a single carrier type is present in SCLC measurements, recombination is negligible in these simulations. The parameters N_t, E_t, μ_0 and the electron injection barrier are varied to obtain the best fit for each device at each level of degradation. (See Methods for further details). The model of a Gaussian distribution of traps was selected in preference to an exponential tail of states or a more complex DoS with multiple features because it provided the best fit to the data with the fewest fitting parameters. Figure 3(a), (b), and (c) show the obtained values of μ_0, N_t, and E_t, respectively for different fractions of O-PCBM using a large set of nominally identical devices in each case. Note that the range of fitted parameters increases with degradation, due to the microstructural variations inherent in the degradation process.

Figure 3(a) shows that the band mobility obtained by this fitting drops by approximately one order of magnitude when the fraction of O-PCBM is increased from 0% to 3.6% (mobility values are taken as the statistical average of a range of repeated runs of fabrication and measurement for each level of O-PCBM studied). At the same time, the density of traps increases by around an order of magnitude. For less degraded samples the trap level lies around 0.2 eV below the transport level of PCBM, while for higher O-PCBM concentrations the trap level and transport level are seen to approach each other as shown in Figure 3(c), although the sample-to-sample variation in the extracted trap depth becomes large. The barrier for charge injection was found to be insensitive to degradation at around

0.3 eV (Supplementary Fig. 9(f)). The SCLC results are consistent with the formation of both shallow and deep states below the LUMO of the PCBM, as expected from the quantum chemical calculations discussed in the previous section. The shallow states would serve both to push down the effective transport level and to reduce the 'band' mobility. This is illustrated schematically in Figure 3(d).

By accounting for the data calculated in the SCLC analysis, we were able to reproduce the qualitative trend in current-voltage response under solar illumination of devices with increasing fraction of O-PCBM (Figure 1d). We used the parameters obtained from SCLC for the DoS and band electron mobilities of the pristine, 1.8% degraded and 3.6% degraded films to represent the cases of fresh, partly and fully degraded films, respectively, and included band-to-band (R_{direct} = 2.2 × 10^{-20} m^3s^{-1}) and band-to-trap recombination, governed by the electron and hole densities along the capture and emission rate coefficients for electrons and holes (which were all set to the same value, $C_0^- = C_+^- = C_0^+ = C_-^+ = 10^{-16}$ m^3s^{-1}), as well as series and shunt resistances (R_S = 4 Ω cm^2 and R_P = 1.9 kΩ cm^2, respectively). Our modelling strategy was to choose the recombination coefficients, parasitic resistances and hole mobility to best fit the J-V curve of the fresh device, and then modify only the parameters related to electron transport (i.e., the electron band mobility, trap density and position of the electron transport level relative to the trap level) according to the values obtained from the SCLC analysis for different levels of degradation. In this way, we could reproduce the trend in current-voltage sweeps observed in the real devices, specifically, the losses in V_{oc}, J_{sc} and fill factor with increasing O-PCBM content. The effect of degradation modelled this way is less severe than that observed experimentally. This could arise either from the variation in the electronic effect of a given fraction of O-PCBM (evident from the scatter in SCLC device behaviour at high levels of degradation) or from neglecting the impact of O-PCBM on another, secondary quantity, for example on hole mobility. Nevertheless, the qualitative reproduction of the trend in all parameters corroborates the link between traps and device performance.

Effects of fullerene oxidation on blend film recombination and transport kinetics. In order to further understand the effect of fullerene oxidation on device performance, particularly on V_{oc}, charge-carrier densities and lifetimes were measured by transient photocurrent (TPC), transient photovoltage (TPV) and charge-extraction (CE) measurements. The measured charge-carrier density at open circuit, as a function of device V_{oc} under increasing illumination intensity, is plotted in Figure 4(a)**.** Figure 4(b) shows the charge-carrier lifetimes measured as a function of these charge-carrier densities*,* under the same illumination conditions. As it can be observed in Figure 4(a), in all devices the charge density rises approximately exponentially with V_{oc}, consistent with the presence of a tail of states in the band gap. We also note that these density of states curves are shifted substantially to lower energy with increasing fraction of O-PCBM: for a given charge-carrier density of 4.3×10^{16} cm^{-3}, for example, the energetic differences are ≅ 140 mV between the devices with 0% and 0.4% O-PCBM, and ≅ 130 mV between those with 0.4% and 1% O-PCBM. Therefore, in order to achieve the same electron quasi-Fermi level position and therefore the same V_{oc}, much more charge has to be injected in the devices with O-PCBM, due to the deeper distribution of states within the band gap. Figure 4(d) shows, for comparison, the charge-carrier density – V_{oc} behaviour expected for the DoS parameters for differently degraded devices obtained by modelling the devices with the same set of parameters obtained from SCLC analysis and used to model the J-V curves in Fig. 1(d) above. The approximately exponential form of the $n(V_{oc})$ curves and the shift to lower V_{oc} with degradation are reproduced, supporting the idea that the changes in transport and density of states both arise from the introduction of electron trap states.

Figure 4(b) shows that the devices with higher O-PCBM fractions exhibit longer charge lifetimes at fixed charge density. Longer charge-carrier lifetimes are consistent with increased trapping in localized states, which can slow down recombination at a given charge density by reducing the rate at which charge carriers meet. The V_{oc} values calculated from these two opposing effects, i.e. longer lifetimes and higher density of sub-gap states with increasing O-PCBM fraction, match the measured V_{oc} values at varying illumination intensity as shown in Figure 4(c) (see Supplementary Information

for the mathematical background), consistent with this analysis. The introduction of electron trap states results in slower recombination at fixed charge density but that does not benefit V_{oc} because a higher charge density (which leads to faster recombination) is needed to achieve the same quasi-Fermi level separation.

TPV measurements provide information on the total recombination in a device, but cannot discriminate between different mechanisms, such as band-to-band, trap mediated or surface recombination. A first indication of the dominant recombination mechanism comes from the ideality factors measured from the dependence of V_{oc} on light intensity [Figure 4(c)]. The ideality factors are related to the reaction order of recombination such that n_{id} tends to increase from ≅ 1 to ≅ 2 either when recombination becomes stronger in the bulk of the active layer compared to its interfaces with the electrodes, or when the recombination involves deeper trap states in the band gap.[35] Here, the increase in n_{id} with O-PCBM fraction indicates that the recombination mechanism changes with increasing oxidation. Both scenarios (more bulk traps and deeper traps) are consistent with the n_{id} behaviour. The same trends found in devices containing O-PCBM were found in devices prepared from blends degraded as films, as seen in Supplementary Fig. 10, eliminating electrode degradation as the cause of the change in TPV behaviour.

Finally, charge-extraction measurements carried out at short circuit (rather than at open circuit as above), allow us to assay the average (combining electron and hole) charge-carrier mobility in the OPV devices. The mobility inferred from these charge extraction data decreased with increasing fraction of O-PCBM (Supplementary Fig. 11), consistent with increased carrier trapping and in qualitative agreement with the SCLC data discussed above. The magnitude of the reduction of mobility upon degradation is lower than obtained by SCLC, however the mobility estimated from charge extraction includes hole mobility, which should be less affected by fullerene oxidation.

Electroluminescence analysis of the effect of fullerene photooxidation on voltage losses. As a complementary probe of the effect of degradation on blend DoS we characterised the series of

PCDTBT:(PCBM:O-PCBM) devices using electroluminescence (EL) and sub-band gap external quantum efficiency (EQE) measurements. Shown in Figure 5a are normalised EL spectra for fresh and degraded devices. The peak at ≅ 1.2 eV is assigned to radiative decay of the charge-transfer state at the PCDTBT:PCBM interface, in agreement with previous measurements.[36] Control experiments on pure PCDTBT or PCBM confirmed that the emission did not arise from band-to-band recombination from either species (Supplementary Fig. 12). The emission of the charge-transfer state is shifted to slightly lower energies in samples containing increasing fractions of O-PCBM, and its quantum yield decreases (higher injection current is required to obtain a detectable emission). The lower emission efficiency observed in devices with oxidised PCBM is consistent with both poorer transport and a higher degree of non-radiative recombination compared to radiative recombination.

Also shown in Figure 5(a) are sub-band gap EQE spectra, obtained by combining measured EQE with the measured EL spectra, using a detailed balance approach (for devices containing other fractions of O-PCBM see Supplementary Fig. 13).[37] The presence of an increasing fraction of charge-transfer states with lower energy than in fresh blends is evident from the decreasing slope of the sub-band-gap EQE curves, which indicates that the contribution to EQE of the sub-band-gap density of states becomes more pronounced with increasing O-PCBM fraction.

From the sub-band-gap EQE data we were able to calculate the V_{oc} that could theoretically be obtained if the only loss mechanism was radiative recombination ($V_{oc,rad}$) following a previously reported approach.[37] This value is normally lower than the V_{oc} in the Shockley–Queisser limit for single junction solar cells because of the non-step-like absorption profile of practical devices such as these. The difference between the resulting radiative-limit $V_{oc,rad}$ and the measured V_{oc} can be assigned to non-radiative recombination losses ($\Delta V_{oc,non\text{-}rad}$). Shown in Figure 5(b) are the contributions to V_{oc} losses. The relative size of the $\Delta V_{oc,non\text{-}rad}$ component for different devices in a series should reflect the degree of non-radiative recombination, as described above, for devices with different fractions of O-PCBM. The losses due to non-radiative recombination clearly increase with increasing fraction of O-PCBM, consistent with the formation of sub-band gap trap states that slow

down carrier collection and increase the overall likelihood of non-radiative recombination. (See Supplementary Table 8 for all the V_{oc} values.) These results are in good agreement with the clear increase in trap-mediated recombination inferred from the ideality factors (Figure 4(c)).

Discussion

Environmental stability has become a primary concern for the realisation of low-cost manufacture of opto-electronic devices using approaches that typically involve air processing and minimal encapsulation. Despite the significant amount of research effort, the origin of the limited environmental stability of devices such as polymer:fullerene solar cells remains unclear. It is recognised that different stress factors (oxygen, water, heat) are involved and that different components of the device are vulnerable (semiconductors, interlayers electrodes) but few studies unambiguously relate particular chemical degradation mechanisms to their impact on electrical performance. Whilst substantial research efforts have addressed the photochemical and photophysical stability of conjugated donor polymers ,[5,6,8,38] the environmental stability of fullerenes and their impact on device performance have received relatively little attention.[22-25] A further consideration is that in most studies to date the chemical nature of defects is not identified and so the precise relationship between degradation mechanism and device behaviour cannot be explored. Here, we used a systematic study of the impact of fullerene oxidation on solar cell performance to demonstrate that common products of the photo-oxidation of PCBM, specifically fullerene epoxides and carbonyls, act as electron traps in OPV devices. Whilst prior studies had shown that epoxides[27] and other oxygenic defects[21,31] were expected to form on fullerenes, and that in practice oxygen exposure changes the electronic structure of fullerenes[22] with impact on device performance,[23] the link between chemical nature of such defects and electrical properties of devices had not previously been investigated. Previous approaches to simulate the effect of degradation have typically addressed the effect on photocurrent collection of oxidative p-doping of the active layer,[39,40] or invoked trap states to explain changes in electrical response,[41-43] but without a clear origin for those

defects. In this work, we have established a quantitative relationship between the presence of specific oxidative defects which act as electron traps and the resulting change in electronic properties of the OPV devices made from the oxidised fullerene, which has not been established previously. Specifically, electron mobility, charge lifetime and density of states measurements are all consistent with the presence of a distribution of electron trap states centred around 0.2 eV below the conduction band edge, which increases with fraction of oxidised fullerene. Shallow traps in this energy range have been previously observed in PCBM without any intentional degradation.[44] By using a device model to account for the effect of these trap states on charge carrier densities, electron transport and recombination, we could show how the introduction of oxidised PCBM causes losses in device open-circuit voltage, short-circuit current and fill factor. More generally, this study demonstrates, at least for similar systems, that when the chemical mechanism of degradation, or the degradation products, are known, we can, in principle, predict the consequences for electronic processes.

Interestingly, we have found that even exposure to low light conditions, typical of laboratory environments, is sufficient to drive the photo-oxidation of fullerenes in polymer:fullerene solar cells, corroborating previous studies on fullerene films (Supplementary Fig. 1).[22] This observation suggests that inadvertent exposure to light and oxygen during sample preparation and characterisation (e.g. optical measurements) is as problematic as illumination of the device under operation. Finally, the results reported herein suggest that PCBM, one of the most commonly used fullerene derivatives in the community to date, may not be an ideal candidate for the commercialisation of stable opto-electronic devices due to their intrinsic instability. Alternative small-molecular acceptor materials, which do not undergo epoxide formation so readily as fullerenes, could be good candidates to extend the lifetime of organic solar cells. Preliminary studies suggest that photodegradation is slower using some non-fullerene acceptors,[4] but more detailed studies are needed. Our findings thus highlight the importance of developing alternative electron accepting/transporting materials with

improved photochemical stability. Our findings are also relevant for stability of perovskite devices, where PCBM is commonly used as an electron collecting interlayer.[45]

It should be re-iterated that the degradation of organic solar cells results from the interplay of multiple concurrent pathways, typically induced by different environmental stress factors. In order to achieve overall environmental stability of organic solar cells, all of these degradation mechanisms need to be identified and addressed. For example, it has been demonstrated that some donor polymers may act as supressing agents to fullerene oxidation,[20] likely owing to their low oxygen solubility and short triplet lifetime.[14,46] While the work presented here demonstrates the important role of fullerenes in the environmental stability of organic solar cells, the development of environmentally stable donor materials, interlayers and electrodes are of equal importance in addressing the stability challenge of organic electronic devices.

Methods

Materials. PCDTBT was purchased from 1-Materials. All fullerene were purchased from Solenne BV. Chlorobenzene (CB), zinc acetate dihydrate, 2-methoxyethanol, and ethanolamine were purchased from Sigma Aldrich. MoO_3 was purchased from Strem Chemicals. All materials were used as received.

Device fabrication. ITO glass substrates were cleaned sequentially with Hellmanex detergent, deionized water, acetone, and isopropyl alcohol in ultrasonic bath. Poly(3,4-ethylenedioxythiophene)-poly(styrenesulfonate), Heraeus Clevios P VP AI 4083, (PEDOT:PSS) or ZnO precursor solution (109.8 mg of zinc acetate dihydrate dissolved in 1 ml of 2-methoxyethanol and 30.2 µl of ethanolamine) was spin-coated on plasma treated ITO substrates at 4000 rpm for 40 s, followed by thermal annealing at 150 ^{o}C for 10 minutes. For the devices using MoO_3 as the interlayer, 10 nm of MoO_3 was thermally evaporated on the ITO coated glasses under vacuum of 2×10^{-5} mbar. PCDTBT and PCBM (1:2) were co-dissolved in CB at 60 °C and stirred at 1300 rpm with a total concentration of 18 mg/ml for over 12 hours in nitrogen filled glovebox. The blend solution was spin-

coated on PEDOT:PSS, MoO_3, or ZnO coated substrates in air, resulting in active layers with a thickness of ~70nm. Finally, 30 nm of calcium and 100 nm of aluminium (or 10 nm of MoO_3 and 100 nm of silver for ZnO device) were thermally evaporated on the blend layer under vacuum of 2×10^{-5} mbar, defining active area of 0.15 cm^2. The devices were encapsulated by glass slides using epoxy in nitrogen filled glovebox prior to measurement. Current density–voltage (*J–V*) characterizations were performed by a Keithley 2400 sourcemeter under AM1.5G illumination, Newport 92193A-1000 solar simulator with a light intensity of 90 mW/cm^2.

Degradation. PCDTBT:PCBM films fabricated on PEDOT:PSS coated ITO glass substrates were degraded under AM1.5G illumination in dry air (relative humidity ~30%) for different periods of time mentioned in the main text. PCBM solution for selective degradation study was prepared by dissolving PCBM (24 mg) in CB (1 ml) in a 15 ml vial at 60 °C with stir speed of 1300 rpm in a nitrogen filled glovebox for at least 12 hours. The vial of PCBM solution was then filled with air and degraded under AM1.5G illumination with stir speed of 300 rpm for 72 hours in air.

XPS measurements. XPS data were obtained using a Kratos Axis Supra (Kratos Analytical, Manchester, U.K.) using a monochromated Al Kα source. All spectra were recorded using a charge neutralizer to limit differential charging. The main carbon peak is charge referenced to 284.5 eV.[47,48] Depth profiles of different samples were generated by rastering a 2.5 kV Ar_{500}^+ cluster beam over a 3 mm × 3 mm area giving a typical sample current of 5.53 nA. The data was fitted using CASA XPS with Shirley backgrounds.

MALDI-TOF measurements. All samples were dissolved in chlorobenzene at an approximate concentration of 1mg/mL. MALDI matrix trans-2-[3-(4-tert-butylphenyl)-2-methyl-2-propenylidene]malononitrile (DCTB) was purchased from Insight Biotechnology Ltd. (Wembley, U.K.), and dissolved in chlorobenzene at 20mg/mL. Solutions of sample and matrix were mixed together so the matrix is in ~250-1000 fold molar excess, typically 1µL of sample to 49µL of matrix. 0.5 µL of each of these mixture solutions for each sample was spotted onto the MALDI plate and dried in air.

MALDI-TOF spectra were acquired in negative-reflectron mode using an ultrafleXtreme mass spectrometer (Bruker Daltonics, Bremen, Germany), which is equipped with a Smartbeam-II Nd:YAG laser (λ = 355 nm). Data was acquired using flexControl software v3.4, while post-acquisition processing of data was performed by flexAnalysis software v3.4. PCBM and oxidised analogues were observed as negative radical ion species ($M^{-\bullet}$). The percentage of photo-oxidised fullerenes was determined by calculating the peak areas of the oxidised fullerene species.

DFT calculations. We performed single point energy calculations on optimised structures in Gaussian09 for *N, N+1* and *N-1* electron systems. The HOMO (and LUMO) levels are then found by computing the difference between total energy for the *N* electron system with the *N-1* (*N+1*) system. All calculations were done at the B3LYP level of theory with the 6-31g* basis set.[49]

Electroluminescence. EL was measured using a spectrograph (Andor Shamrock 303) combined with a InGaAs photodiode array (Andor iDUS 491) cooled to -90 °C, calibrated with a Bentham CL2 quartz halogen lamp with known emission spectrum. EL spectra were collected at injection current densities up to 100 mA/cm^2, on at least 4 devices for each fraction of O-PCBM.

External quantum efficiency. EQE was measured using a grating spectrometer (CVI DIGIKROM 240) to create monochromatic light combined with a tungsten halogen light source. The monochromatic light was modulated at 290 Hz with a chopper, and a Stanford Research Systems SR380 lock-in amplifier, with an internal transimpedance amplifier of 106 V/A, was used to detect the photocurrent. Long pass filters at 780 and 850 nm were used to filter out the scattered light from the monochromator. The spectra were taken from 300 to 1000 nm and calibrated by a silicon photodiode.

Electron only devices. glass substrates containing a predefined layer (≈ 70 nm) of indium doped tin oxide (ITO) were ultrasonicated in an acetone bath, and subsequently in an IPA bath, for 10 minutes, respectively. The substrates were dried using nitrogen. Titanium dioxide (TiO_2) films were deposited

onto the ITO by spin coating of a precursor solution containing 70 µL titanium isopropoxide, 55 µL ethanolamine and 1 mL 2-methoxyethanol. The substrates were sintered in an oven for 1 hour at 500 °C. The resulting TiO_2 film is approximately 20 nm think. The pre-degraded PCBM was spun onto the substrates with a target film thickness of around 80 nm. The back contact was applied by thermal annealing under high vacuum ($< 5 \times 10^{-6}$ Torr). Calcium (Ca) was evaporated at a rate 1 Å/s with a final thickness of around 30 nm. A thick layer of aluminium was subsequently evaporated at a rate of 20 Å/s with a resulting layer thickness of 150 nm. The resulting electron-only device had the following device architecture: glass/ITO/TiO_2/PCBM/Ca/Al. The devices were stored and measured under inert atmosphere (N_2) and in the dark.

SCLC measurements. The current density-voltage (*J–V*) curves were recorded using a source measurement unit (SMU) using a slow scan rate to ensure that the device was in a steady-state condition. J-V curves were recorded in both forward (0 → 5V) and in reverse (0 → -5 V) bias. Since no difference in the magnitude or the shape of the current was observed irrespective of bias polarity, the presence of built-in voltages across the device can be ruled out. The J-V curves were analysed using a commercially available drift-diffusion solver called Advanced Semiconductor Analysis (ASA). The software uses a multiple trapping-release model which assumes that all charge carriers must be released from charge traps to the transport level in order to contribute to the current. Traps were modelled using a Gaussian distribution of states below the conduction band edge, where we allowed for the Gaussian density and the trap level to vary while the Gaussian standard deviation was set to 0.1 eV. To fit the experimental *J–V* curves with the model we allowed the trap density, trap depth, electron band mobility and barrier for electron injection to vary simultaneously.

References

1 Cui, Y. *et al.* Fine-Tuned Photoactive and Interconnection Layers for Achieving over 13% Efficiency in a Fullerene-Free Tandem Organic Solar Cell. *J. Am. Chem. Soc.* **139**, 7302-7309 (2017).

2 Liu, Y. *et al.* Aggregation and morphology control enables multiple cases of high-efficiency polymer solar cells. *Nature Communications* **5**, 5293, doi:10.1038/ncomms6293 (2014).

3 Zhao, W. *et al.* Fullerene-Free Polymer Solar Cells with over 11% Efficiency and Excellent Thermal Stability. *Advanced Materials* **28**, 4734-4739, doi:10.1002/adma.201600281 (2016).

4 Baran, D. *et al.* Reducing the efficiency-stability-cost gap of organic photovoltaics with highly efficient and stable small molecule acceptor ternary solar cells. *Nature Materials* **16**, 363-369 (2017).

5 Jørgensen, M., Norrman, K. & Krebs, F. C. Stability/degradation of polymer solar cells. *Solar Energy Materials and Solar Cells* **92**, 686-714 (2008).

6 Jørgensen, M. *et al.* Stability of Polymer Solar Cells. *Advanced Materials* **24**, 580-612 (2012).

7 Emmott, C. J. M. *et al.* In-situ, long-term operational stability of organic photovoltaics for off-grid applications in Africa. *Sol. Energy Mater. Sol. Cells* **149**, 284-293 (2016).

8 Kawano, K. *et al.* Degradation of organic solar cells due to air exposure. *Solar Energy Materials and Solar Cells* **90**, 3520-3530, doi:10.1016/j.solmat.2006.06.041 (2006).

9 Ahmed, R., Simbrunner, C., Schwabegger, G., Baig, M. A. & Sitter, H. Air stability of C60 based n-type OFETs. *Synth. Met.* **188**, 136-139 (2014).

10 Heumueller, T. *et al.* Morphological and electrical control of fullerene dimerization determines organic photovoltaic stability. *Energy & Environmental Science* **9**, 247-256, doi:10.1039/C5EE02912K (2016).

11 Heumueller, T. *et al.* Reducing burn-in voltage loss in polymer solar cells by increasing the polymer crystallinity. *Energy & Environmental Science* **7**, 2974-2980, doi:10.1039/C4EE01842G (2014).

12 Li, Z. *et al.* Performance enhancement of fullerene-based solar cells by light processing. *Nat. Commun.* **4:2227** (2013).

13 Wood, S. *et al.* Natures of optical absorption transitions and excitation energy dependent photostability of diketopyrrolopyrrole (DPP)-based photovoltaic copolymers. *Energy & Environmental Science* **8**, 3222-3232, doi:10.1039/C5EE01974E (2015).

14 Soon, Y. W. *et al.* Correlating triplet yield, singlet oxygen generation and photochemical stability in polymer/fullerene blend films. *Chemical Communications (Cambridge, United Kingdom)* **49**, 1291-1293, doi:10.1039/c2cc38243a (2013).

15 Distler, A. *et al.* Effect of PCBM on the Photodegradation Kinetics of Polymers for Organic Photovoltaics. *Chem. Mater.* **24**, 4397-4405 (2012).

16 Rao, A. M. *et al.* Photoinduced Polymerization of Solid C_{60} Films. *Science* **259**, 955-957 (1993).

17 Eklund, P. C., Rao, A. M., Zhou, P., Wang, Y. & Holden, J. M. Photochemical transformation of C_{60} and C_{70} films. *Thin Solid Films* **257**, 185-203 (1995).

18 Distler, A. *et al.* The Effect of PCBM Dimerization on the Performance of Bulk Heterojunction Solar Cells. *Adv. Energy Mater.* **4**, 1300693 (2014).

19 Piersimoni, F. *et al.* Influence of fullerene photodimerization on the PCBM crystallization in polymer: Fullerene bulk heterojunctions under thermal stress. *J. Polym. Sci. Part B: Polym. Phys.* **51**, 1209-1214 (2013).

20 Shogo, Y. *et al.* MALDI-TOF MS Study of the Photooxidation of PCBM and Its Suppression by P3HT. *Chemistry Letters* **44**, 339-341, doi:10.1246/cl.141025 (2015).

21 Xiao, Z. *et al.* Synthesis of [59]Fullerenones through Peroxide-Mediated Stepwise Cleavage of Fullerene Skeleton Bonds and X-ray Structures of Their Water-Encapsulated Open-Cage Complexes. *J. Am. Chem. Soc.* **129**, 16149-16162 (2007).

22 Anselmo, A. S., Dzwilewski, A., Svensson, K. & Moons, E. Photodegradation of the electronic structure of PCBM and C60 films in air. *Chem. Phys. Lett.* **652**, 220-224 (2016).

23 Hansson, R. *et al.* Photo-degradation in air of the active layer components in a thiophene-quinoxaline copolymer:fullerene solar cell. *Phys. Chem. Chem. Phys.* **18**, 11132-11138 (2016).

24 Yamane, S. *et al.* Photooxidation studies on indene-C60 adducts. *Sol. Energy Mater. Sol. Cells* **143**, 135-140 (2015).

25 Matsuo, Y. *et al.* Deterioration of bulk heterojunction organic photovoltaic devices by a minute amount of oxidized fullerene. *Chem. Commun. (Cambridge, U. K.)* **48**, 3878-3880 (2012).

26 Volonakis, G., Tsetseris, L. & Logothetidis, S. Impurity-related degradation in a prototype organic photovoltaic material: A first-principles study. *Org. Electron.* **14**, 1242-1248 (2013).

27 Reese, M. O. *et al.* Photoinduced Degradation of Polymer and Polymer–Fullerene Active Layers: Experiment and Theory. *Adv. Funct. Mater.* **20**, 3476-3483 (2010).

28 Peters, C. H. *et al.* High Efficiency Polymer Solar Cells with Long Operating Lifetimes. *Adv. Energy Mater.* **1**, 491-494, doi:10.1002/aenm.201100138 (2011).

29 Jeranko, T., Tributsch, H., Sariciftci, N. S. & Hummelen, J. C. Patterns of efficiency and degradation of composite polymer solar cells. *Sol. Energy Mater. Sol. Cells* **83**, 247-262 (2004).

30 Shoaee, S. & Durrant, J. R. Oxygen diffusion dynamics in organic semiconductor films. *J. Mater. Chem. C* **3**, 10079-10084 (2015).

31 Silva, H. S., Cresson, J., Rivaton, A., Bégué, D. & Hiorns, R. C. Correlating geometry of multidimensional carbon allotropes molecules and stability. *Org. Electron.* **26**, 395-399 (2015).

32 Zeman, M. & Krc, J. Optical and electrical modeling of thin-film silicon solar cells. *J. Mater. Res.* **23**, 889-898 (2008).

33 Dacuña, J. & Salleo, A. Modeling space-charge-limited currents in organic semiconductors: Extracting trap density and mobility. *Phys. Rev. B* **84**, 195209 (2011).

34 Nicolai, H. T., Mandoc, M. M. & Blom, P. W. M. Electron traps in semiconducting polymers: Exponential versus Gaussian trap distribution. *Phys. Rev. B* **83**, 195204 (2011).

35 Kirchartz, T., Deledalle, F., Tuladhar, P. S., Durrant, J. R. & Nelson, J. On the Differences between Dark and Light Ideality Factor in Polymer:Fullerene Solar Cells. *J. Phys. Chem. Lett.* **4**, 2371-2376 (2013).

36 Faist, M. A. *et al.* Competition between the Charge Transfer State and the Singlet States of Donor or Acceptor Limiting the Efficiency in Polymer:Fullerene Solar Cells. *Journal of the American Chemical Society* **134**, 685-692, doi:10.1021/ja210029w (2012).

37 Yao, J. *et al.* Quantifying Losses in Open-Circuit Voltage in Solution-Processable Solar Cells. *Phys. Rev. Applied* **4**, 014020 (2015).

38 Nicolai, H. T. *et al.* Unification of trap-limited electron transport in semiconducting polymers. *Nat. Mater.* **11**, 882-887 (2012).

39 Seemann, A. *et al.* Reversible and irreversible degradation of organic solar cell performance by oxygen. *Solar Energy* **85**, 1238-1249 (2011).

40 Schafferhans, J., Baumann, A., Wagenpfahl, A., Deibel, C. & Dyakonov, V. Oxygen doping of P3HT:PCBM blends: Influence on trap states, charge carrier mobility and solar cell performance. *Org. Electron.* **11**, 1693-1700 (2010).

41 Khelifi, S. *et al.* Investigation of defects by admittance spectroscopy measurements in poly (3-hexylthiophene):(6,6)-phenyl C61-butyric acid methyl ester organic solar cells degraded under air exposure. *J. Appl. Phys.* **110**, 094509 (2011).

42 Lenes, M. *et al.* Electron Trapping in Higher Adduct Fullerene-Based Solar Cells. *Adv. Funct. Mater.* **19**, 3002-3007 (2009).

43 Pacios, R. *et al.* Effects of Photo-oxidation on the Performance of Poly[2-methoxy-5-(3′,7′-dimethyloctyloxy)-1,4-phenylene vinylene]:[6,6]-Phenyl C61-Butyric Acid Methyl Ester Solar Cells. *Adv. Funct. Mater.* **16**, 2117-2126 (2006).

44 Schafferhans, J., Deibel, C. & Dyakonov, V. Electronic Trap States in Methanofullerenes. *Adv. Energy Mater.* **1**, 655-660 (2011).

45 Correa-Baena, J.-P. *et al.* The rapid evolution of highly efficient perovskite solar cells. *Energy Environ. Sci.* **10**, 710-727 (2017).

46 Soon, Y. W. *et al.* Material Crystallinity as a Determinant of Triplet Dynamics and Oxygen Quenching in Donor Polymers for Organic Photovoltaic Devices. *Advanced Functional Materials* **24**, 1474-1482, doi:10.1002/adfm.201302612 (2013).
47 Richter, M. H., Friedrich, D. & Schmeißer, D. Valence and Conduction Band States of PCBM as Probed by Photoelectron Spectroscopy at Resonant Excitation. *BioNanoScience* **2**, 59-65, doi:10.1007/s12668-011-0034-1 (2012).
48 Díaz, J., Paolicelli, G., Ferrer, S. & Comin, F. Separation of the sp3 and sp2 components in the C1s photoemission spectra of amorphous carbon films. *Physical Review B* **54**, 8064-8069 (1996).
49 Jones, R. O. & Gunnarsson, O. The density functional formalism, its applications and prospects. *Rev. Mod. Phys.* **61**, 689-746 (1989).

Author Contributions

Device fabrication and stability studies were carried out by H.K.H.L. and Z.L. MALDI-TOF measurements were carried out by M.F.W. AFM measurements were carried out by J.R.S and XPS depth profiles by J.M. DFT calculations were performed by B.R. EL measurements were performed by A.M.T., and sub-band gap EQE measurements were carried out by S.M.T. and A.D.C.M. SCLC measurements and *J*–*V* simulations were carried out by J.A.R. TPV and CE measurements were carried out by J.W. J.M., T.W., E.S. and S.P. contributed to sample preparation and device fabrication. H.K.H.L., J.R.D., A.M.T., T.K. and W.C.T. contributed to project planning and discussions. Z.L. and J.N. had the idea, led the project, and prepared the manuscript. All authors contributed to the manuscript preparation.

Acknowledgements

The authors would like to acknowledge the funding support from the Welsh Assembly Government funded Sêr Cymru Solar Project, and the National Research Network in Advanced Engineering and Materials, the European Commission's CHEETAH Project (FP7-Energy-2013- Grant no. 609788) and EPSRC grants EP/M025020/1 and EP/K030671/1. ZL thanks the Welsh Assembly Government Sêr Cymru II fellowship scheme, AMT thanks the Imperial College Junior Research Fellowship scheme, ADCM thanks CNPq-Brazil PDE fellowship (Grant 207507/2014-7), JAR thanks the EPSRC Doctoral

Training Centre in Plastic Electronics (EP/G037515/1) and BR thanks the EPSRC Doctoral Training Centre in Theory and Simulation of Materials (EP/G036888/1) for funding.

Competing Financial Interests Statement

The authors declare no competing financial interests.

Figure legends

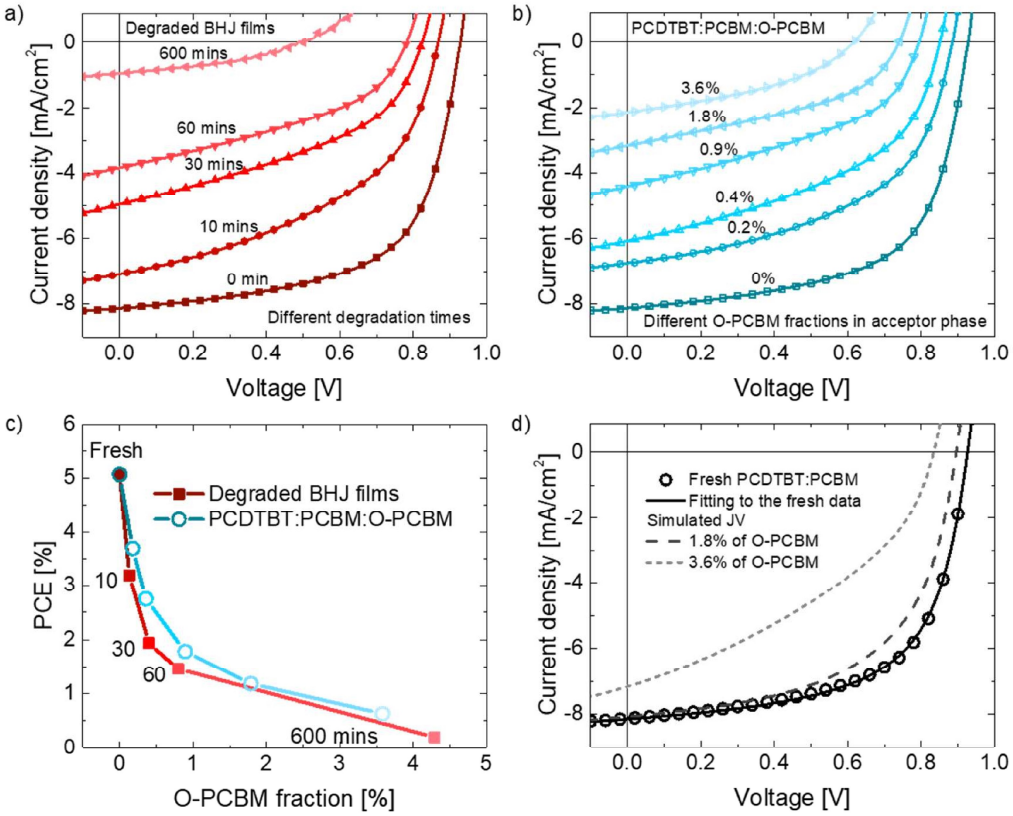

Figure 1 Impact of fullerene photo-oxidation on OPV devices behaviour. (a) Current density-voltage (*J-V*) characteristic of ITO/PEDOT:PSS/PCDTBT:PCBM (1:2)/Ca/Al devices with different degradation times under simulated AM1.5G illumination in air (the films were exposed to solar simulated light prior to back contact deposition); (b) *J-V* characteristic of PCDTBT:PCBM blend devices made with

different fractions of degraded PCBM (the PCBM was degraded in solution prior to active layer processing), the percentages indicating the mass fraction of O-PCBM in the fullerene phase. All devices were encapsulated in nitrogen before characterisation. (c) PCE as a function of O-PCBM fraction for degraded PCDTBT:PCBM devices and pre-degraded PCBM devices; and (d) experimental (open circles) and simulated *J-V* characteristics for a device with pristine PCDTBT:PCBM (black); also simulated *J-V* characteristics for devices with increasing fraction of O-PCBM (dark grey dash line: 1.8 % and light grey short dash line: 3.6 %), reconstructed using the mobilities, trap energies and trap densities obtained from the space-charge-limited current analysis (see Figure 3). Full device parameters are summarised in Supplementary Table 1 and Table 2.

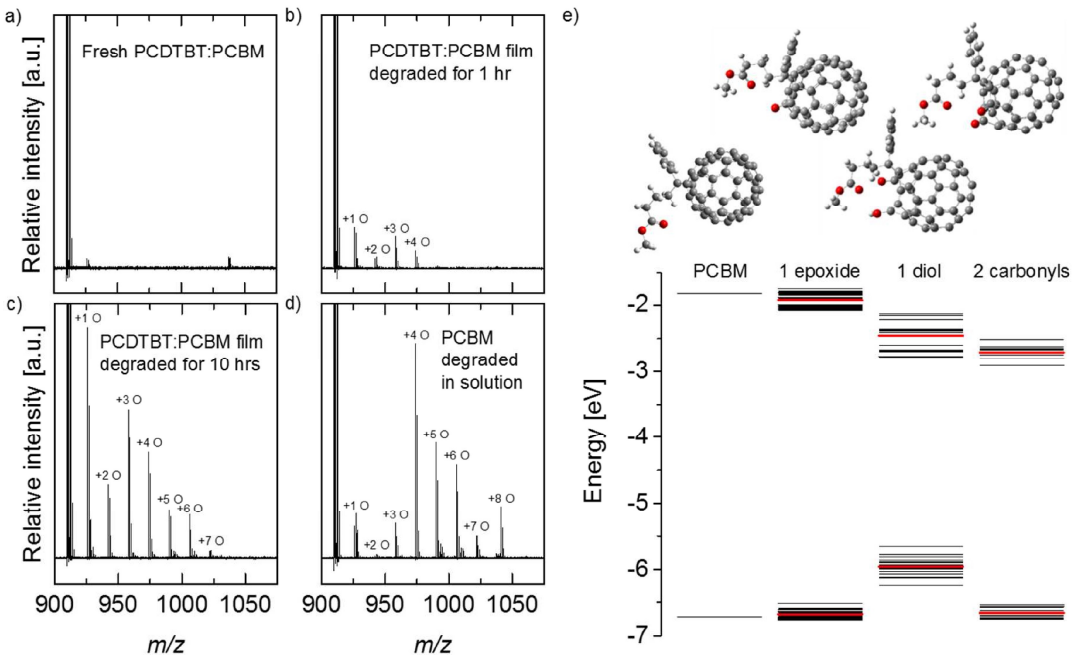

Figure 2 Possible mechanisms of fullerene photo-oxidation. Negative ion mode MALDI-TOF measurement of (a) fresh PCDTBT:PCBM blend films; PCDTBT:PCBM blend films degraded under one sun in dry air for (b) 1 hour and (c) 10 hours; and (d) PCBM degraded in solution under one sun in dry air for 72 hours (see Supplementary Fig. 8 for raw data). (e) From left to right: HOMO and LUMO energies (calculated using a delta-SCF method) for neat PCBM, PCBM with one epoxide, PCBM with

one diol and PCBM with two carbonyls defects. The different energies correspond to different possible positions of the defects on the fullerene cage. Boltzmann averages, based on total energy calculations, are given by the red lines. The molecular structures of PCBM, and an example of each defect type, are shown above their corresponding energy level diagram.

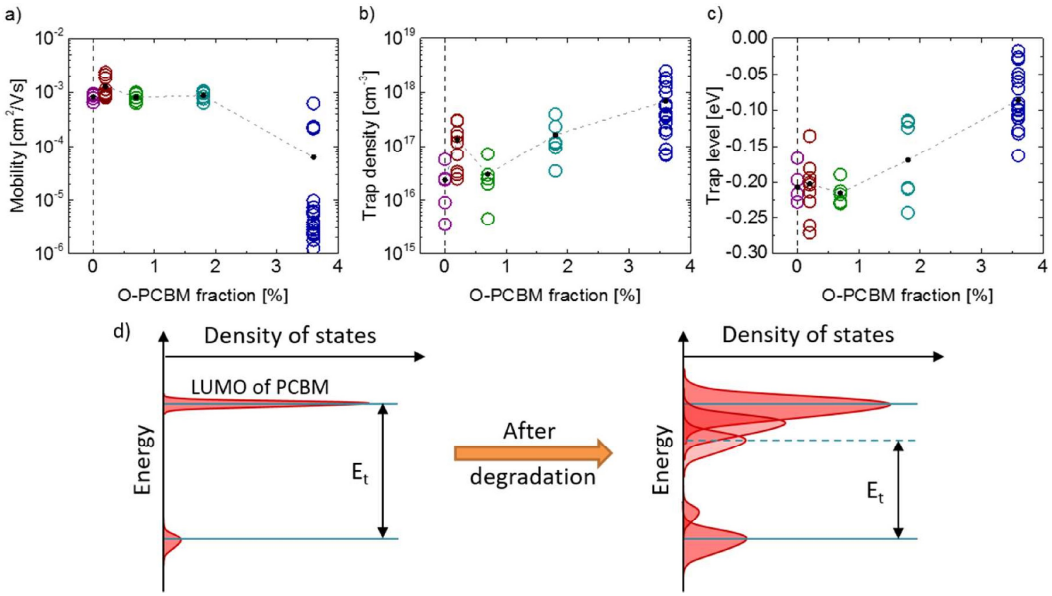

Figure 3 Effects of fullerene oxidation on charge transport kinetics in neat PCBM films. Parameters obtained from analysis of space-charge-limited current measurements for PCBM electron-only devices with increasing fractions of O-PCBM: (a) electron "band" mobilities; (b) density of deep (Gaussian) traps; (c) depth of trap level below the LUMO of the pristine PCBM. (d) Schematic illustrating how the density of electron states may evolve during photo-oxidation. A number of repeated studies of fabrication and measurement were performed due to increasing variations of the band mobility, trap density and trap levels with increasing O-PCBM fraction caused by more severe film irregularity.

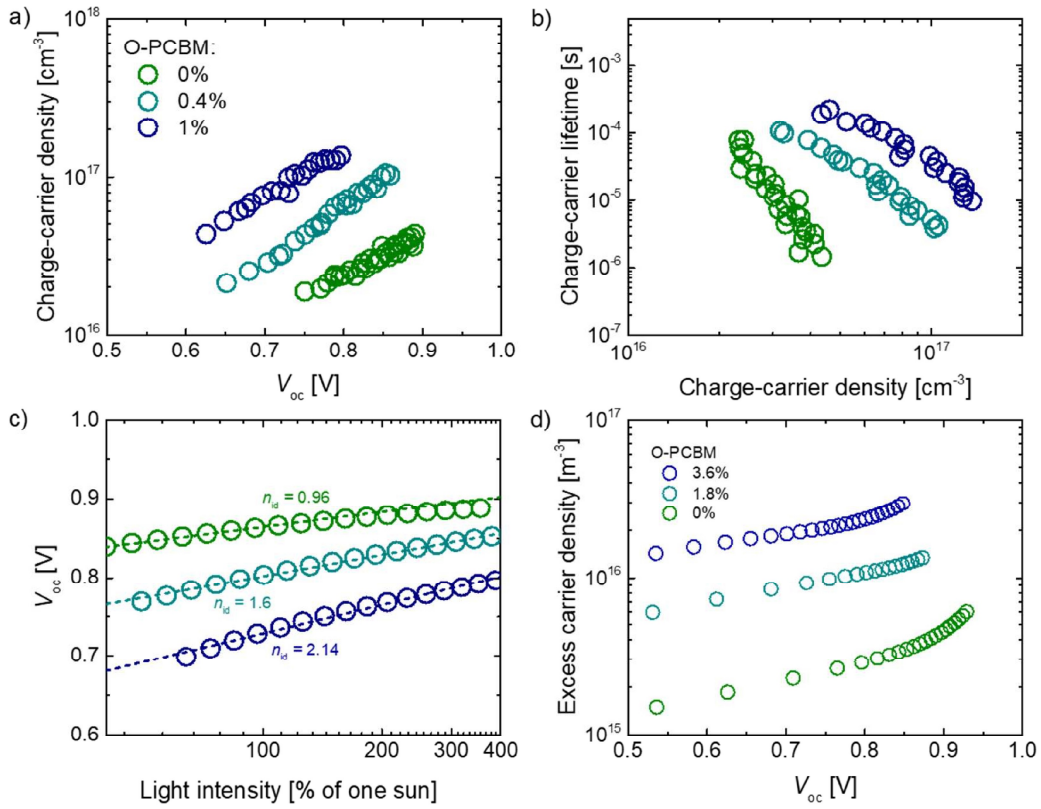

Figure 4 Effects of fullerene oxidation on blend film recombination and transport kinetics. CE,TPV and TPC analysis of PCDTBT:PCBM devices with increasing fraction of O-PCBM: (a) Charge-carrier density at varying V_{oc} (produced by varying the illumination intensity); (b) charge-carrier lifetimes at varying charge-carrier density [calculated from (a)]; (c) measured V_{oc} (open circles) at varying illumination intensities (the dashed lines indicate linear fits to the data); (d) simulated charge carrier density versus V_{oc} for different levels of degradation. Note that the devices under study exhibited high shunt currents under low illumination conditions (below 0.3 suns), and therefore those data were not included in the analysis.